NOVEL BIOBASED RESINS USING SUCROSE ESTERS OF PLANT OILS

A Dissertation
Submitted to the Graduate Faculty
of the
North Dakota State University
of Agriculture and Applied Science

By

Xiao Pan

In Partial Fulfillment of the Requirements
for the Degree of
DOCTOR OF PHILOSOPHY

Major Department:
Coatings and Polymeric Materials

May 2011

Fargo, North Dakota

North Dakota State University
Graduate School

Title

Novel Biobased Resins using Sucrose Esters of Plant Oils

By

Xiao Pan

The Supervisory Committee certifies that this ***disquisition*** complies with North Dakota State University's regulations and meets the accepted standards for the degree of

DOCTOR OF PHILOSOPHY

North Dakota State University Libraries Addendum

To protect the privacy of individuals associated with the document, signatures have been removed from the digital version of this document.

ABSTRACT

Pan, Xiao, Ph.D., Department of Coatings and Polymeric Materials, College of Science and Mathematics, North Dakota State University, May 2011. Novel Biobased Resins Using Sucrose Esters of Plant Oils. Major Professor: Dr. Dean C. Webster.

Interest in using renewable raw materials to prepare biobased monomers, polymers, and materials is rapidly increasing. The goal of the research described is to develop branched polyesters of plant oil fatty acids, using different core polyols (i.e. sucrose, dipentaerythritol, and tripentaerythritol) and plant oils (i.e. linseed, safflower, and soybean), into curing systems that have potential uses in applications such as coatings, composites, and adhesives. This study is mainly focused on the use of sucrose as the core polyol in the soyate resins.

Sucrose esters and their derivatives have a compact structure, high density, and high functionality—double bonds, epoxides, or hydroxyls. When considering the use of sucrose ester compounds to form crosslinked materials, the rigid core of sucrose can potentially impart hardness to the thermoset, and the high functionality can lead to rapid gelation and high crosslink density. Thus, these novel biobased resins using sucrose esters of plant oils have the potential to be a significant advance in biobased resin technology, as well as to be competitive with the conventional petroleum-based resins.

ACKNOWLEDGMENTS

I joined NDSU in August of 2007. With immense gratitude I would like to thank all the people with whom I spent the past four years.

I sincerely thank my wonderful advisor—Dr. Dean C. Webster—one of the most important people in my life. He offered me the opportunity to join the CPM graduate program. He accepted my will to work in his group. He supported me constantly as much as he could in research and spent a lot of time revising my papers. I really wish that I could create the words that no one else used before to express my greatest thanks to him.

I would like to thank my other committee members, Dr. Bret Chisholm, Dr. Andriy Voronov, and Dr. Kalpana Katti, for their assistance, guidance and time contributions to this committee, and efforts for reading and advising this dissertation.

I must thank Partha Sengupta, Thomas J. Nelson, and Adlina Paramarta, who were and are working with me closely in the project. I appreciate the receiving, giving and sharing in this team, no matter of just some random thoughts, which might initiate a new idea. I would like to thank Chavanin Siripirom for playing soccer with me on weekends without which I would have lost most of the fun in Fargo's winter. I would like to thank Stacy Sommer for taking care of my safety in the lab and bringing delicious cookies to group meetings. I would like to thank Erin Pavlacky for inviting me to her wonderful wedding with Drew Pavlacky who was my lab partner in Coatings I lab. I also would like to thank the other members in Dr. Webster's group for the lab and equipment help. Special thanks must be given to the CPM staff, Carol Johnson, Jacinda Wollan, and Heidi Docktor, for their great help.

DEDICATION

I would like to dedicate this doctoral dissertation to my wife, Jingyan, who sacrified for my American dream. It would be doubtful that I could complete this process without her constant love, understanding, and support. This dissertation is also dedicated to my son, James, who specially encouraged me to work harder and think more.

To my mother (Shuping Wang) and my mother-in-law (Shumei Zhang), thank you for being in Fargo with me and taking care of James. The honor of this successful completion of my Ph.D. not only belongs to me, but also belongs to both of you.

TABLE OF CONTENTS

ABSTRACT iii

ACKNOWLEDGMENTS iv

DEDICATION v

LIST OF TABLES xiii

LIST OF FIGURES xv

CHAPTER 1. GENERAL INTRODUCTION 1

1.1. Green/Sustainable Chemistry 1

1.2. Challenges of Green Chemistry 2

1.3. Renewable Raw Materials 3

1.3.1. Plant Oils 3

1.3.1.1. Composition and structure 3

1.3.1.2. Oil-based paints and coatings 6

1.3.1.3. Alcoholysis 9

1.3.2. Carbohydrates 12

1.3.2.1. Sucrose 12

1.3.3. Sucrose Esters of Plant Oils 13

1.4. References 15

CHAPTER 2. NOVEL BIOBASED DUAL-CURE COATING SYSTEM 19

2.1. Abstract 19

2.2. Introduction 19

2.3. Experimental 21

2.3.1. Raw Materials 21

2.3.2. Synthesis of Acetoacetylated Sucrose Soyate (ASS) 22

2.3.3. Synthesis of Acetoacetylated Sucrose (AS) 22

2.3.4. Synthesis of Enamine Alkyl Substituted Acetoacetylated Sucrose (EAS).... 23
2.3.5. Characterization on Resins 23
2.3.6. Compatibility Studies 24
2.3.6.1. Enamine alkyl chain length 24
2.3.6.2. Degree of enamine alkyl substitution 25
2.3.7. Coating Formulation 25
2.3.8. Coating Measurements 26
2.3.9. Drying Time 26
2.4. Results and Discussion 27
2.4.1. Synthesis and Characterization of Acetoacetylated Sucrose Soyate (ASS) .. 27
2.4.2. Synthesis of Acetoacetylated Sucrose and Their Enamine Derivatives 30
2.4.2.1. Acetoacetylated sucrose 31
2.4.2.2. Fully enamine alkyl substituted AS (f-EAS) 33
2.4.3. Partially Enamine Alkyl Substituted AS (p-EAS) 37
2.4.4. Coating Properties 41
2.4.4.1. Autoxidation curing of SS based materials 41
2.4.4.2. Enamine formation curing of EAS based materials 42
2.4.4.3. Dual-curing of SS/EAS blends via autoxidation and enamine formation.. 43
2.4.5. Drying Time Studies 45
2.5. Conclusions 46
2.6. References 47
CHAPTER 3. NOVEL BIOBASED EPOXY COMPOUNDS: EPOXIDIZED SUCROSE ESTERS OF FATTY ACIDS 49
3.1. Abstract 49
3.2. Introduction 50
3.3. Experimental 52

3.3.1. Raw Materials 52
3.3.2. Epoxidation of Sucrose Esters 52
3.3.3. Characterization on Epoxy Resins 53
3.4. Results and Discussion 56
3.4.1. Epoxidation 56
3.4.2. Functional Groups and Molecular Structure 58
3.4.2.1. FTIR results 58
3.4.2.2. ^{1}H-NMR results 58
3.4.2.3. ^{13}C-NMR results 61
3.4.3. Composition and Molecular Weight 62
3.4.4. Density 65
3.4.5. Bulk Viscosity 66
3.4.6. Intrinsic Viscosity 67
3.4.7. Thermal Properties 68
3.4.7.1. DSC results 68
3.4.7.2. TGA results 69
3.4.8. Structure and Property Relationships 70
3.5. Conclusions 72
3.6. References 73
CHAPTER 4. HIGH BIOBASED CONTENT EPOXY-ANHYDRIDE THERMOSETS FROM EPOXIDIZED SUCROSE ESTERS OF FATTY ACIDS 76
4.1. Abstract 76
4.2. Introduction 77
4.3. Experimental 80
4.3.1. Raw Materials 80
4.3.2. Preparation of Epoxidized Sucrose Esters of Fatty Acids 80

4.3.3. Epoxy-anhydride Formulation and Curing 81
4.3.4. Characterization on Epoxy-anhydride Thermosets 81
4.3.4.1. Differential scanning calorimetry (DSC) 81
4.3.4.2. Soxhlet extraction 82
4.3.4.3. Fourier transform infrared (FTIR) spectroscopy 83
4.3.4.4. Tensile testing 83
4.3.4.5. Dynamic mechanical analysis (DMA) 84
4.3.4.6. Nanoindentation 84
4.3.4.7. Thermogravimetric analysis (TGA) 85
4.3.4.8. Coating measurements 85
4.4. Results and Discussion 85
4.4.1. Properties of The Epoxy Compounds 85
4.4.2. Curing Reaction Mechanism 86
4.4.3. The Degree of Cure or Conversion 89
4.4.4. Sol Content 91
4.4.5. Biobased Content 95
4.4.6. Tensile Properties 95
4.4.7. Dynamic Mechanical Properties 99
4.4.8. Nanomechanical Properties 102
4.4.9. Thermal Stability 106
4.4.10. Coating Properties 107
4.4.11. Structure-property Relationships 109
4.5. Conclusions 110
4.6. References 111
CHAPTER 5. IMPACT OF STRUCTURE & FUNCTIONALITY OF CORE POLYOL IN HIGHLY FUNCTIONAL BIOBASED EPOXY RESINS 113

5.1. Abstract 113
5.2. Introduction 114
5.3. Experimental 118
5.3.1. Raw Materials 118
5.3.2. Preparation of DPE/TPE Esters of Soybean Oil Fatty Acids 118
5.3.3. Preparation of Epoxidized Soyate Compounds 120
5.3.4. Characterization on Epoxidized Soyate Compounds 120
5.3.5. Epoxy-anhydride Formulation and Curing 122
5.3.6. Characterization on Epoxy-anhydride Thermosets 122
5.4. Results and Discussion 123
5.4.1. Synthesis of Epoxidized Soyate Compounds 123
5.4.1.1. GPC results 124
5.4.1.2. FTIR results 125
5.4.1.3. ^{1}H-NMR results 126
5.4.2. Structure-property Relationships in Epoxy Compounds 128
5.4.3. Structure-property Relationships in Epoxy-anhydride Thermosets 132
5.5. Conclusions 136
5.6. References 137
CHAPTER 6. NOVEL BIOBASED HIGH FUNCTIONALITY POLYOLS AND THEIR USE IN POLYURETHANE COATINGS 139
6.1. Abstract 139
6.2. Introduction 140
6.3. Experimental 142
6.3.1. Raw Materials 142
6.3.2. Synthesis of Sucrose Soyate Polyols 143
6.3.2.1. Acid-epoxy reaction 143

6.3.2.2. Alcohol-epoxy reaction 144
6.3.3. Characterization on Polyols 145
6.3.4. Polyurethane (PU) Formulation and Curing 145
6.3.5. Characterization on PU Thermosets 146
6.4. Results and Discussion 148
6.4.1. Polyol Synthesis 148
6.4.1.1. Base-catalyzed acid-epoxy reaction 148
6.4.1.2. Acid-catalyzed alcohol-epoxy reaction 153
6.4.2. Properties of PU Thermosets 159
6.4.2.1. Biobased content 159
6.4.2.2. Coatings properties 160
6.4.2.3. Tensile, dynamic mechanical, and thermal properties of PU films 163
6.4.2.4. Thermal stabilities of PU thermosets 166
6.5. Conclusions 167
6.6. References 168
CHAPTER 7. SUCROSE SOYATE-BASED WATER DISPERSIBLE POLYOLS AND THEIR USE IN TWO-COMPONENT AQUEOUS POLYURETHANE COATINGS 170
7.1. Abstract 170
7.2. Introduction 171
7.3. Experimental 174
7.3.1. Raw Materials 174
7.3.2. Synthesis of Maleinized Sucrose Soyate 174
7.3.3. Synthesis of Sucrose Soyate-based Water Dispersible Polyol 175
7.3.4. Water Dispersion Stability of Polyol 175
7.3.5. Formulation of 2K Waterborne Polyurethane (PU) 176

7.3.6. Characterization on Resins and PU Coatings 176
7.4. Results and Discussion 177
7.5. Conclusions 182
7.6. References 182
CHAPTER 8. OVERALL CONCLUSIONS 185
CHAPTER 9. FUTURE WORK 187
9.1. Acetoacetate Chemistry in Sucrose and Sucrose Soyate 187
9.2. Epoxidized Sucrose Esters (ESSs) 188
9.2.1. Quantitative Analysis of ESSs Using MALDI-TOF MS 188
9.2.2. Solvent Compatibility and Dilution Curve 188
9.2.3. High Temperature Curing of Epoxy-anhydride System 189
9.2.4. Corrosion Protection Evaluation 189
9.3. Biobased High Functionality Polyols 189
9.3.1. Polyols with 100% Biobased Content 189
9.3.2. Comparison with Triglyceride Polyols in Polyurethane 190

LIST OF TABLES

Table		Page
1.1.	Typical fatty acid composition of selected plant oils	5
2.1.	Acetoacetylated sucrose (AS) and fully enamine alkyl substituted acetoacetylated sucrose (f-EAS)	33
2.2.	Compatibilities between fully enamine alkyl substituted acetoacetylated sucrose (f-EAS) and sucrose soyate in solution/solvent-free (Y = compatible; N = incompatible)	37
2.3.	Acetoacetylated sucrose (AS) and enamine alkyl substituted acetoacetylated sucrose with different degrees of enamine substitution	38
2.4.	The effect of degree of enamine substitution on the compatibility between SS and f-EAS	41
2.5.	Properties of SS based coatings cured via autoxidation	42
2.6.	Properties of EAS based coatings cured via enamine formation	42
2.7.	Properties of dual-cured coatings	45
3.1.	Descriptions of sucrose esters of fatty acids used in this study	52
3.2.	The conversions of epoxidation and epoxide functionalities of epoxidized sucrose esters of fatty acids (ESEFAs)	57
3.3.	Compositions and molecular weights of epoxidized sucrose esters	65
4.1.	Properties of ESEFAs and ESO control used in this study	86
4.2.	The degrees of cure or conversions of epoxy-anhydride thermosets with an equivalent ratio of epoxide to anhydride of 1:0.5	91
4.3.	The tensile properties of epoxy-anhydride thermosetting thin films with an equivalent ratio of epoxide to anhydride of 1:0.5	97
4.4.	The tensile properties of epoxy-anhydride thermosetting thick samples with an equivalent ratio of epoxide to anhydride of 1:0.75 and 1:0.5	99
4.5.	Dynamic mechanical properties and crosslink densities of epoxy-anhydride thermosets	99
4.6.	Properties of epoxy-anhydride coatings	108

5.1. The properties of polyester esters of soybean oil fatty acids before and after epoxidation 128

5.2. The tensile, dynamic mechanical and thermal properties of epoxy-anhydride thermosets 133

6.1. Ester-sucrose soyate polyols prepared in acid-epoxy reactions 149

6.2. Ether-sucrose soyate polyols prepared in alcohol-epoxy reactions 155

6.3. Properties of polyurethane coatings 162

6.4. Young's modulus, tensile strength at maximum load, and elongation at break of polyurethane films in tensile testing 163

6.5. Dynamic mechanical and thermal properties of polyurethane films 165

7.1. Water dispersion stability of polyol in different degrees of neutralization and solids contents 181

7.2. Properties of waterborne 2K polyurethane coatings 181

LIST OF FIGURES

Figure		Page
1.1.	Schematic representation of plant oil structure	4
1.2.	Chemical structures of fatty acids in plant oils	6
1.3.	Transesterification of a triglyceride with methanol	10
1.4.	Synthetic strategies of fatty acid methyl ester (FAME)	11
1.5.	Chemical structure of sucrose (β-D-fructofuranosyl-(2→1)-α-D-glucopyranoside)	12
1.6.	Sucrose ester of plant oil fatty acid with full substitution	14
2.1.	Schematic sketch of the determination of drying times using BK 3-Speed Drying Recorder in 24 hours travel	27
2.2.	Synthesis of acetoacetylated sucrose soyate (ASS)	28
2.3.	GPC plots of partially esterified sucrose soyate (p-SS) and acetoacetylated sucrose soyate (ASS)	28
2.4.	FT-IR spectra of partially esterified sucrose soyate (p-SS) and acetoacetylated sucrose soyate (ASS)	29
2.5.	^{1}H-NMR spectra of partially esterified sucrose soyate (p-SS) and acetoacetylated sucrose soyate (ASS)	30
2.6.	Synthesis of acetoacetylated sucrose (AS) and enamine substituted acetoacetylated sucrose (EAS)	31
2.7.	FT-IR spectra of sucrose and acetoacetylated sucrose (AS)	32
2.8.	^{1}H-NMR spectrum of acetoacetylated sucrose (AS)	32
2.9.	GPC plots of fully enamine alkyl substituted acetoacetylated sucrose (f-EAS) and acetoacetylated sucrose (AS)	34
2.10.	^{1}H-NMR spectrum of dodecylamine enamine substituted acetoacetylated sucrose (D-EAS)	35
2.11.	DSC curves indicating glass transition of fully enamine alkyl substituted acetoacetylated sucrose (f-EAS) prepared using different length of primary monoamines	36

2.12. DSC curves of dodecylamine-EAS (D-EAS) and octadecylamine-EAS (O-EAS) 36

2.13. GPC plots of acetoacetylated sucrose (AS) and dodecylamine enamine substituted acetoacetylated sucrose (D-EAS) with different degrees of enamine substitution 39

2.14. FT-IR spectra of acetoacetylated sucrose (AS) and dodecylamine enamine substituted acetoacetylated sucrose (D-EAS) with different degrees of enamine substitution 39

2.15. DSC curves indicating the glass transitions of acetoacetylated sucrose (AS) and dodecylamine enamine substituted acetoacetylated sucrose (D-EAS) with different degrees of enamine substitution 40

2.16. Schematic of the dual-cure process of blend of ASS and O/D-EAS-3 in the presence of diamine crosslinker (PACM) and metal salt driers 44

2.17. Drying times of coatings. a. SS based coatings cured via autoxidation; b. EAS based coatings; c. Dual-cure blends of O/D-EAS-3 and ASS 46

3.1. Reactions mechanism for *in situ* epoxidation with peroxyacid 51

3.2. FT-IR spectra of (a) sucrose linseedate (SL) and epoxidized sucrose linseedate (ESL); (b) sucrose soyate B6 (SSB6) and epoxidized sucrose soyate B6 (ESSB6) 59

3.3. The ^{1}H-NMR spectra of sucrose safflowerate (SSF) and epoxidized sucrose safflowerate (ESSF) 60

3.4. The ^{13}C-NMR spectra of sucrose safflowerate (SSF) and epoxidized sucrose safflowerate (ESSF) 61

3.5. Positive ion MALDI-TOF mass spectra of epoxidized sucrose esters: (a) epoxidized sucrose linseedate (ESL); (b) epoxidized sucrose safflowerate (ESSF); (c) epoxidized sucrose soyate (ESS); (d) epoxidized sucrose soyate B6 (ESSB6) 64

3.6. (a) Density of sucrose ester versus iodine value; (b) density of epoxidized sucrose ester versus epoxide functionality 65

3.7. (a) Bulk viscosity and iodine value of sucrose ester; (b) bulk viscosity and epoxide functionality of epoxidized sucrose esters 66

3.8. Intrinsic viscosities of soybean oil, sucrose esters, and their epoxy products in THF at 25°C 67

3.9. DSC curves indicating glass transition temperatures of (a) sucrose esters; (b) epoxidized sucrose esters 68

3.10. TGA thermograms of (a) sucrose esters; and (b) epoxized sucrose esters (Experiments were carried out in a nitrogen atmosphere) 69

3.11. The effect of *cis* configuration of double bonds and epoxides on fatty acid morphology: a) naturally occurring *cis* double bonds bend fatty acid chains, with the assumption that the C-C single bonds are all in *trans*; b) *cis* double bonds produce *cis* epoxides with the bond length and bond angle slightly changed 71

4.1. Epoxidized sucrose ester of fatty acids (ESEFAs) 78

4.2. Chemical formulae of the reactants used for epoxy-anhydride 87

4.3. Reaction mechanism of epoxy-anhydride in the presence of DBU amidine catalyst and hydroxyls 89

4.4. Typical DSC temperature scans at 10°C/min of ESO-anhydride curing system (a) and ESS-anhydride curing system (b) that have been cured at 85°C for 0 hour, 12 hours and 48 hours 90

4.5. Sol content (wt %) of epoxy-anhydride thermosets that have been cured at 85°C for 12 and 48 hours 92

4.6. Overlaid FTIR spectra of samples from ESS/MHHPA/DBU system that has been cured at 85°C for 0, 12, and 48 hours 93

4.7. Overlaid FTIR spectra of sol and gel samples of ESS/MHHPA/DBU system that has been cured for 12 hours 94

4.8. Typical stress-strain curves of epoxy-anhydride thermosetting thin films with an equivalent ratio of epoxide to anhydride of 1:0.5 97

4.9. Typical stress-strain curves of epoxy-anhydride thermosetting thick samples with an equivalent ratio of epoxide to anhydride of 1:0.75 and 1:0.5 98

4.10. Temperature dependence of loss factor tan δ (a) and storage modulus *E'* (b) of epoxy-anhydride thermosets using ESEFAs (The equivalent ratio of epoxide to anhydride is 1:0.5) 100

4.11. Temperature dependence of loss factor tan δ (a) and storage modulus *E'* (b) of ESL thermosets (The equivalent ratios of epoxide to anhydride are 1:0.5, 1:0.4, and 1:0.3) 101

4.12. Temperature dependence of loss factor tan δ (a) and storage modulus E' (b) of soyate epoxy (i.e. ESS, ESSB6, and ESO) thermosets (The equivalent ratio of epoxide to anhydride is 1:0.5) 102

4.13. Typical load-displacement curves of soyate epoxy thermosets in nanoindentation tests (The equivalent ratio of epoxide to anhydride is 1:0.5) 104

4.14. The sample modulus E_s (a) and indentation hardness H (b) of soyate epoxy thermosets in nanoindentation tests (The equivalent ratios of epoxide to anhydride are 1:0.5 and 1:0.75) 105

4.15. TGA curves of epoxy-anhydride thermosets in nitrogen at a heating rate of 20°C/min: (a) ESL thermosets in different epoxide/anhydride molar ratios; (b) ESEFAs thermosets with epoxide:anhydride=1:0.5; (c) Soyate epoxy thermosets with epoxide:anhydride=1:0.5; (d) Soyate epoxy thermosets with epoxide:anhydride=1:0.75 106

4.16. The onset decomposition temperatures of epoxy-anhydride thermosets 107

5.1. Molecular structures of dipentaerythritol (DPE) and tripentaerythritol (TPE) 114

5.2. Glycerol, dipentaerythritol, tripentaerythritol, and sucrose were used as core polyols in the polyol esters of epoxidized soybean oil fatty acids 117

5.3. GPC plots of polyol esters of soybean oil fatty acids before and after epoxidation. (a) Unsaturated polyol esters: FAME, soybean oil, dipentaerythritol soyate, tripentaerythritol soyate B6, and tripentaerythritol soyate; (b) Epoxidized polyol esters: epoxidized soybean oil, epoxidized dipentaerythritol soyate, epoxidized tripentaerythritol soyate B6, and epoxidized tripentaerythritol soyate 124

5.4. Overlaid FTIR spectra of polyol esters of soybean oil fatty acids before and after epoxidation. (a) DPES and EDPES; (b) TPES and ETPES; (c) ETPES and ETPESB6; SSB6 and ESSB6 125

5.5. Overlaid ^{1}H-NMR spectra of (a) polyol esters of soybean oil fatty acids and (b) their epoxy products 127

5.6. Positive ion MALDI mass spectra of epoxidized polyol esters of soybean oil fatty acids: (a) ESO; (b) EDPES; (c) ETPESB6; (d) ETPES; (e) ESS; (f) ESSB6. Sodiated peaks are labeled according to the m/z ratios 130

5.7. Comparison of the physical properties of polyol esters of fatty acids before and after epoxidation 131

5.8. Molecular structure of dodecenylsuccinic anhydride (3-(dodec-1-enyl)oxolane -2,5-dione) 132

5.9. Comparison of the properties of epoxy-anhydride thermosets using different epoxidized polyol esters 134

5.10. Comparison of the properties of epoxy-anhydride coatings using different epoxidized polyol esters 135

6.1. Reaction strategies of producing triglyceride polyols by transforming double bonds to hydroxyls 141

6.2. GPC plots of the f-ESS starting material and the ester-polyols prepared by reaction with 2-ethylhexanoic acid (EHA) in different acid/epoxide molar ratios 150

6.3. FT-IR spectra of the f-ESS starting material and the ester-polyols prepared by reaction with 2-ethylhexanoic acid (EHA) in different acid/epoxide molar ratios 151

6.4. The overlaid ^{1}H-NMR spectra of the ester-polyols prepared by reaction with 2-ethylhexanoic acid (EHA) in different acid/epoxide molar ratios 152

6.5. The epoxide conversions of the ester-polyols using 2-ethylhexanoic acid (EHA) in different acid/epoxide molar ratios 153

6.6. GPC plots of the starting material ESSs and ester polyol products: (a) f-ESS and MESSs; (b) ESSB6 and MESSB6 156

6.7. FTIR spectra of the starting material ESSs and the ether-polyol products: (a) f-ESS and MESS; (b) ESSB6 and MESSB6 157

6.8. ^{1}H-NMR spectra overlaid of the starting material f-ESS and its ether-polyol product MESS_1 158

6.9. Aliphatic diisocyanate trimers 159

6.10. The overlaid FTIR spectra of MESS_1/IPDI trimer PU thermosets with different NCO/OH ratios 161

6.11. Young's moduli and elongations at break of polyurethanes films 164

6.12. TGA curves in nitrogen of polyurethanes (PUs) at a heating rate of 20°C/min: (a) PUs using ester-polyols. (b) PUs using ether-polyols 166

7.1. Synthesis of maleinized sucrose soyate (MSS) in free-radical initiated maleinization 178

7.2. GPC plots of sucrose soyate (SS) and maleinized sucrose soyate (MSS) in the reaction in a MA/SS molar ratio of 6:1 179

7.3. Overlaid FTIR spectra of sucrose soyate (SS), maleinized sucrose soyate (MSS), the mixture of MSS and PDO, and the product of polyol 180

CHAPTER 1. GENERAL INTRODUCTION

1.1. Green/Sustainable Chemistry

Sustainability is the long-term vision on the endurance of the earth to human beings. To reduce the negative human impact on the dimension of environmental sustainability, green chemsitry is becoming the most responsible research goal in academic and industrial chemistry.

Green chemistry, also called sustainable chemistry, is a philosophy of chemical research and engineering that encourages the design of products and processes that minimize the use and generation of hazardous substances.[1] As a chemical philosophy, green chemistry applies to organic chemistry, inorganic chemistry, biochemistry, analytical chemistry, and even physical chemistry. Green chemistry applies across the life cycle of a chemical product, including its design, manufacture, and use.

The United States Environmental Protection Agency (EPA) developed *the 12 Principles of Green Chemistry*.[2] The utilization of natural products has been considered as one of the approaches (the 7th principle of green chemistry: Use of Renewable Feedstocks) that can contribute to green chemistry. Plants function as natural battery that harvests solar energy through photosynthesis, a process that converts carbon dioxide into organic compounds. Thus, the utilization of renewable raw materials results in recycling carbon dioxide that doesn't contribute to green house effects. Furthermore, the resulting products are highly possible to take advantage of the synthetic potential of nature, such as a built-in design of degradation (the 10th principle of green chemistry: Design for Degradation) and

an expected lower toxicity to human beings (the 3rd and 4th principles of green chemistry: Less Hazardous Chemical Syntheses, and Designing Safer Chemicals).

The rapid increasing interest in biofeedstock-based chemistry is also due to the foreseeable limits of fossil raw materials as they are depleting and are irreplaceable. Although we do not exactly know that when fossil raw materials will have become so expensive that biofeedstocks are an economically competitive alternative, the transition to a more biobased production is pressing, and somehow the field of inexpensive, large-scale-accessible biobased chemicals is expanding year by year.

1.2. Challenges of Green Chemistry

Today chemical industry is still in an early stage of the transition from petroleum-based production to biobased production due to a variety of obstacles:

a) Fossil raw materials are still economic and readily available at present, although what we are witnessing today is that chemical industry is fighting with the rising costs of fossil oil and gas.

b) The present technology for transforming fossil raw materials into chemicals is exceedingly well developed and basically different from that required for transforming biobased raw materials into chemicals with industrial application profiles. The cost of new investment needs to be considered.

c) Markets are not willing to give up the cost and currently achieved properties only for the sake of green chemistry.

Thus, the task of scientists in this particular era lies in developing new chemicals from renewable raw materials which are economical and processing-friendly while yielding

the product properties and functions demanded in today's applications. From one challenge to one opportunity—the role of business in tomorrow's society, people are willing to advance the understanding, development and application of technologies and methods of biofeedstock-based chemistry, as well as the commercialization of biobased chemcials.

1.3. Renewable Raw Materials

A screening of natural products in the earth consists of the plant kingdom, the microbial world, the marine world, animal sources, and venoms and toxins. Plants provide a large variety of renewable raw materials, including plant oils, polysaccharides (mainly cellulose and starch), sugars, waxes, lignin, proteins, woods, and others.

1.3.1. Plant Oils

Plants oils are the most important renewable raw materials in the chemicals industry today for the production of surfactants, cosmetic products, lubricants, paint formulations, and thermoset materials.[3-9]

1.3.1.1.Composition and structure

Plant oils are lipid materials derived from plants. Physically, plant oils are liquid at room temperature. Chemically, plants oils are naturally occurring triglycerides of fatty acids, i.e. glycerol triesters of fatty acids (Figure 1.1). Although many different parts of plants may yield oil, in commercial practice, oil is extracted primarily from seeds. Therefore, plant oils are also called seed oils. Most naturally occurring fatty acids have a chain of an even number of carbon atoms, from 4 to 28. Three key parameters are driving

differences among plants oils: the length of fatty acid chains, the number of double bonds, and the stereochemistry of double bonds (i.e. *cis* or *trans* configuration).

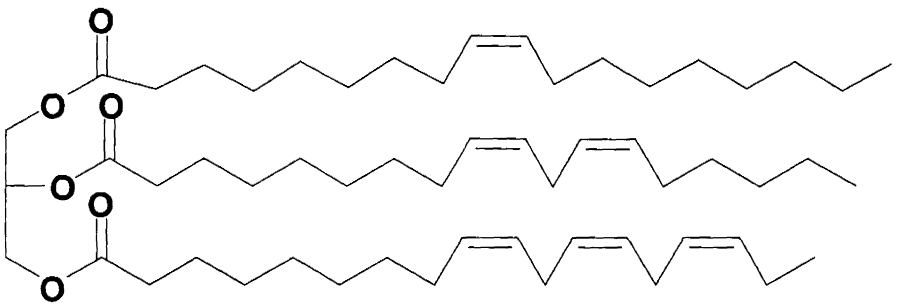

Figure 1.1. Schematic representation of plant oil structure

The reactive sites in most plant oils are the ester groups and the double bonds; however, some oils may naturally contain hydroxy (e.g. ricinoleic acid) and epoxy (e.g. vernolic acid) groups. Ester bonds are the cleavable sites where the reactions transferring fatty acids take place. Double bonds are the functionalizable sites where new functional groups may be derived. Crosslinking or derivatizing reactions of fatty acids mainly occur on double bonds, thus the content of double bonds (or the degree of unsaturation) of plant oils is the most important parameter affecting the physical and chemical properties of plant oils, as well as the properties of their derivatives. The degree of unsaturation of plant oil is expressed by iodine value (IV, the amount of iodine (in gram) that can react with double bonds present in 100 g of sample), which usually varies from zero to 200 g I_2/100 g. Iodine value has been used to correlate with the classification of oils, which are divided into three classes that are roughly classified from the observations of oil behaviors during the exposure to air: drying oils (IV > 140; e.g. linseed oil), semi-drying oils (125 < IV < 140; e.g. soybean oil) and non-drying oils (IV < 125; e.g. coconut oil).

In this study, three types of plant oils have been used and their compositions expressed as the percentage by weight are shown in Table 1.1. Soybean oil is the most readily available plant oil in the world and United States is the Top 1st producer. The farm value of U.S. soy production in 2008/09 was $29.6 billion; the second-highest value among U.S. produced crops, trailing only corn.[10] United States is the Top 3rd producer of linseed oil in the world trailing Canada and China, and the U.S. linseed oil production in 2008/09 was 188,552 metric tons.[11] Safflower is a minor crop today, with about 600,000 metric tons of safflower seeds being produced commercially in more than sixty countries worldwide. India and United States are the leading producers with the safflower seeds production in 2008/09 was 189,000 and109,756 metric tons, respectively.[11] Overall, soybean, linseed, and safflower oils are the most available unsaturated plant oils in U.S.

Five dominating fatty acids are in these three plant oils, two saturated— palmitic acid (C16:0) and stearic acid (C18:0), and three unsaturated— oleic acid (C18:1), linoleic acid (C18:2), and linolenic acid (C18:3). The first number designates the number of carbon atoms in a fatty acid chain and the second represents the number of double bonds. According to the iodine values, linseed and safflower oils are drying oils and soybean oil is semi-drying oil. The unsaturation in linseed oil is highly contributed by linolenic acids, but the unsaturations in safflower and soybean oils are mainly contributed by linoleic acids.

Table 1.1. Typical fatty acid composition of selected plant oils

Carbon atoms: Double bonds	16:0	18:0	18:1	18:2	18:3	Iodine value	Average double bonds per molecule
Linseed oil	5	5	22	16	52	>177	6.3
Safflower oil	7	4	13	75	1	140-150	5.0
Soybean oil	10	5	25	51	9	123-139	4.6

Figure 1.2 displays the chemical structures of the plant oil fatty acids in Table 1. It is noted that all double bonds are in *cis* configuration. The positions of the first double bonds are located on the 9^{th} and 10^{th} carbons; the second are located on the 12^{th} and 13^{th} carbons; the third are located on the 15^{th} and 16^{th} carbons. Thus, the double bonds in linseed, safflower, and soybean oils are non-conjugated. They are separated by a methylene group that makes them less reactive in autoxidation. Some oils (e.g. tung oil) have conjugated double bonds and they polymerize easily when exposed to air.

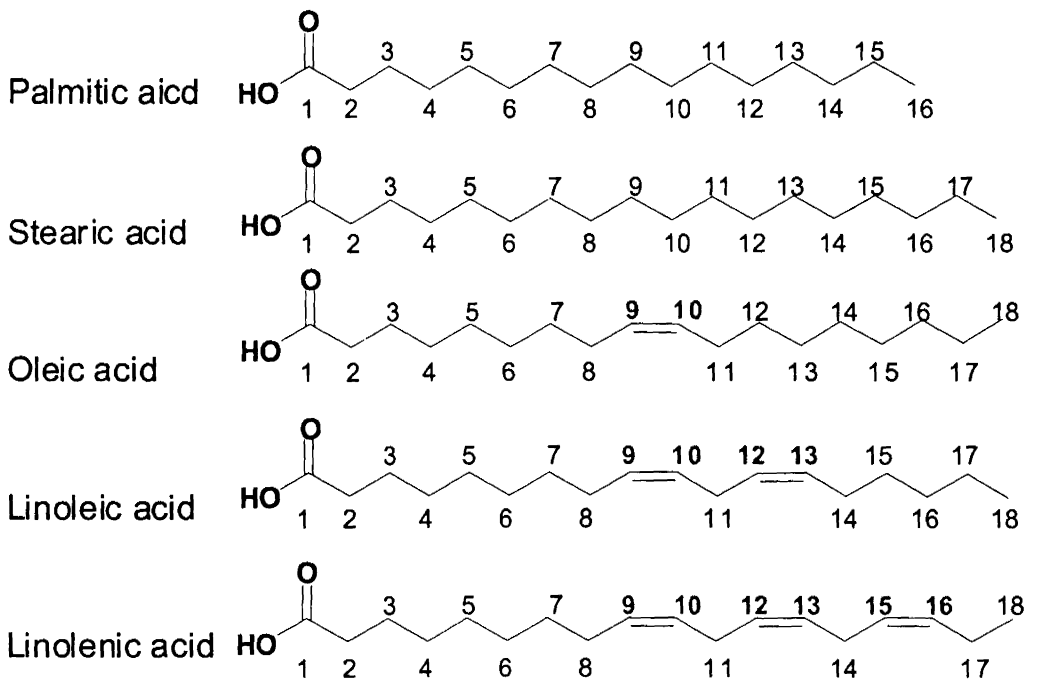

Figure 1.2. Chemical structures of fatty acids in plant oils

1.3.1.2.Oil-based paints and coatings

Drying oils, triglycerides of unsaturated fatty acids, have been used as the key component of coating binder systems for centuries. Prior to the 1920s, the main ingredient in paints and varnishes was the drying oil such as linseed oil. Crosslinking via autoxidation

with atmospheric oxygen, the use of drying oils allows for the preparation of liquid paints that are stable in a closed container, but cure when applied in a thin film to a surface with exposure to atomospheric oxygen.

By concerning with the different concepts relating to the drying properties, a considerable volume of research was undertaken to improve and modify drying oils in the early 20th century, including bodied oils, blown oils, dimerized/oligomerized oils, reconstituted oils, maleic anhydride-treated oils, and copolymer-type oils (e.g. styrenation), etc.[12]

In the late 1920s polyester resins incorporating petrochemical monomers along with oils—alkyd resins—were developed and, due to the large variety of compositions possible, rapidly grew to dominate the coatings industry by the 1940s.[13] The petrochemical monomers are typically dicarboxylic acids or anhydrides such as phthalic anhydride or maleic anhydride, and polyols such as trimethylolpropane, glycerine, or pentaerythritol. Alkyds resins were developed that overcame many of the limitations of drying oils. By synthesizing resins from oils or fatty acids in combination with the petrochemical monomers, resins could be made that resulted in improved initial drying time, higher viscosity, and harder films. By varying oil content, oil type, monomer composition and degree of polymerization, a large variety of alkyd resins could be tailored for almost any coating applications.

The preparation of alkyds from oils typically undergoes a two-step process. The first process is called alcoholysis/mono-glyceride process, in which the raw drying oil is combined with an additional polyol and heated to cause transesterification of the triglycerides into a mixture of mono-polyol esters of fatty acids. Secondly, mono-polyol

esters react with dicarboxylic acids or anhydrides to produce the final alkyd. One key aspect that has limited the adaptability of alkyd reisns to ever more strigent environmental regulations is that there is little control over the structure of the resin. Due to the stochastic nature of the polyesterification process, a broad distribution of polymer chains are formed during alkyd synthesis, which is magnified as the molecular weight is reduced to achieve higher solids, resulting in poor quality coating films. To overcome this limitation, currently, the concept of alkyd resins is being reinvented using approaches such as hyperbranched polyols to yield high-solids alkyd resins.[14-17]

The further development of coatings resins based on natural products has largely stalled during the last 50 years due to a focus on new technology—acrylic resins, polyurethanes, epoxy systems, and latex coatings. These petrochemical derivatives are economical and readily available, and they have provided many new curing technologies which have led to extraordinary coating properties. While the demise of alkyd resins was said to be imminent, alkyd resins continue to be produced in large quantities today.

The incorporation of acetoacetate chemistry into alkyds has been achieved by using tertiary-butyl acetoacetate (t-BAA) to efficiently acetoacetylate the hydroxyls of alkyds.[18-19] The benefits of acetoacetyl chemistry in alkyd coatings are attributed to the reduced solution viscosity, additional cross-linking capabilities, improved adhesion to metals, and etc. Especially, it has been observed that acetoacetate facilitates the autoxidation process of fatty esters in the systems of conventional alkyds.[20]

Oil-based polyurethanes have an extensive use in coatings. As the most common oil-based urethane varnishes, urethane alkyds (uralkyds) are usually prepared using diisocyanate, partial glycerides, and phthalic anhydride.[21] Plant oil-based water reducible

polyurethane dispersions can be achieved by reacting diisocyanates with diol, monoglyceride, and dimethylol propionic acid (DMPA).[22]

Epoxidation of double bonds of fatty esters will convert alkyds into epoxy compounds. However, the utilization of epoxidized alkyds in coatings has never been reported. Due to the low reactivity of the internal epoxy groups and the flexibility of fatty acid chains, epoxidized plant oils have been used as stabilizers and plasticizers for poly(vinyl chloride) structural materials, or reactive toughening agents for rigid thermosetting plastics (e.g. phenolic resins).[23-26] It has also been shown that epoxidized oils can be cured using cationic photopolymerization of epoxides to form coatings.[27-29] However, the extensive use of epoxidized oils in cationic UV curing is still prevented by the relative low reactivity of the internal epoxy groups.[30-31]

It is important to explore new processes to broaden the applications of the plant oil epoxides in UV curable coatings. Acrylation of epoxy fatty compound is a chemical pathway to prepare free-radical UV curable oil-based resins. Biobased acrylate UV curable compounds have been prepared by reacting epoxidized vegetable oil with acrylic acids.[32-34] Soy-based UV curable thiol-ene coating resins have been prepared using the Lewis acid-catalyzed ring opening reaction of epoxidized soybean oil with multifunctional thiols or hydroxyl functional allyl compounds.[35]

1.3.1.3.Alcoholysis

An example of an alcoholysis reaction is the reaction of a triglyceride with a simple alcohol such as methanol or ethanol to give the methyl or ethyl esters of fatty acids,

as well as glycerol. This reaction is more commonly known as a transesterification reaction due to the exchange of the alcohol fragments.

Alcoholysis reaction is a very significant chemical reaction that allows building up a new polymer/macromolecule with the intact oil fatty acids. Usually, the transplantation of fatty acids to other molecules containing hydroxyls necessarily undergoes an intermediate product— fatty acid methyl ester (FAME). FAMEs are also called biodiesel that can be used as an alternative fuel for internal combustion engines. The preparation of biodiesel has been explored as a very attractive issue of using bioenergy.[36-37] Figure 1.3 displays the transesterification reaction between methanol and oil to synthesize FAME.

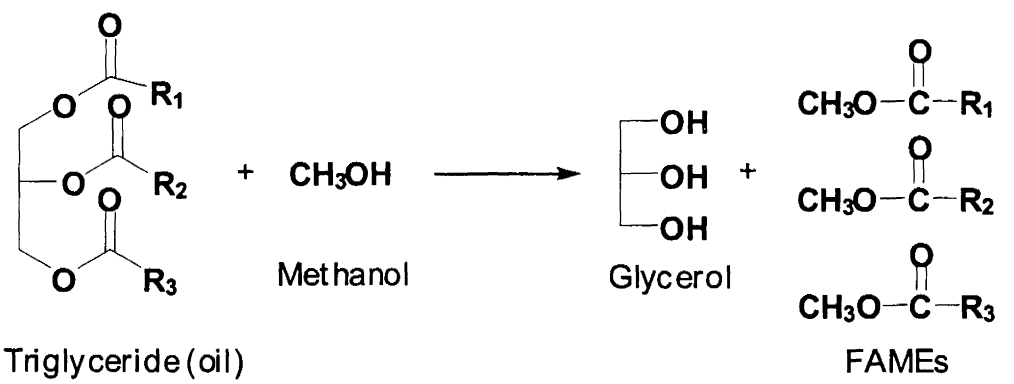

Figure 1.3. Transesterification of a triglyceride with methanol

The variables affecting the production of FAME include free fatty acids content and water content inside of crude plant oil.[36-37] The experimental variables in lab-scale synthesis of FAME include alcohol type, molar ratio of alcohol to oil, type and amount of catalyst, reaction temperature, rate and mode of stirring, and final purification.

FAME synthesis process can be classified as catalytic and non-catalytic, and the catalytic process consists of heterogeneous and homogeneous types. The non-catalytic process is mainly the supercritical fluids conditions (e.g. methanol).[38] The catalytic process is mainly carried out using homogeneous catalysts, which are basic alkaline compounds, such as sodium/potassium hydroxides, carbonates or alkoxides.[39-40] Enzymes are also can be used as a biocatalytic catalyst.[41] Plant oils with rich free fatty acid content usually undergo acid-catalyzed transesterification to suppress foaming.[42] Organotin compounds, i.e. tin(IV) complexes, are very efficient to catalyze alcoholysis of oils.[43] The use of heterogeneous catalysts can effectively suppress homogeneous process problems, such as the production of soaps, separation and purification of products.[44] Figure 1.4 displays the synthetic strategies of FAME.

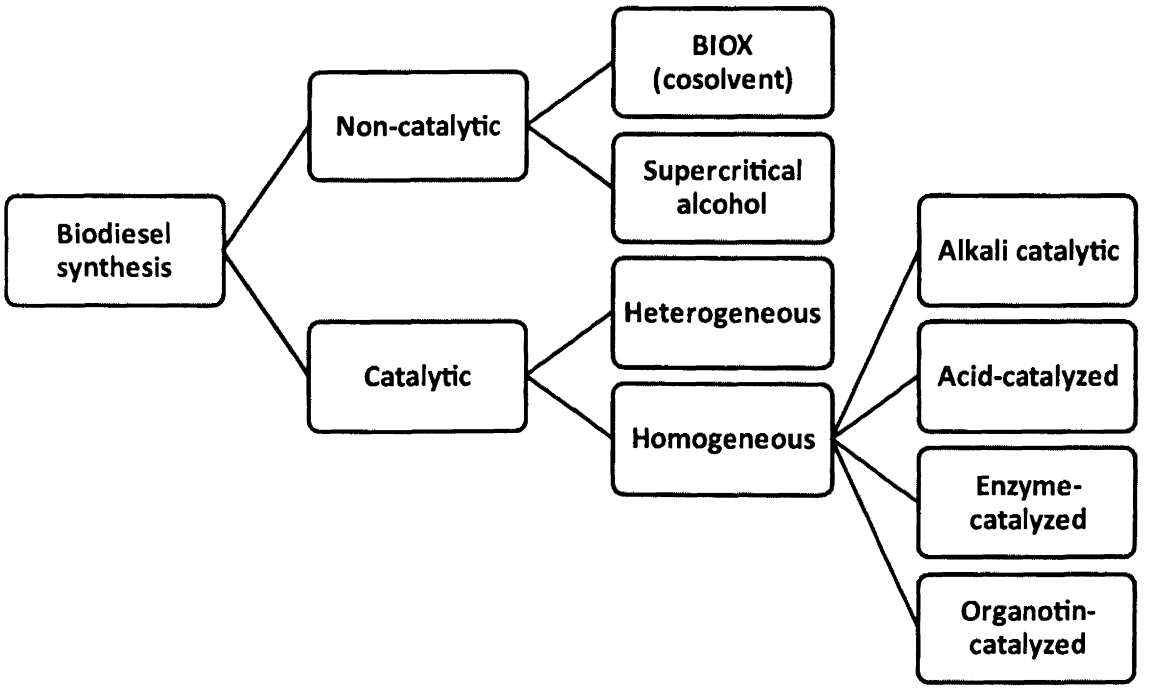

Figure 1.4. Synthetic strategies of fatty acid methyl ester (FAME)

1.3.2. Carbohydrates

The most important class of available natural products in terms of volume is carbohydrates, as they represent roughly 75% of the annually renewable biomass of about 200 billion tons. Whereas the bulk of the annually renewable carbohydrate biomass are polysaccharides, their non-food utilization is confined to textile, paper, and coating industries. Organic commodity chemicals are more expediently obtained from low molecular weight carbohydrates than from polysaccharides. The versatile industrial work of transforming mono- and di-saccharides (e.g. sucrose, glucose and fructose) into products having the potential to replace petrochemical products is very attractive.[45]

1.3.2.1.Sucrose

Sucrose is a non-reducing disaccharide, systematically made of β-D-fructofuranosyl-(2→1)-α-D-glucopyranoside glycosidically linked through their anomeric carbon atoms (Figure 1.5). Sucrose contains eight hydroxyls, three of which are primary and the remaining five are secondary. Sucrose decomposes as it melts at 186 °C (367 °F) to form caramel. Like other carbohydrates, it combusts to carbon dioxide and water.

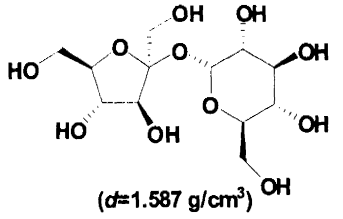

Figure 1.5. Chemical structure of sucrose (β-D-fructofuranosyl-(2→1)-α-D-glucopyranoside)

1.3.3. Sucrose Esters of Plant Oils

Before the 1960s, esters using the mono-/di-saccharides of sugars (i.e. glucose, fructose, and sucrose) didn't have practical value, because this family of natural polyols caramelize and char at the high temperatures used in esterification reaction. Sucrose esters of unsaturated fatty acids were first explored as coating vehicles in the 1960s, and they were prepared using base-catalyzed transesterification between FAME and sucrose.[46-47] While these early studies indicated that the highly substituted sucrose esters had low viscosities, rapid air-drying times and good coatings properties, obtaining a high degree of substitution of fatty acids on the sucrose proved to be challenging. It appears that these resins were never commercialized at that time. In the 1970s, sucrose esters with a full substitution were developed by Procter & Gamble (P&G) Chemicals as a fat substitute, called Olestra or known as the brand name Olean. In the late 1990s, Olestra became infamous in the U.S for its unpleasant side effects.[48]

In 2002, P&G Chemicals had developed an efficient process for industrially producing highly substituted sucrose ester resins under the brand name Sefose.[49-51] Sefose resins were commercialized with a focus on marketing to the lubricant and paint industry. These commercially available products are mixtures of sucrose hexa-, hepta-, and mainly octa-esters (a minimum of 70 wt % of total ester mixture). The viscosities of Sefose sucrose esters are only 300-400 mPa·s. In 2009, Sefose-based alkyd resin technology enabled P&G Chemicals and Cook Composites and Polymers (CCP) to jointly win the "Presidential Green Chemistry Challenge Award for Designing Greener Chemicals" from the U.S. Environmental Protection Agency (EPA) on behalf of the White House, due to the

formulation of coatings having less than half the Volatile Organic Compounds (VOCs) of traditional solventborne alkyd coatings.[52]

Figure 1.6 displays the possible molecular structure of sucrose ester of plant oil fatty acids with a full substitution of fatty acids on the core sucrose. Derived from vegetable oil and sugar, sucrose ester is non-persistent, non-toxic and 100% biodegradable. It can be tailored for different applications by selecting the right plant oil to achieve desired oil content, fatty acid chain length distribution, unsaturation level and degree of esterification.

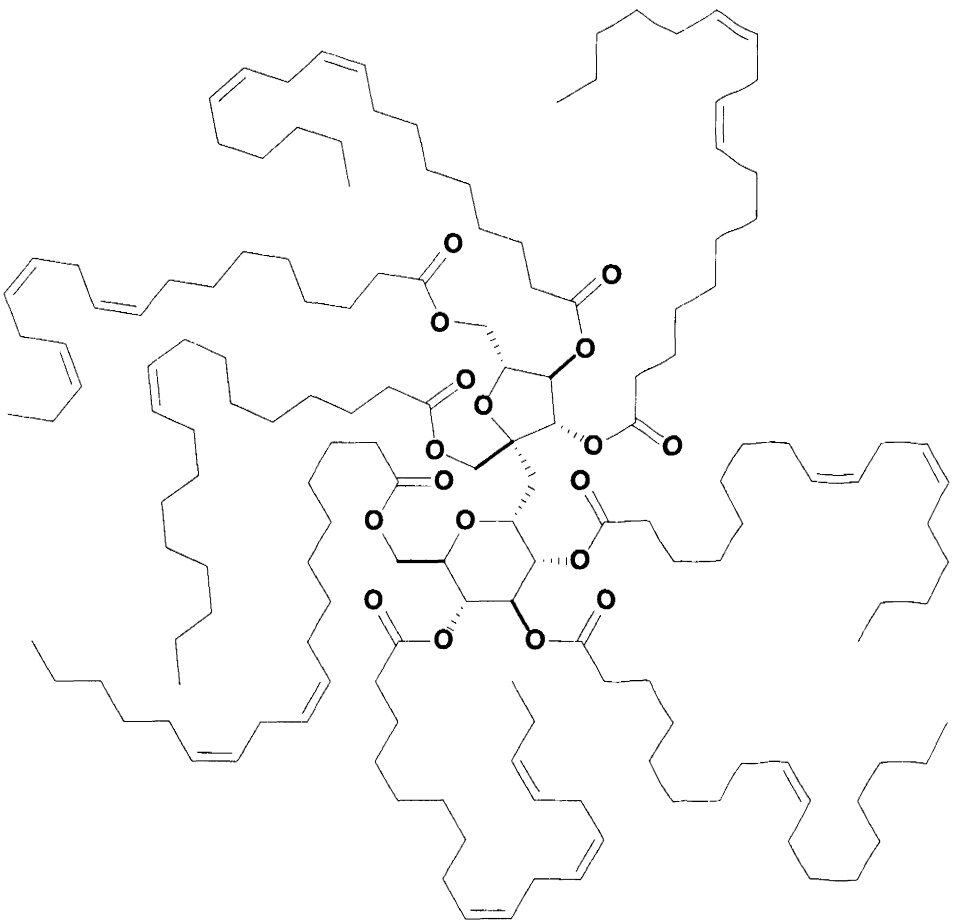

Figure 1.6. Sucrose ester of plant oil fatty acid with full substitution

1.4. References

1. Green Chemistry, the United States Environmental Protection Agency (EPA). http://www.epa.gov/greenchemistry/. (Accessed April 6, 2011).
2. Twelve Principles of Green Chemistry, the United States Environmental Protection Agency (EPA). http://www.epa.gov/greenchemistry/pubs/principles.html. (Accessed April 6, 2011).
3. Meier, M. A. R.; Metzger, J. O.; Schubert, U. S. *Chem. Soc. Rev.* **2007**, *36*, 1788.
4. Baumann, H.; Bühler, M.; Fochem, H.; Hirsinger, F.; Zoebelein, H.; Falbe, J. *Angew. Chem. Int. Ed. Engl.* **1998**, *27*, 41.
5. Biermann, U.; Friedt, W.; Lang, S.; Lühs, W.; Machmüller, G.; Metzger, J. O.; Klaas, M. B.; Schäfer, H. J.; Schneider M. P. *Angew. Chem. Int. Ed.* **2000**, *39*, 2206.
6. Khot, S. N.; Lascala, J. J.; Can, E.; Morye, S. S.; Williams, G. I.; Palmese, G. R.; Kusefoglu, S. H.; Wool, R. P. *J. Appl. Polym. Sci.* **2001**, *82*, 703.
7. Güner, F. S.; Yağcı, Y.; Eriyes, A. Y. *Prog. Polym. Sci.* **2006**, *31*, 633.
8. Sharma, V.; Kundu P. P. *Prog. Polym. Sci.* **2006**, *31*, 983.
9. Xia, Y., Larock, R. C. *Green Chem.* **2010**, *12*, 1893.
10. United States Department of Agriculture, Agricultural Statistics 2009. http://www.ers.usda.gov/Briefing/SoybeansOilCrops/. (Accessed March 15, 2011).
11. Food and Agricultural Organization of United Nations: Economic and Social Department: The Statistical Division. http://faostat.fao.org/site/291/default.aspx. (Accessed March 15, 2011).
12. Rheineck, A. E. *J. Oil Colour Chem. As.*, **1959**, *36*, 574.

13. Patton, T. C. *Official Digest, Federation of Societies for Paint Technology* **1960**, *32*, 1544.

14. Bat, E.; Gündüz G.; Kisakürek, D.; Akhmedov, İ. M. *Prog. Org. Coat.* **2006**, *55*, 330.

15. Mańczyk, K.; Szewczy P. *Prog. Org. Coat.* **2002**, *44*, 99.

16. Karakaya, C.; Gündüz, G.; Aras, L.; Mecidoğlu, İ. A. *Prog. Org. Coat.* **2007**, *59*, 265.

17. Haseebuddin, S.; Parmar, R.; Waghoo, G.; Ghosh, S. K. *Prog. Org. Coat.* **2009**, *64*, 446.

18. Bors, D. A.; Lavoie, Alvin C.; Emmons, W. D. *U.S. Pat. No. 5,484,849*, **1996**.

19. Kuo, T.; Grosso, P. V.; Spilman, G. E.; Clark, M. D. *U.S. Pat. No. 6,794,049*, **2004**.

20. Kuo, T.; Grosso, P. V.; Spilman, G. E.; Clark, M. D. *U.S. Pat. No. 6,780,523*, **2004**.

21. Guner, F. S.; Gumusel, A.; Calica, S.; Erciyes, A. T. *J. Coat. Technol.* **2002**, *74*, 55.

22. Lu, Y.; Larock, R. C. *Biomacromolecules* **2007**, *8*, 3108.

23. Karmalm, P.; Hjertberg, T.; Jansson, A.; Dahl R. *Polym. Degrad. Stab.* **2009**, *94*, 2275.

24. Fenollar, O.; García, D.; Sánchez, L.; López, J.; Balart, R. *Eur. Polym. J.* **2009**, *45*, 2674.

25. Bueno-Ferrer, C.; Garrigós, M.C.; Jiménez, A. *Polym. Degrad. Stab.* **2010**, *95*, 2207.

26. Miyagawa, H.; Misra, M.; Drzal, L. T. *Polym. Eng. Sci.* **2005**, *45*, 487.

27. Crivello, J. V.; Narayan, R. *Chem. Mater.* **1992**, *4*, 692.

28. Thames, S. F.; Yu, H. *Surf. Coat. Technol.* **1999**, *115*, 208.

29. Ortiz, R. A.; López, D. P.; Cisneros, M. d. L. G.; Valverde, J. C. R.; Crivello J. V. *Polymer* **2005**, *46*, 1535.

30. Zou, K.; Soucek, M. D. *Macromol. Chem. Phys.* **2005**, *206*, 967.

31. Sangermano, M.; Malucelli, G.; Bongiovanni, R.; Gozzelino, G.; Peditto, F.; Priola, A. *J. Mater. Sci.* **2002**, *37*, 4753.

32. Scala, J. L.; Wool, R. P. *J. Am. Oil Chem. Soc.* **2002**, *79*, 59.

33. Scala, J. L., Wool, R. P. *Polymer* **2005**, *46*, 61.

34. Pelletier H.; Belgacem, N.; Gandini A. *J. Appl. Polym. Sci.* **2006**, *99*, 3218.

35. Chen, Z.; Chisholm, B. J.; Patani, R.; Wu, J. F.; Fernando, S.; Jogodzinski, K.; Webster, D. C. *J. Coat. Tech. & Res.* **2010**, *7*, 603.

36. Demirbas, A. *Energy Convers. Manage.* **2009**, *50*, 14.

37. Sharma, Y.C.; Singh, B. *Renewable Sustainable Energy Rev.* **2009**, *13*, 1646.

38. Demirbas, A. *Biomass Bioenergy* **2009**, *33*, 113.

39. Rashid, U.; Anwar, F.; Moser, B. R.; Ashraf, S. *Biomass Bioenergy* **2008**, *32*, 1202.

40. Rashid, U.; Anwar, F. *Fuel* **2008**, *87*, 265.

41. Dizge, N.; Keskinler, B. *Biomass Bioenergy* **2008**, *33*, 1274.

42. Zhang, J.; Jiang, L. *Bioresour. Technol.* **2008**, *99*, 8995.

43. Ferreira, D. A.C.; Meneghetti, M. R.; Meneghetti, S. M. P.; Wolf, C. R. *Appl. Catal., A* **2007**, *317*, 58.

44. Albuquerque, M. C. G.; Santamará-González, J.; Mérida-Robles, J. M.; Moreno-Tose, R.; Rodríguez-Castellón, E.; Jiménez-López, A.; Azevedo, D. C. S.; Cavalcante-Jr, C. L.; Maireles-Torres, P. *Appl. Catal., A* **2008**, *347*, 162.

45. Lichtenthaler, F. W.; Peters, S. *C. R. Chim.* **2004**, *7*, 65.

46. Bobalek, E. G.; Walsh, T. J.; Ciang, H. *Official Digest* **1961**, 453.

47. Walsh, T. J.; Bobalek, E. G.; Hall, D. R. *Div. Org. Coatings Plastic Chem.* **1961**, *21*, 125.

48. The Problems with Olestra, Center for Science in the Public Interest. http://www.cspinet.org/olestra/11cons.html. (Accessed on April 15, 2011).

49. Howie, J. K.; Schaefer, J. J.; Trout, J. E. *U.S. Pat. No. 6,995,232*, **2002**.

50. Corrigan, P. J. *U.S. Pat. No. 6,620,952*, **2000**.

51. Schaefer, J. J., Trout, J. E. *U.S. Pat. No. 6,887,947*, **2002**.

52. Chempol® MPS wins the 2009 Presidential Green Chemistry Challenge Awards. http://www.pgsefose.com/sefose-in-the-news.html. (Accessed February 8, 2011).

CHAPTER 2. NOVEL BIOBASED DUAL-CURE COATING SYSTEM

2.1. Abstract

Sucrose esters consisting of acetoacetates and fatty acids were invented as novel biobased amine-cured and autoxidation dual-cure coating systems, in the presence of diamine crosslinker and metal salt driers. Acetoacetylated sucrose soyate (ASS) was an intramolecular system containing both acetoacetates and fatty acids in the same molecule. Miscible bicomponent blends, made of ASS and partially enamine alkyl substituted acetoacetylated sucrose (p-EAS), was an intermolecular curing system. Compatibility between the two components was achieved by reacting acetoacetylated sucrose (AS) with alkyl amines, in which the compatibility could be adjusted by either the alkyl chain length or the degree of enamine alkyl substitution, DES. Sucrose esters were characterized by gel permeation chromatography (GPC), Fourier transform infrared (FTIR) spectroscopy, nuclear magnetic resonance (NMR) spectroscopy, and differential scanning calorimetry (DSC). The properties and drying times of coatings cured through autoxidation, amine-acetoacetate reactions, and by dual-curing were studied. It was found that acetoacetate chemistry improved the attributes of sucrose ester of fatty acids in ambient curing conditions, as well as providing dual-cure coatings having a good balance of properties.

2.2. Introduction

Acetoacetylated sucrose (AS) is an attractive sucrose ester compound with acetoacetates as the functional groups. The synthesis was first reported in the 1960s by reacting diketene with sucrose in dimethylformamide in the presence of triethylamine

catalyst.[1] About twenty years later, Elam et al. improved the preparation of saccharide acetoacetates by reacting saccharides with 2,2,6-trimethyl-4H-1,3-dioxin-4-one, requiring neither a catalyst nor a solvent.[2] In the 1990s, new products and synthesis techniques started to be available to facilitate the preparation of AS by reacting sucrose with alkyl (i.e. methyl, ethyl, and t-butyl) acetoacetates via transesterification.[3]

The broad variety of promising applications of acetoacetate chemistry in the preparation of thermoset coatings were explored by chemists at Eastman Chemical Company, who showed that acetoacetylated polymers can be derivatized or crosslinked using a variety of chemicals, such as melamines, isocyanates, aldehydes, amines (enamine formation), and acrylates (Michael Reaction).[4-5] In the early 2000s, the two most common and efficient methods for covalently bonding acetoacetates to make high-solids coatings resins were: a) free-radical polymerization of acetoacetoxyethyl methacrylate (AAEM) with other vinyl monomers; b) transesterification of t-butyl acetoacetate (*t*-BAA) with polymers containing pendant hydroxyl groups.[6] In the latter method, the attractive attributes of substituting hydroxyls with acetoacetates on polyester resins include reduced solution viscosity and glass transition temperature. Therefore, acetoacetate chemistry provides coating resins with wide latitude for the formulation of high-solids systems with crosslinking versatility for both high temperature and ambient curing.

Acetoacetate chemistry has been introduced into alkyd resins, which contain unsaturated fatty acids as functional groups for autoxidation. Bors et al. disclosed air-drying curable alkyd latex (emulsion polymerization) formulated by pendant acetoacetate functionalized polymer, unsaturated fatty acids and metal salt driers (i.e. cobalt drier).[7] Kuo et al. disclosed high-solids solventborne and waterborne air-drying curable acetoacetate

functionalized alkyds via transesterification.[8-9] Interestingly, the observations in both studies indicated that acetoacetate promoted the autoxidation process. Powell et al. made the statement that acetoacetate is able to work as a reactive copromoter in alkyd resins.[10] "Copromoter" means that acetoacetate has the capability of facilitating hydroperoxide decomposition (either oxidation or reduction) by interacting with cobalt, which accelerates autoxidation. "Reactive" means that acetoacetate can cure into the polymer matrix. However, the details of the exact reactions occurring have not been demonstrated, nor has an extensive study on the influence of acetoacetate groups on autoxidation been reported.

Sucrose fatty esters are 100% biobased resins only containing fatty acids as functional groups, but they possess more promising autoxidation curing than normal triglycerides due to their higher functionalities and unique macromolecular structure. Based on the above literature studies, the work reported herein was initiated by the idea of chemically introducing acetoacetates into sucrose fatty ester resins or blending acetoacetylated sucrose with sucrose fatty esters. The novel coating system would consist of sucrose esters having both acetoacetates and fatty acids as the functional groups. This coating system could be dual-cured by enamine formation and autoxidation. The applications of acetoacetate chemistry on sucrose fatty ester resins are promising, and enamine derivatizing and crosslinking using amines was explored in this study.

2.3. Experimental

2.3.1. Raw Materials

Sucrose (assay≥99.5%, HPLC), β-D-Fructofuranosyl-α-D-glucopyranoside, was purchased from Sigma-Aldrich, Inc (St. Louis, MO). Tertiary-butyl acetoacetate (*t*-BAA,

>98%) was kindly supplied by Eastman Chemical Company (Kingsport, TN). Butylamine, hexylamine, octylamine, decylamine, dodecylamine and octadecylamine were purchased from Sigma-Aldrich, Inc. (St. Louis, MO. Fully esterified sucrose soyate (SS, SEFOSE 1618U) and partially esterified sucrose soyate (p-SS, SEFOSE 1618U B6) were kindly supplied by Procter & Gamble Chemicals (Cincinnati, OH). COBALT HEX-CEM (12%) and ZIRCONIUM HEX-CEM (18%) were provided by OMG (Westlake, OH). Nuxtra Zinc (8%) was provided by DURA Chemicals, Inc. (Alameda, CA). These metal salts were used as driers in autoxidation. AMICURE PACM curing agent (AHEW = 52.5 g/mole), 4, 4'-methylenebiscycloheexanamine, was a gift from Air Products and Chemicals, Inc. (Allentown, PA). All materials were used as received without further purification.

2.3.2. Synthesis of Acetoacetylated Sucrose Soyate (ASS)

In a 500 mL four-neck flask equipped with a mechanical stirrer, nitrogen inlet, thermocouple, reflux condenser and Dean-Stark trap, 100 g (0.054 moles) of p-SS (SEFOSE 1618U B6) and 17.2 g of *t*-BAA (0.108 moles) were added. After 30 minutes nitrogen pre-purge, the reactants were heated to 130°C. During the reaction, the nitrogen inner pressure was kept positive, and 9.1 g of *t*-butanol (0.108 moles) was collected in the Dean-Stark trap as a byproduct. The reaction was stopped when no more *t*-butanol evolved. A light yellow liquid was produced, called acetoacetylated sucrose soyate (ASS).

2.3.3. Synthesis of Acetoacetylated Sucrose (AS)

In a 500 mL four-neck flask equipped with a mechanical stirrer, nitrogen inlet, thermocouple, reflux condenser and Dean-Stark trap, 50.0 g (0.146 moles) of sucrose and

184.9 g of *t*-BAA (1.169 moles) were added. The reactants were stirred and heated to 130°C. During the reaction, the nitrogen inner pressure was kept positive, and 84.8 g of *t*-butanol (1.145 moles) was collected in the Dean-Stark trap as a byproduct. The reaction was stopped when no more *t*-butanol evolved. A yellow viscous product was obtained, known as acetoacetylated sucrose (AS).

2.3.4. Synthesis of Enamine Alkyl Substituted Acetoacetylated Sucrose (EAS)

A series of enamine alkyl substituted acetoacetylated sucrose compounds (EASs) were prepared with different enamine alkyl chain lengths and different degrees of enamine substitution (DES) by reacting AS with primary monoamines. Here, a specific reaction using dodecylamine to synthesize EAS with full enamine substitution is used as an example. In the same reaction setup for AS preparation, 50.0 g (0.050 moles) of AS and 73.0 g (0.400 moles) of dodecylamine were added. The reactants were stirred and heated to 110°C. During the reaction, the nitrogen inner pressure was kept positive, and 7.1 g of water (0.400 moles) was collected in the Dean-Stark trap as a byproduct. The reaction was stopped when no more water evolved. Finally, a red-yellow viscous product was obtained. Other compounds were synthesized using a similar procedure.

2.3.5. Characterization on Resins

Molecular weight was determined using a Waters 2410 gel permeation chromatograph equipped with refractive index detector. Polystyrene standards were used for calibration. A 1.5% sample solution in THF using a flow rate of 1 ml/min was used. FTIR measurements were done with a Thermo Scientific Nicolet 8700 FTIR spectrometer.

Samples were prepared in THF solution, and the concentration was exactly controlled as 4 mg/ml. For each sample solution, a 200 μL drop was deposited by micropipette and naturally spread out on the center of potassium bromide salt crystal. After the evaporation of the THF, a thin layer of sample was formed. Spectra acquisitions were based on 32 scans with data spacing of 4.0 cm^{-1}, and the data were set for auto gain to monitor spectral ranges of 4000–500 cm^{-1}. ^{1}H-NMR measurements were done at 23°C using a JEOL-ECA (400 MHz) NMR spectrometer with an autosampler accessory. All measurements were made using $CDCl_3$ as solvent. The data was processed using the Delta software package. A Q1000 DSC from TA Instruments with an autosampler was used for glass transition temperature (T_g) and melting point (T_m) determinations. Samples were subjected to a heat–cool–heat cycle from -90 to +100 °C by ramping at 10 °C/min for both heating and cooling cycles. The second heating cycle was used to characterize the samples.

2.3.6. Compatibility Studies

2.3.6.1.Enamine alkyl chain length

The effect of enamine alkyl chain length on compatibility was studied using fully enamine alkyl substituted acetoacetylated sucrose (f-EAS) and sucrose soyate (SS). Different alkyl amine resulted in different length of enamine alkyl chain on f-EAS. The f-EAS/SS bicomponent mixtures were mixed in a weight ratio of 1:1. The two components were mixed in xylene solution (80 wt% solid content). The mixtures were allowed to stand for three days before assessing compatibility. Compatibility was visually assessed by the absence of two layers.

2.3.6.2.Degree of enamine alkyl substitution

The effect of the degree of enamine alkyl substitution on the compatibility was studied using partially enamine alkyl substituted acetoacetylated sucrose (p-EAS) and SS. The p-EAS/SS bicomponent mixtures were formulated in the weight ratio of 1:1 in the absence of solvent. The mixtures were allowed to stand for three days before assessing compatibility. Compatibility was visually assessed as the absence of two layers.

2.3.7. Coating Formulation

The sucrose fatty ester based coatings were formulated solvent-free. Cobalt, zinc and zirconium driers were added to the resin at 0.04 wt%, 0.03 wt% and 0.1 wt% (based on resin solids), respectively. Sonication was used for one hour to disperse the driers. The EAS based coatings were formulated in xylene solution (80 wt% of solid content). PACM diamine crosslinker was used in the ratio of amine to acetoacetate equivalents as 1:1. The bicomponent dual-cure coatings were formulated in xylene solution (80 wt% of solid content). The driers were added with the same weight percent as above based on ASS, and then PACM diamine crosslinker was used in the ratio of amine to acetoacetate equivalents as 1:1. All coatings were cast on solvent-cleaned QD-36 steel panels using a draw-down bar with a gap of 4 mils. The coatings were kept at ambient for two days for network formation. Tack free samples were further cured in an oven at 80°C for two hours, and then kept at ambient conditions for 3 more days before testing.

2.3.8. Coating Measurements

The thickness of the cured coating was the average of 10 measurements taken using a Byko-Test 8500 coating thickness gauge at different locations on the film and the uncertainty is the standard deviation. König pendulum hardness and pencil hardness were measured using ASTM D 4366 and ASTM D 3363, respectively. The adhesion of cured coatings was evaluated using crosshatch adhesion ASTM D 3359. Methyl ethyl ketone (MEK) double rub test was carried out following ASTM D 5402. Impact resistance was characterized using ASTM D 2794. Mandrel bend test was carried out based on ASTM D 522, and the results were reported as the elongation of the coating at cracking.

2.3.9. Drying Time

The drying times of coatings were characterized using a BK 3-Speed Drying Recorder (MICKLE Laboratory Engineering Co. Ltd., United Kingdom). The instrument was designed as a needle carrier holding six hemispherical ended needles traveled the length of the six 305*25 mm glass test strips in 6, 12 or 24 hours. In this study, the paint films were cast using a stainless steel cubic film applicator with a gap of 76 MU (film width 13mm, thickness 75μm). Each hemispherical ended steel needle was equipped with a brass weight (5 grams) to study the through-drying properties. The needle travel time was selected for 24 hours. The drying times were evaluated as (I) Open time, (II) Dust free time and (III) Tack free time, and they are illustrated in Figure 2.1.[11]

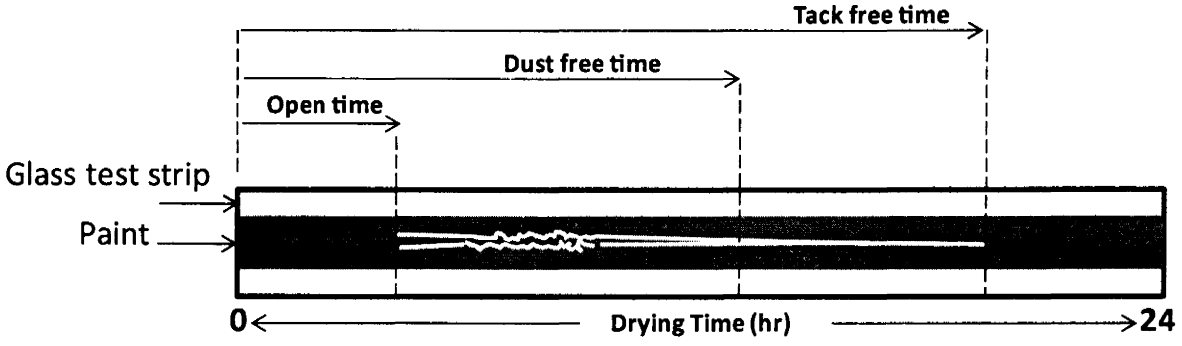

Open time: the end time of the line traced by the needle and closed up again
Dust free time: the end time of the line scratched (contains skinning) by the needle
Tack free time: the end time of a straight line which does not close up

Figure 2.1. Schematic sketch of the determination of drying times using BK 3-Speed Drying Recorder in 24 hours travel

2.4. Results and Discussion

2.4.1. Synthesis and Characterization of Acetoacetylated Sucrose Soyate (ASS)

The dual-cure design of sucrose ester, intramolecularly consisting of both acetoacetate and fatty acid groups, can be achieved by the acetoacetylation of a partially esterified sucrose soyate resin with *t*-BAA. SEFOSE 1618U B6 is a partially esterified sucrose soyate (p-SS) having an average of six soybean fatty acids and two hydroxyls per molecule. The substitution of hydroxyls with acetoacetates produces ASS having an average of six fatty acids and two acetoacetates per molecule, as illustrated in Figure 2.2.

Figure 2.3 shows the GPC plots of p-SS and ASS, and it is observed that the molecular weight of ASS is slightly higher than that of p-SS; however the relatively narrow molecular weight distribution is retained. Figure 2.4 shows the overlaid FTIR spectra of p-SS and ASS. The FTIR spectrum of p-SS shows a small hydroxyl absorption band at 3300-

3500 cm^{-1}, which disappears in the FTIR spectrum of ASS. The FTIR spectrum of ASS also shows a small acetoacetate carbonyl absorption band at 1720 cm^{-1}.

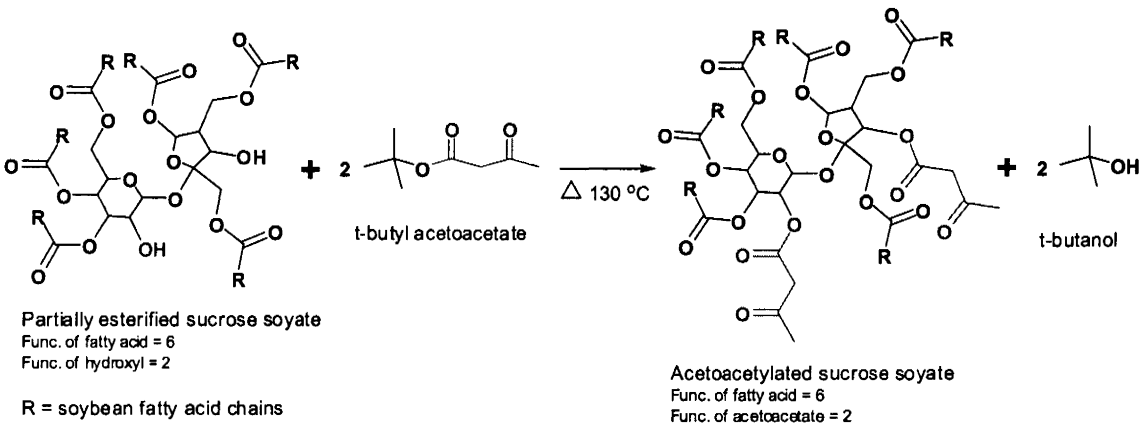

Figure 2.2. Synthesis of acetoacetylated sucrose soyate (ASS)

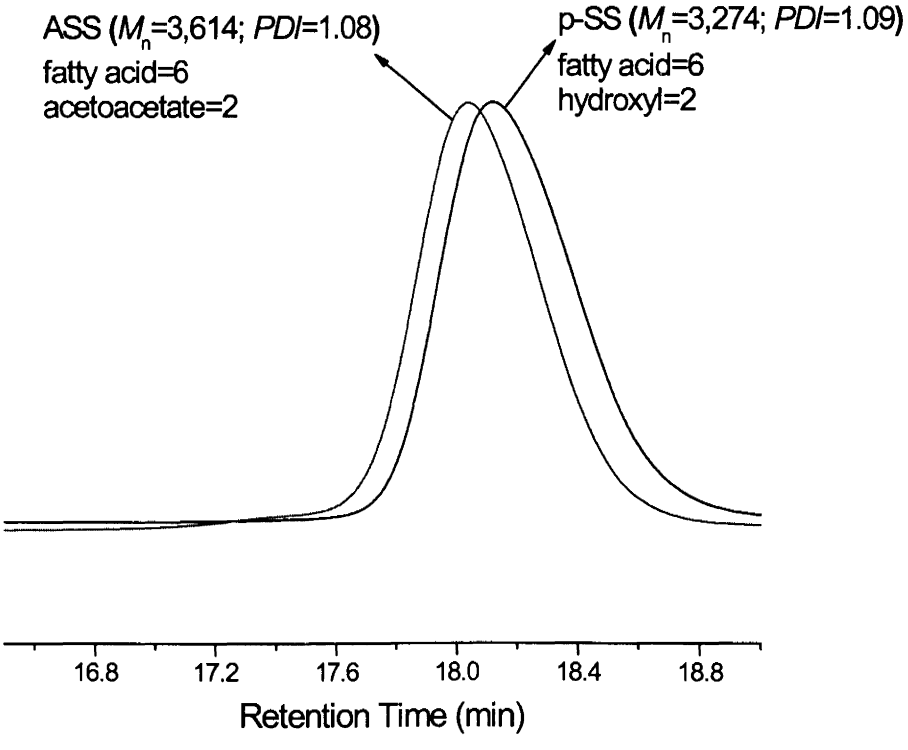

Figure 2.3. GPC plots of partially esterified sucrose soyate (p-SS) and acetoacetylated sucrose soyate (ASS)

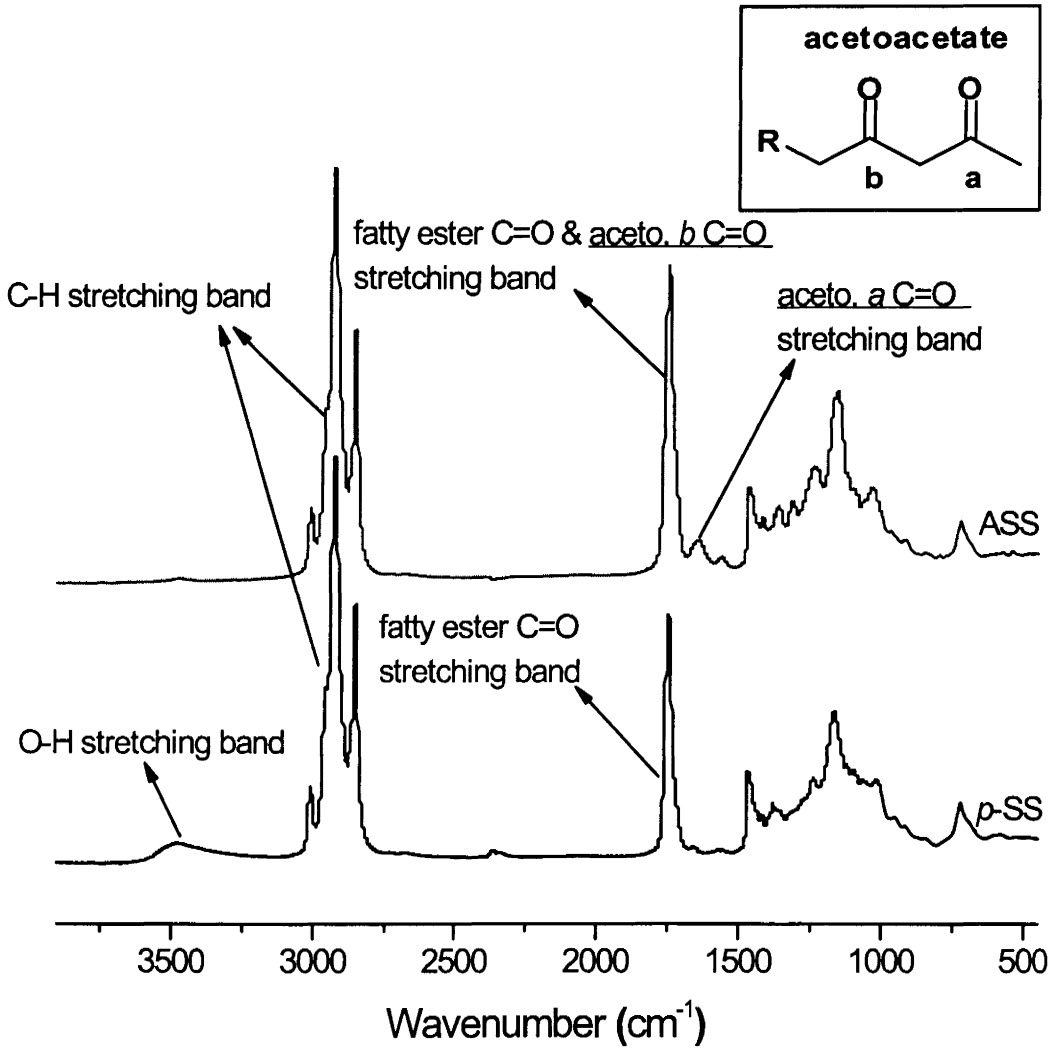

Figure 2.4. FT-IR spectra of partially esterified sucrose soyate (p-SS) and acetoacetylated sucrose soyate (ASS)

Figure 2.5 shows the overlaid ^{1}H-NMR spectra of p-SS and ASS. In the ^{1}H-NMR spectrum of ASS, the substitution of hydroxyls with acetoacetates is confirmed by the peaks of the methyl protons of acetoacetate at 2.23 ppm and methylene protons of acetoacetate at 3.34 ppm.

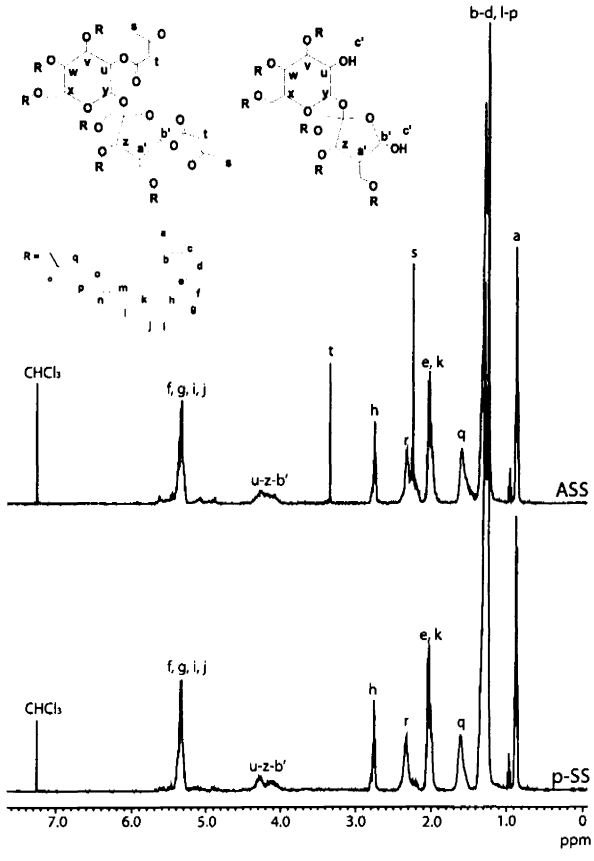

Figure 2.5. ^{1}H-NMR spectra of partially esterified sucrose soyate (p-SS) and acetoacetylated sucrose soyate (ASS)

2.4.2. Synthesis of Acetoacetylated Sucrose and Their Enamine Derivatives

The dual-cure design of sucrose esters, intermolecularly consisting of acetoacetates and fatty acids, can be achieved by blending acetoacetylated sucrose (AS) with sucrose fatty ester resin, however, the acetoacetylated sucrose is not compatible with sucrose fatty ester resins and rapidly phase separates. The compatibility of AS with sucrose soyate can potentially be improved by the reaction of the acetoacetate group of AS with alkyl amines

to form the enamine substituted AS. The effects of enamine alkyl chain length and the degree of enamine substitution of AS on the compatibility are explored.

2.4.2.1.Acetoacetylated sucrose

Acetoacetylated sucrose (AS) is the sucrose ester consisting of acetoacetates as functional groups, and it was prepared from the reaction of sucrose with t-BAA via transesterification, as illustrated in Figure 2.6. In the overlaid FTIR spectra of sucrose and AS shown in Figure 2.7, the formation of AS is confirmed by the complete disappearance of the broad hydroxyl band at 3000-3600 cm^{-1} and the appearance of two carbonyl bands at 1735 cm^{-1} and 1780 cm^{-1}. In the ^{1}H-NMR spectrum of AS (Figure 2.8), the formation of AS is confirmed by the appearance of the peaks of methyl protons of acetoacetate at 2.1-2.3 ppm and methylene protons of acetoacetates at 3.4-3.7 ppm.

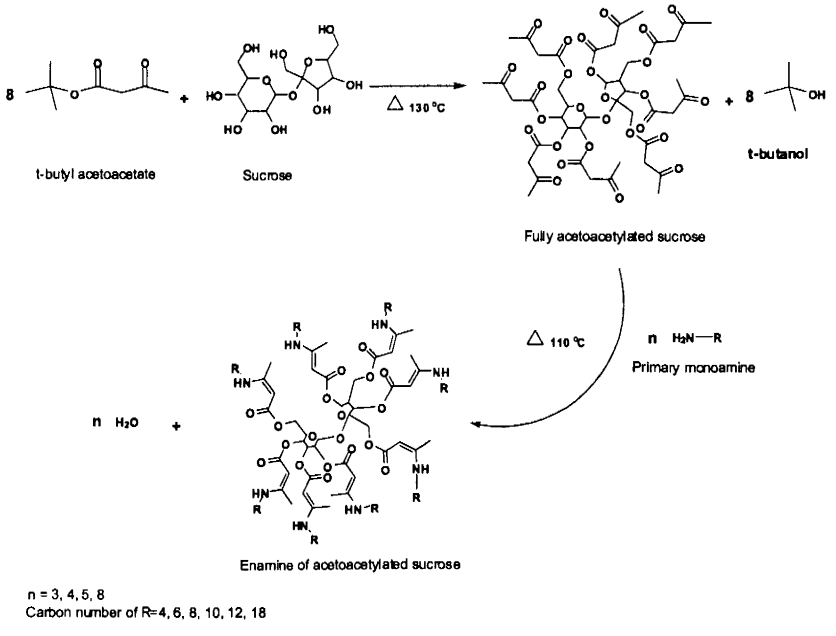

Figure 2.6. Synthesis of acetoacetylated sucrose (AS) and enamine substituted acetoacetylated sucrose (EAS)

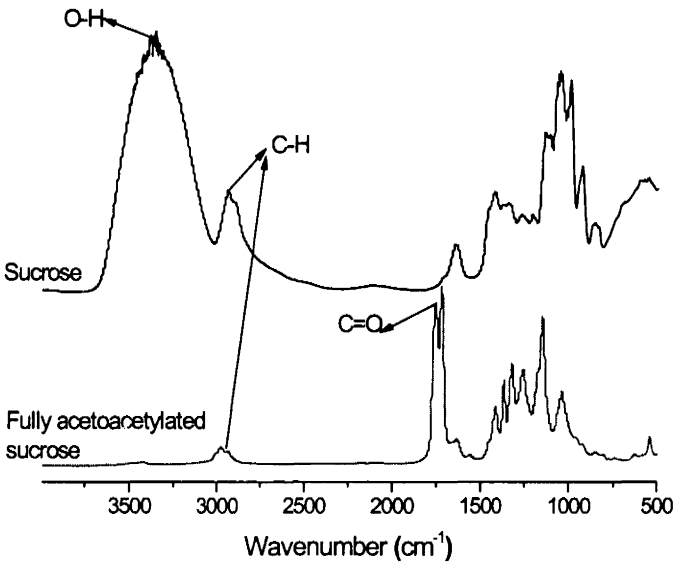

Figure 2.7. FT-IR spectra of sucrose and acetoacetylated sucrose (AS)

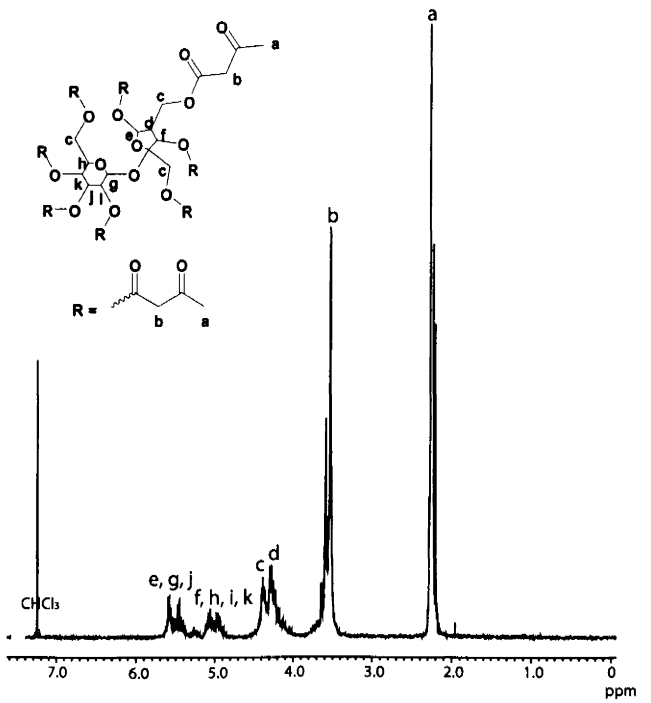

Figure 2.8. ^{1}H-NMR spectrum of acetoacetylated sucrose (AS)

2.4.2.2.Fully enamine alkyl substituted AS (f-EAS)

To explore the effect of enamine alkyl length on the compatibility with SS, a series of fully enamine alkyl substituted acetoacetylated sucrose (f-EAS) compounds were prepared. The reactions of acetoacetates with a series of primary monoamines were used to prepare f-EAS. Butylamine, hexylamine, octylamine, decylamine, dodecylamine and octadecylamine are the primary monoamines used in this study. The characteristics of the f-EAS compounds with different enamine alkyl lengths are summarized in Table 2.1.

Table 2.1. Acetoacetylated sucrose (AS) and fully enamine alkyl substituted acetoacetylated sucrose (f-EAS)

f-EAS samples	GPC			DSC		Appearance at ambient condition
	Mn	*Mw*	*PDI*	T_g (°C)	T_m (°C)	
AS	854	1,036	1.21	-31	-	Viscous liquid
Butylamine-EAS	1,438	1,777	1.24	-33	-	Viscous liquid
Hexylamine-EAS	1,668	2,012	1.21	-40	-	Viscous liquid
Octylamine-EAS	2,477	2,723	1.10	-41	-	Viscous liquid
Decylamine-EAS	2,943	3,215	1.09	-38	-	Viscous liquid
Dodecylamine-EAS	3,259	3,482	1.07	-49	-	Viscous liquid
Octadecylamine-EAS	4,562	4,933	1.08	-	46	Crystalline solid

Different lengths of enamine alkyl chains result in different hydrodynamic volumes of f-EAS in THF solution, and lead to different retention times in GPC (Figure 2.9). The compounds have a narrow molecular weight distribution. An example ^{1}H-NMR of the dodecylamine enamine substituted acetoacetylated sucrose (D-EAS) is shown in Figure 2.10. The generation of enamine alkyl is confirmed by the secondary amine (-NH-) proton peaks at 8.44 ppm, vinyl proton peak at 3.51 ppm, and methyl protons (attached to vinyl) at

2.22 ppm. In Figure 2.11, it can be seen that the glass transition temperatures of f-EAS decrease with the increase of enamine alkyl chain length, from butylamine-EAS to dodecylamine-EAS. The longer alkyl chain provides a larger volume between f-EAS molecules, which gives more degrees of freedom available to molecule segmental mobility. However, once the alkyl chain is long enough to be conducive to packing into a crystalline state, it can crystallize. Thus, octadecylamine-EAS (O-EAS) is a brittle crystalline material at room temperature, and it shows a large melting peak without a detectable glass transition (Figure 2.12). From butylamine-EAS to dodecylamine-EAS, f-EAS are completely amorphous with one T_g. Probably, f-EAS synthesized using an alkyl amine having a chain length between dodecylamine and octadecylamine is semicrystalline, which is able to present both T_g and T_m.

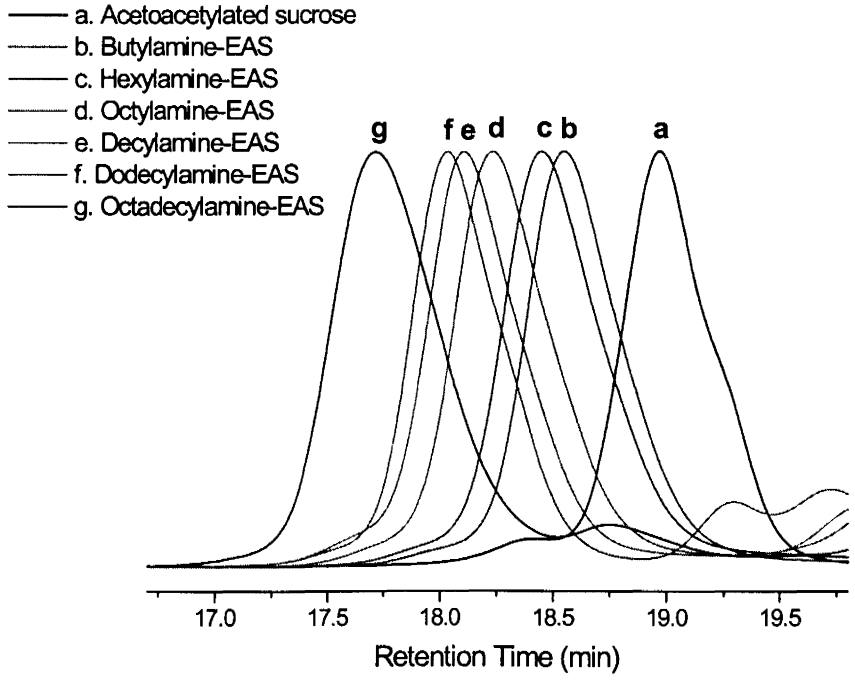

Figure 2.9. GPC plots of fully enamine alkyl substituted acetoacetylated sucrose (f-EAS) and acetoacetylated sucrose (AS)

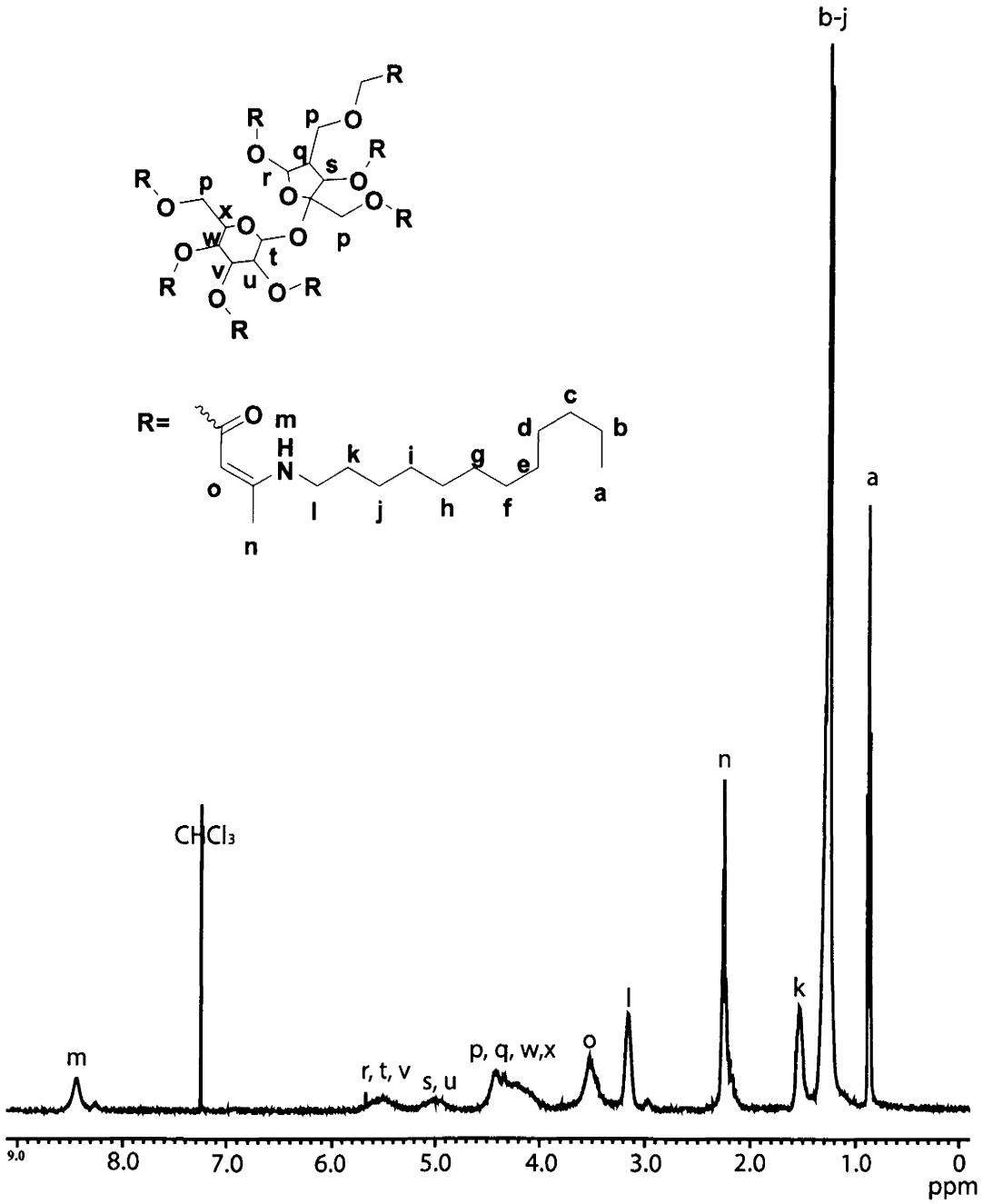

Figure 2.10. ^{1}H-NMR spectrum of dodecylamine enamine substituted acetoacetylated sucrose (D-EAS)

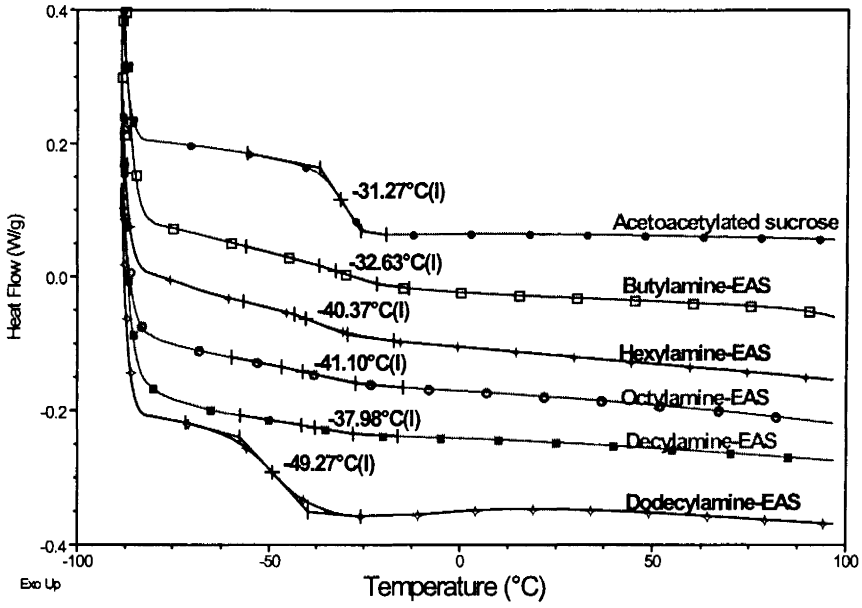

Figure 2.11. DSC curves indicating glass transition of fully enamine alkyl substituted acetoacetylated sucrose (f-EAS) prepared using different length of primary monoamines

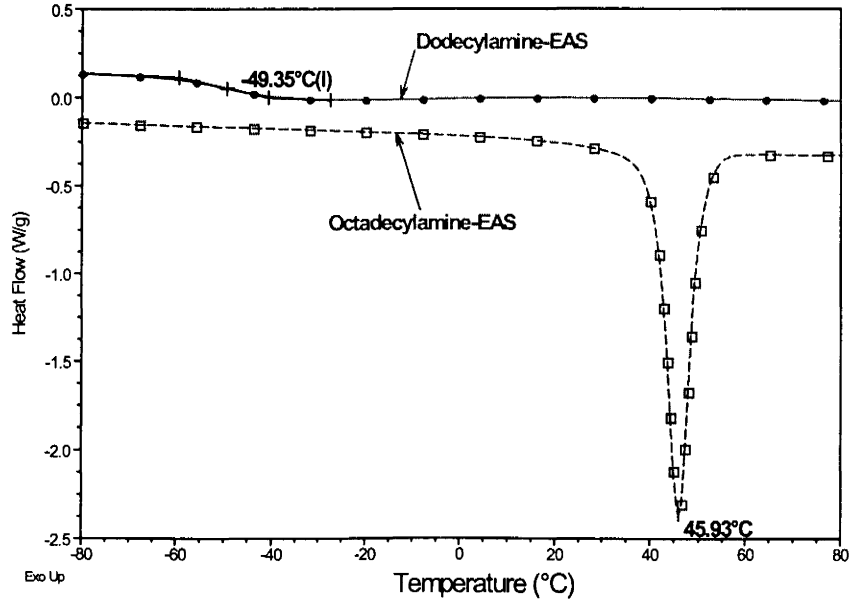

Figure 2.12. DSC curves of dodecylamine-EAS (D-EAS) and octadecylamine-EAS (O-EAS)

The effect of enamine alkyl length on the compatibility of f-EAS with sucrose soyate is shown in Table 2.2. Decylamine-EAS is the boundary, which is miscible with SS in THF, MEK and xylene solutions, but not in acetone or solvent-free. Dodecylamine-EAS is the only f-EAS compatible with SS in all the listed conditions at room temperature. Octadecylamine-EAS is compatible with SS in the melt state (m. p. = 46°C), but phase separation occurs upon cooling because of its crystalline nature at ambient conditions.

Table 2.2. Compatibilities between fully enamine alkyl substituted acetoacetylated sucrose (f-EAS) and sucrose soyate in solution/solvent-free (Y = compatible; N = incompatible)

f-EAS samples	Compatibility results				
	Solvent-free	Acetone	THF	MEK	xylene
Butylamine-EAS	N	N	N	N	N
Hexylamine-EAS	N	N	N	N	N
Octylamine-EAS	N	N	N	N	N
Decylamine-EAS	N	N	Y	Y	Y
Dodecylamine-EAS	Y	Y	Y	Y	Y
Octadecylamine-EAS (melted)	Y	Y	Y	Y	Y

2.4.3. Partially Enamine Alkyl Substituted AS (p-EAS)

Based on the above studies, dodecylamine-EAS (D-EAS) is a suitable composition for further exploration of the effect of the degree of enamine substitution on the compatibility of p-EAS with SS. As an additional composition, octadecylamine/dodecylamine-EAS (O/D-EAS, octadecylamine: dodecylamine = 1:2) was also prepared. The characteristics of EAS with different degrees of enamine substitution are shown in Table 2.3. The number in the compound name represents the degree of

enamine substitution based on the average number of acetoacetate groups reacted with amine. There are two glass transition temperatures in the p-EAS samples, and they are listed from lower to higher as T_{g1} and T_{g2}.

Table 2.3. Acetoacetylated sucrose (AS) and enamine alkyl substituted acetoacetylated sucrose with different degrees of enamine substitution

p-EAS samples	GPC			DSC		Appearance at ambient condition
	Mn	*Mw*	*PDI*	T_{g1} (°C)	T_{g2} (°C)	
AS	854	1,036	1.21	-31	-	Viscous liquid
D-EAS-3	1,902	2,244	1.18	-66	-9	Viscous liquid
O/D-EAS-3	2,387	2,663	1.12	-59	-15	Viscous liquid
D-EAS--4	2,572	2,886	1.16	-56	-17	Viscous liquid
D-EAS--5	2,615	3,031	1.12	-56	-14	Viscous liquid
D-EAS--8	3,259	3,482	1.07	-	46	Viscous liquid

Different degrees of enamine substitution resulted in different hydrodynamic volumes of p-EAS in THF solution, and different retention times in GPC (Figure 2.13). Since the FTIR samples were carefully prepared to obtain the same film thickness, FTIR absorption spectra of p-EAS samples are suitable for both qualitative and quantitative analysis. In Figure 2.14, higher enamine substitution results in a higher intensity of the secondary amine N-H band at 3500 cm^{-1}, the C-H band (both sp^3 and sp^2 hybrid) at 2900-3100 cm^{-1}, the enamine carbonyl C=O band at 1658 cm^{-1}, and the enamine C=C band at 1610 cm^{-1}. In Figure 2.15, the DSC thermograms of p-EAS show glass transitions without the presence of crystalline melting transitions; they are amorphous. Interestingly, each p-EAS possesses two glass transitions. Presumably, because each compound contains two functional groups—acetoacetates and enamine alkyls—two glassy phases are formed.

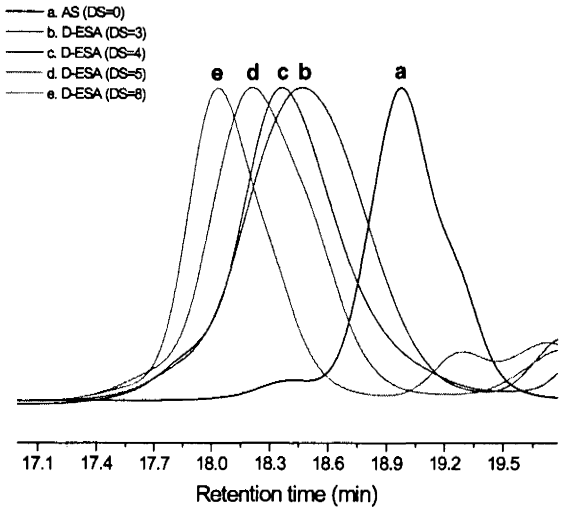

Figure 2.13. GPC plots of acetoacetylated sucrose (AS) and dodecylamine enamine substituted acetoacetylated sucrose (D-EAS) with different degrees of enamine substitution

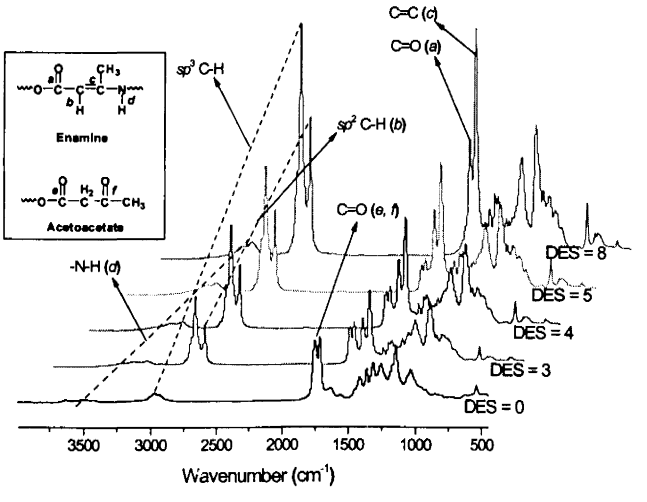

Figure 2.14. FT-IR spectra of acetoacetylated sucrose (AS) and dodecylamine enamine substituted acetoacetylated sucrose (D-EAS) with different degrees of enamine substitution

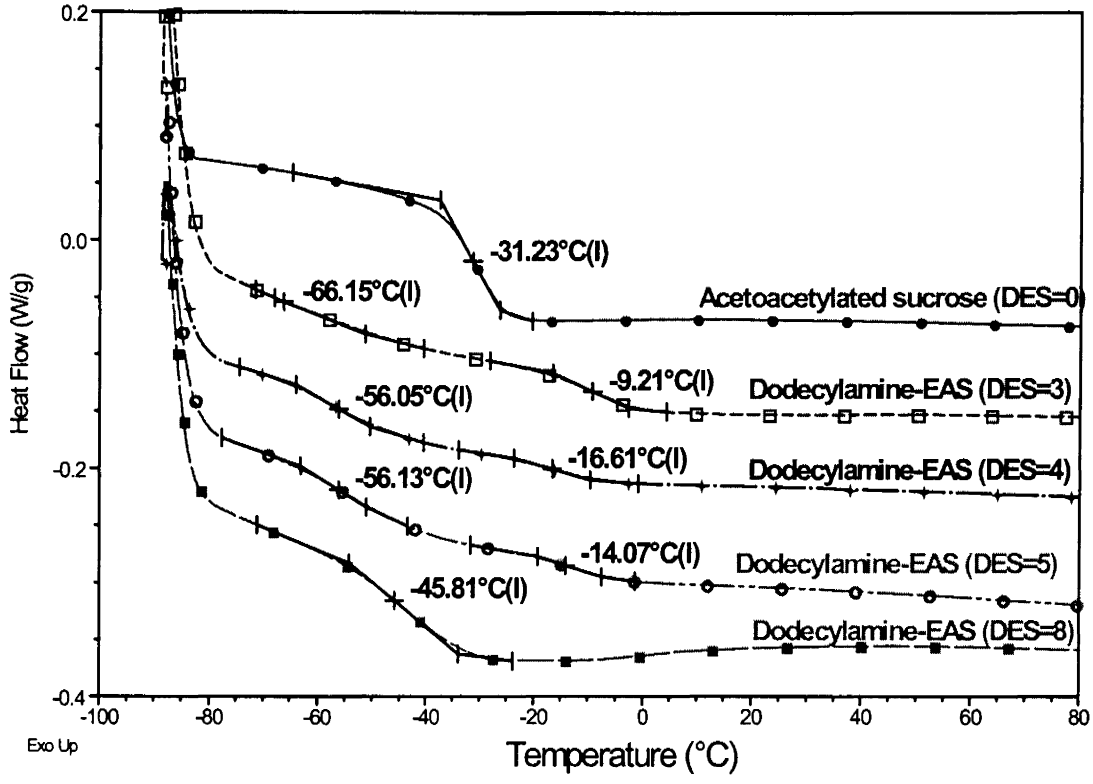

Figure 2.15. DSC curves indicating the glass transitions of acetoacetylated sucrose (AS) and dodecylamine enamine substituted acetoacetylated sucrose (D-EAS) with different degrees of enamine substitution

The effect of the degree of enamine substitution on the compatibility of p-EAS with sucrose soyate is shown in Table 2.4. D-EAS becomes miscible with SS when its degree of substitution is four. Interestingly, O/D-EAS-3 (octadecylamine: dodecylamine = 1:2) is miscible with SS and ASS when its degree of substitution is three. The miscible bicomponent made of O/D-EAS-3 and ASS consists of seven acetoacetates and six soyate fatty acid groups for dual-curing, and three enamine alkyls to provide compatibility.

Table 2.4. The effect of degree of enamine substitution on the compatibility between SS and f-EAS

Entry (mixture)	Compatibility rating	Compound 1	Functionality		Compound 2	Functionality	
			FA	*AA*		*EA*	*AA*
1	N	SS	8	0	AS	0	8
2	N	SS	8	0	D-EAS-3	3	5
3	Y	SS	8	0	D-EAS-4	4	4
4	Y	SS	8	0	D-EAS-5	5	3
5	Y	SS	8	0	D-EAS-8	8	0
6	Y	SS	8	0	O/D-EAS-3	3	5
7	Y	ASS	6	2	O/D-EAS-3	3	5

FA: fatty acid; AA: acetoacetate; EA: enamine; Y = compatible; N = incompatible

2.4.4. Coating Properties

2.4.4.1.Autoxidation curing of SS based materials

Fully esterified sucrose soyate (f-SS), partially esterified sucrose soyate (p-SS) and acetoacetylated sucrose soyate (ASS) are all sucrose soyate based materials. Their unsaturated soybean fatty acids are capable of undergoing autoxidation curing. In an autoxidation formulation, a combination of cobalt, zinc and zirconium salts were used as driers (0.04 wt%, 0.03 wt% and 0.1 wt%, based on the weight of sucrose soyate material). Additionally, since ASS has both unsaturated fatty acid and acetoacetate functional groups, it was dual-cured by both enamine formation reactions and autoxidation in the presence of PACM diamine crosslinker (acetoacetate:amine = 1:1) with the same drier content.

The coating properties are shown in Table 2.5. It is observed that autoxidation cured SS based coatings are soft, flexible, and have low solvent resistance. However, the dual-cured ASS coating present has much higher hardness and solvent resistance.

Table 2.5. Properties of SS based coatings cured via autoxidation

Sample names	Thickness (μm)	König pendulum hardness (s)	Pencil hardness (gouge)	Cross-hatch adhesion	MEK double rub resistance	Reverse impact (in-lb)	Mandrel bend (elongation -at-break)
f-SS	58 ± 9	14	<EE	4B	32	>172	>28%
p-SS	61 ± 7	13	<EE	4B	16	>172	>28%
ASS	56 ± 6	17	EE	4B	28	>172	>28%
ASS[1]	65 ± 6	37	6B	2B	132	120	>28%

[1]ASS was dual-cured by both enamine formation and autoxidation

2.4.4.2.Enamine formation curing of EAS based materials

Acetoacetylated sucrose (AS), dodecylamine enamine substituted acetoacetylated sucrose (D-EAS) with the degree of enamine substitution 4 and 5, and octadecylamine/dodecylamine enamine substituted acetoacetylated sucrose (O/D-EAS) with the degree of enamine substitution 3 are all acetoacetate functional materials and thus capable of undergoing enamine formation curing using PACM as a difunctional crosslinker. The coatings properties are shown in Table 2.6. It is observed that PACM-cured EAS based coatings are all hard and brittle. Their solvent resistances are reduced with the increase of enamine substitution, due to the decrease of crosslink density.

Table 2.6. Properties of EAS based coatings cured via enamine formation

Sample names	Thickness (μm)	König pendulum hardness (s)	Pencil hardness (gouge)	Cross-hatch adhesion	MEK double rub resistance	Reverse impact (in-lb)	Mandrel bend (elongation -at-break)
AS	56 ± 3	188	3H	1B	>400	<4	<2.5%
D-EAS-5[1]	48 ± 5	100	5B	3B	9	10	>28%
D-EAS-4	51 ± 5	138	4B	3B	55	8	>28%
D-EAS-3	50 ± 6	163	HB	2B	106	4	4%
O/D-EAS-3	47 ± 6	167	HB	2B	109	4	4%

[1]D-EAS-5 represents D-EAS with the degree of enamine substitution (DES) = 5

2.4.4.3.Dual-curing of SS/EAS blends via autoxidation and enamine formation

The autoxidation cured coatings tend to be soft, but flexible, while the amine cured coatings are hard and brittle, so combining the two systems could lead to coatings having an optimum set of peroperties. The bicomponent system comprised of ASS and O/D-EAS-3 was chosen for the exploration of the dual curing system. This blend was capable of maintaining one-phase state throughout the two different curing processes. PACM was used as the diamine crosslinker. As before, a mixture of cobalt, zinc and zirconium salts was used as the metal salt driers.

Since the speed of EF curing using PACM is much faster than autoxidation curing, the dual-cure process is separated into two steps (Figure 2.16): Step I is EF curing, and Step II is autoxidation curing. In Step I, ASS and PACM serve as difunctional reactants, and O/D-EAS-3 serves as a pentafunctional reactant and thus a high degree of crosslinking can be achieved. In the autoxidation curing phase (Step II), only ASS contains the unsaturated fatty acids, which can be crosslinked via autoxidation and accelerated by metal salt driers.

The properties of a series of dual-cured coating made from different radios of ASS and O/D-EAS-3 are shown in Table 2.7. Compared with the properties of autoxidation cured SS based coatings (Table 2.5) and EF cured EAS based coatings (Table 2.6), the dual-cured coatings show properties balanced between the flexibility of SS and rigidity of EAS. The composition of the two components (weight ratio) has an influence on the coating properties. As the content of ASS increases, the coating is softer and more flexible; conversely, more O/D-EAS-3 results in harder and less flexible films.

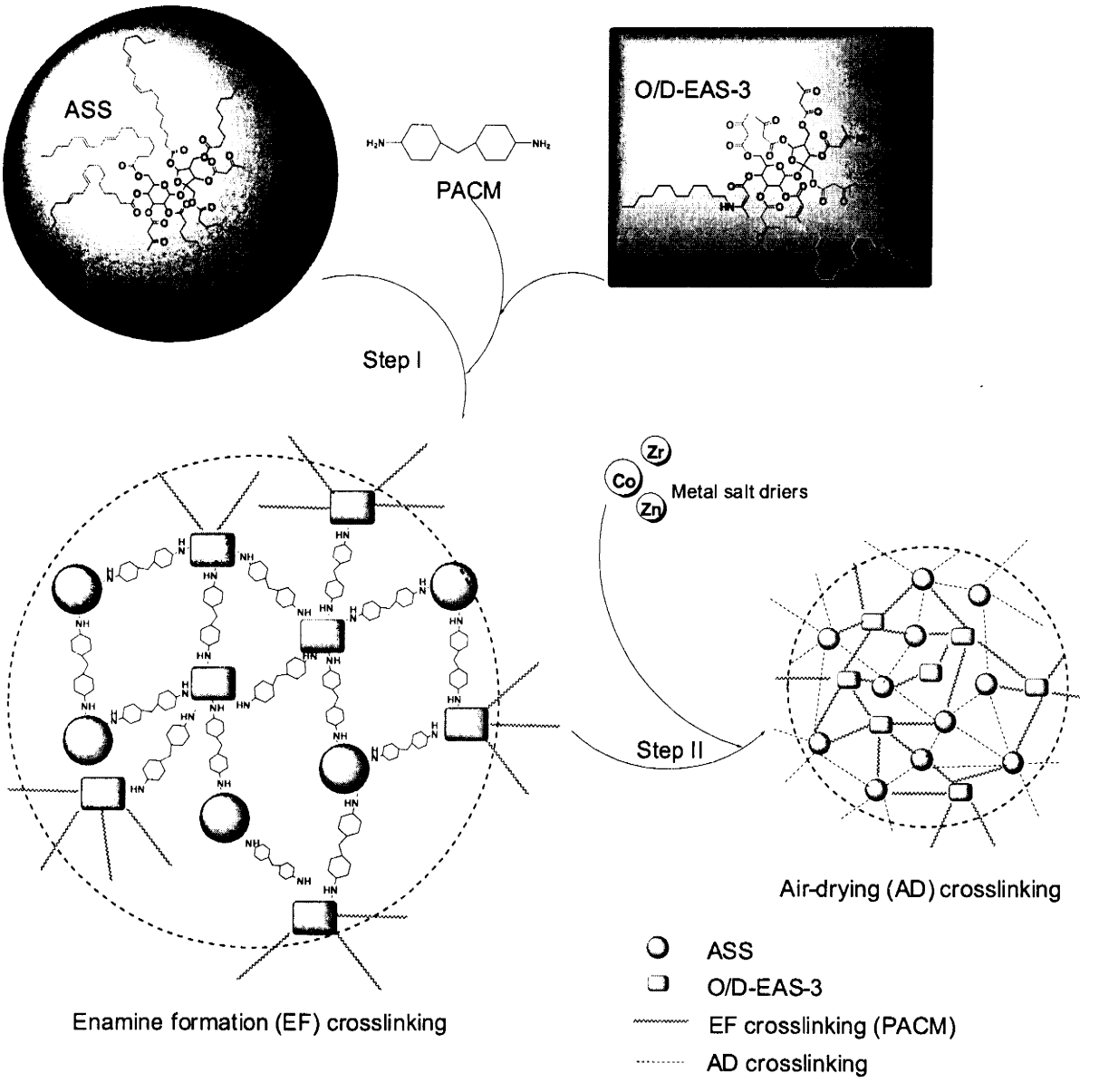

Figure 2.16. Schematic of the dual-cure process of blend of ASS and O/D-EAS-3 in the presence of diamine crosslinker (PACM) and metal salt driers

Table 2.7. Properties of dual-cured coatings

Weight ratio of ASS to O/D-EAS-3	Thickness (μm)	König pendulum hardness (s)	Pencil hardness (gouge)	Cross-hatch adhesion	MEK double rub resistance	Reverse impact (in-lb)	Mandrel bend (elongation -at-break)
3/7	50 ± 4	136	B	2B	121	12	4.5%
5/5	52 ± 6	53	2B	4B	68	20	>28%
7/3	58 ± 8	35	5B	4B	41	40	>28%

2.4.5. Drying Time Studies

The drying times were studied using a drying time recorder for the three systems: autoxidation cured SS based coatings, EF cured EAS based coatings, and dual-cured coatings. The results are shown as the bar graphs in Figure 2.17, in which the open time, dust free time, and tack-free time are defined as the three steps of drying.

In Figure 2.17a, ASS dries slower than f-SS via autoxidation curing. Prior research has indicated that acetoacetates accelerate the autoxidation process in the presence of unsaturated fatty acids and metal driers in conventional alkyd coatings. [20-23] However, this data shows that replacing fatty acid groups with acetoacetate groups slows down the autoxidative curing. Thus, it appears that acetoacetylation on sucrose soyate is not as meaningful as acetoacetylation on conventional alkyd resins, for the purpose of accelerating autoxidation curing.

In Figure 2.17b, the PACM-cured EAS coatings reach the dust free state within one hour. It proves that curing with PACM is much faster than autoxidation curing of fatty acids with driers. The high functionality of acetoacetate groups results in fast curing. In Figure 2.17c, the dual-cured coatings accomplish drying faster than autoxidation curing, but slower than EF curing. As the content of ASS increases, the drying times become longer; conversely, more O/D-EAS-3 results in a shorter drying time.

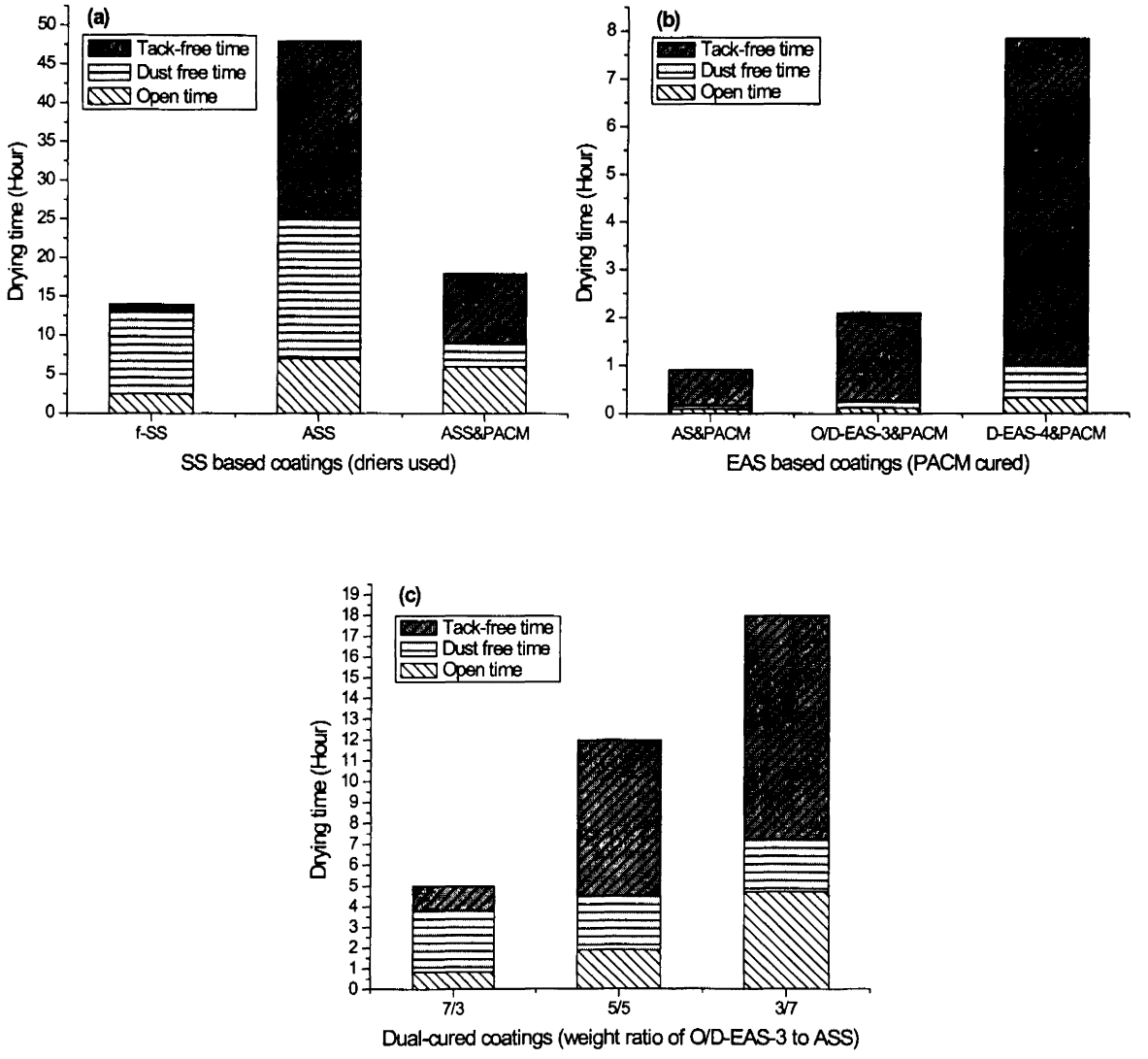

Figure 2.17. Drying times of coatings. a. SS based coatings cured via autoxidation; b. EAS based coatings; c. Dual-cure blends of O/D-EAS-3 and ASS

2.5. Conclusions

In this study, enamine formation reaction between acetoacetate and amine was explored along with autoxidation of fatty acids to formulate dual-cure coating resins. Autoxidation-cured SS based coatings exhibit good flexibility, but low solvent resistance

and hardness. Diamine-cured EAS based coatings have good solvent resistance and hardness, but their rigidity and brittleness results in generally poor mechanical properties. The properties of the dual-cured coatings systems are well balanced between flexibility and rigidity, softness and hardness. In addition, the dual-cure coating systems renders a moderate and adjustable drying time for coating application at ambient conditions.

Acetoacetate chemistry combined with sucrose ester of fatty acids is a highly tunable platform which can be used to develop a wide variety of coatings systems having different properties. The potential of this novel system is worthy of being further explored, since enamine formation is only a part of the reaction versatility of acetoacetate functional compounds.

2.6. References

1. Dalton, L. K. *J. Appl. Chem.* **1963**, *13*, 277.
2. Elam, E. U.; Middleton, M. L. *U.S. Pat. No. 4,551,523*, **1985**.
3. Mafoti, R.; Keegan, R. E.; Schilling, S. L. *U.S. Pat. No. 5,407,596,* **1995**.
4. Rector, F. D.; Blount, W.W.; Leonard, D.R. *J. Coat. Technol.* **1989**, *61*, 31.
5. Witzeman, J. S.; Nottingham, W. D.; Rector, F. D. *J. Coat. Technol.* **1990**, *62*, 101.
6. Marsh, S. J. *Polymer Preprints (American Chemical Society, Division of Polymer Chemistry)* **2003**, *44*, 52.
7. Bors, D. A.; Lavoie, Alvin C.; Emmons, W. D. *U.S. Pat. No. 5,484,849*, **1996**.
8. Kuo, T.; Grosso, P. V.; Spilman, G. E.; Clark, M. D. *U.S. Pat. No. 6,794,049*, **2004**.
9. Kuo, T.; Grosso, P. V.; Spilman, G. E.; Clark, M. D. *U.S. Pat. No. 6,780,523*, **2004**.

10. Powell, J. E.; Honeycutt, A. H. *Composites & Polycon 2007 (American Composites Manufacturers Association)* **2007**, 1.

11. Klaasen, R.P.; van der Leeuw, R.P.C. *Prog. Org. Coat.* **2006**, *55*, 149.

CHAPTER 3. NOVEL BIOBASED EPOXY COMPOUNDS: EPOXIDIZED SUCROSE ESTERS OF FATTY ACIDS

3.1. Abstract

Novel biobased high functionality epoxy resins were synthesized by the epoxidation of sucrose ester resins of vegetable oil fatty acids (SEFA). A series of sucrose esters of fatty acids were epoxidized by peracetic acid generated *in situ* from hydrogen peroxide and acetic acid in the presence of an ion exchange resin catalyst to produce the epoxidized sucrose esters of fatty acids (ESEFA). The conversion of double bonds to epoxides was greater than 99%. The products were characterized by matrix-assisted laser desorption and ionization time-of-flight (MALDI-TOF) mass spectrometry, Fourier-transform infrared (FTIR) spectroscopy, and nuclear magnetic resonance (NMR) spectroscopy. The physical properties were characterized using bulk viscosity, intrinsic viscosity, and density measurements. The thermal properties were characterized by differential scanning calorimetry (DSC) and thermogravimetric analysis (TGA). Since sucrose esters consist of a sucrose core fully substituted with eight vegetable oil fatty acids, both SEFAs and ESEFAs possess well-defined compact macromolecular structures. As novel biobased epoxy compounds, ESEFAs possess high epoxy functionality (8–15 per molecule), high density, and a compact molecular structure. Thus, ESEFAs are very promising in a number of uses from the formation of biobased thermosets by crosslinking of the epoxy groups, to further derivatization by reaction of the epoxy groups.

3.2. Introduction

Epoxides are cyclic ethers also called oxiranes, in which the oxygen atom is contained in a three membered ring. Epoxidation is one of the most important and useful modifications using the double bonds of unsaturated fatty compounds, since epoxide is a reactive intermediate to readily generate new functional groups. Ring-opening of epoxide via nucleophilic addition leads to a large number of products, such as diol, alkoxy alcohol (ether alcohol), hydroxy ester (ester alcohol), amino alcohol, and others. Through epoxide opening of epoxidized soybean oil using alcohols, triglyceride polyols intended for application in polyurethanes have been successfully prepared by Petrovic and co-works.[1-3] Epoxide reaction with unsaturated acids has been widely utilized to synthesize oil-based free-radical UV-curable coating resins by reacting acrylic acids with epoxidized vegetable oils (EVOs).[4-6]

Generally, while there are four techniques that can be employed to produce epoxides from olefinic molecules, the *in situ* performic/peracetic acid (*HCOOOH or CH_3COOOH*) process appears to be the most widely applied method to epoxidize fatty compounds.[7] Figure 3.1 displays the reaction mechanism, which consists of a first step of peroxyacid formation and a second step of double bond epoxidation. Recently, the kinetics of epoxidation of vegetable oils and the extent of side reactions was studied using an acidic ion exchange resin as catalyst and revealed that the reactions were first order with respect to the amount of double bonds and that side reactions were highly suppressed; the conversion of double bonds to epoxides was also high.[8-9] The catalyst, Amberlite IR 120, is an acidic ion exchange resin, a copolymer based on styrene (98 wt%) crosslinked by

divinylbenzene (2 wt%). Its acidity is generated by sulfonic acid groups attached to the polymer skeleton.

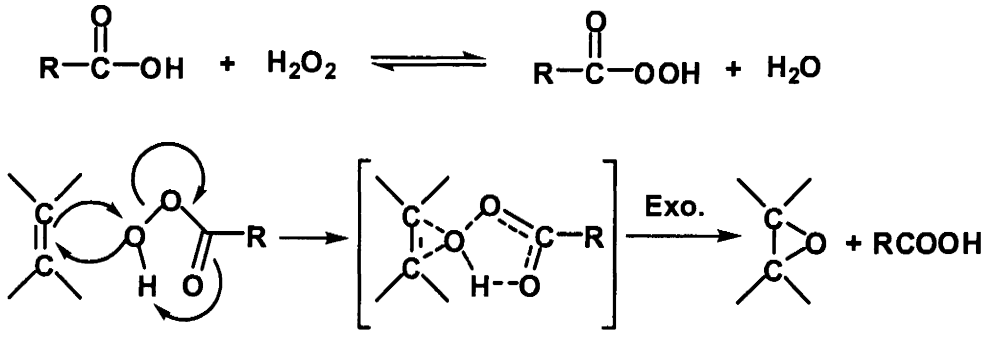

Figure 3.1. Reactions mechanism for *in situ* epoxidation with peroxyacid

Epoxides generated from the epoxidation of double bonds of unsaturated fatty acids are known as internal epoxides—both carbons of the heterocyclic ring are substituted with another carbon. The most commonly used epoxy resins are the bisphenol-A diglycidyl ether resins. The epoxy groups on these resins are of the type known as external epoxides—three of the four substituent groups on the heterocyclic ring are hydrogen atoms. Since internal epoxides are much less reactive than external epoxides in most epoxy curing reactions, the roles traditionally assigned to epoxidized oils are as stabilizers and plasticizers for halogen-containing polymers (i.e. poly(vinyl chloride)), and reactive toughening agents for rigid thermosetting plastics (e.g. phenolic resins).[10-13] It has also been shown that EVOs can be cured using cationic photopolymerization of epoxides to form coatings.[14-16]

In this study, four SEFOSE sucrose esters derived from different vegetable oils (Table 3.1) were epoxidized using peracetic acid generated *in situ* from hydrogen peroxide and acetic acid, in the presence of Amberlite IR 120H as catalyst. The structure-property relationships of sucrose esters before and after epoxidation were explored based on the

studies of their molecular structures, compositions, double bond/epoxide contents, viscosities, and densities.

Table 3.1. Descriptions of sucrose esters of fatty acids used in this study

Name		The type of plant oil	Average degree of substitution	Iodine value, IV_0	Viscosity (mPa·s)
Full	Abbreviated				
Sucrose linseedate	SL	Linseed	7.7	177	236
Sucrose safflowerate	SSF	Safflower	7.7	133	393
Sucrose soyate	SS	Soybean	7.7	117	425
Sucrose soyate B6	SSB6	Soybean	6.0	115	890

3.3. Experimental

3.3.1. Raw Materials

The sucrose esters of fatty acids were kindly provided by *Procter & Gamble* Chemicals (Cincinnati, OH). Acetic acid (ACS reagent, ≥99.7%), diethyl ether (ACS reagent, ≥99.0%), hydrogen peroxide (50 wt% solution in water), Amberlite IR-120H ion-exchange resin, sodium carbonate (ACS reagent), and anhydrous magnesium sulfate (reagent grade, ≥97%) were purchased from Sigma-Aldrich, Inc. (St. Louis, MO). All materials were used as received without further purification

3.3.2. Epoxidation of Sucrose Esters

Epoxidation reactions were carried out in a 500 mL four-neck flask, equipped with a mechanical stirrer, nitrogen inlet, thermocouple and addition funnel. Sucrose linseedate (170g, 0.07 mol) containing 1.17 mol double bonds, acetic acid (35.1 g, 0.585 mol), and Amberite 120H (34g, 20 wt% of sucrose linseedate) were charged to the reaction flask. The molar ratio of acetic acid: hydrogen peroxide (H_2O_2): double bond was controlled as

0.5:2:1. The mixture was rapidly stirred and nitrogen purged, and the temperature was raised to 55°C. Hydrogen peroxide (50 wt% aqueous solution, 160g, 2.35 mol) was added dropwise using an addition funnel at a rate such that the reaction temperature was controlled in the range of 55-65°C. After the completion of the hydrogen peroxide addition, the reaction was stirred at 60°C for 30 minutes. The product was transferred into a separatory funnel and allowed to cool to room temperature. After the aqueous layer was drained, the organic layer was diluted by 300 mL diethyl ether and washed with water five times. A saturated sodium carbonate/water solution was used as the last wash to completely remove the acetic acid. The organic layer was transferred into a beaker and dried with anhydrous magnesium sulfate overnight. The hydrated magnesium sulfate was removed by filtration, and diethyl ether was removed by rotavapping. Finally, a transparent viscous liquid was obtained as the epoxidized sucrose linseedate. The other SEFAs were epoxidized and purified using the same process. Recovered yields were all about 97 percent.

3.3.3. Characterization on Epoxy Resins

MALDI-TOF mass spectra were recorded on a Bruker Ultraflex II spectrometer equipped with a 1.85 m linear flight tube and a Smart beam laser. All mass spectra were obtained in positive ion and linear mode. Samples were dissolved in THF (1 mg/mL), and α-cyano-4-hydroxycinnamic acid (10 mg/mL in THF) was used as matrix, and trifluoroacetic acid (0.1 wt% in water) was used as the dopant. A mixture of 10 μL of the matrix solution, 2 μL of the dopant, and 2 μL of the polymer solution was prepared and a 2 μL sample was spotted on the target plate. All data were processed using Flex analysis and

PolyTools software. FTIR measurements were done by a Thermo Nicolet 8700 FTIR spectrometer. Samples were prepared in THF solution with the concentration of 4 mg/ml. Then, a 200 μL drop of the solution was deposited by micropipette on the center of the potassium bromide salt crystal and the drop was naturally spread out. After the evaporation of the THF, a thin layer of sample film was formed on the crystal. Spectra acquisitions were based on 32 scans with data spacing of 4.0 cm^{-1} in the range of 4000–500 cm^{-1}. NMR measurements were done at 23°C using a JEOL-ECA (400 MHz) NMR spectrometer with an autosampler accessory. All measurements were made using $CDCl_3$ as solvent. The data was processed using the Delta software package. The bulk viscosities of samples were measured using a Brookfield Viscometer (DV-II+ Pro) at 21°C. Intrinsic viscosity [η] of the materials was measured in THF with a Cannon-Fenske viscometer (size 50) at 25°C. The concentration of solution was 3.7-9.0 g/100 mL, and the relative viscosity η_r was controlled in the good range of 1.1-1.6. The extrapolations of reduced viscosity and inherent viscosity were averaged to yield the intrinsic viscosity for each sample. The densities of samples were measured using a BYK-Gardner Weight Per Gallon Cup at 25°C, referring to ASTM D 1475. The Midget Cup having a capacity of 8.32 grams of water at 25°C was used. The net weight of the fluid sample in grams equals the sample's density in pounds per U.S. gallon, which is converted into grams/mL. A Q1000 DSC from TA Instruments (New Castle, DE) with an autosampler was used for glass transition temperature (T_g) determination. Samples were subjected to a heat–cool–heat cycle from -90 to +100°C by ramping at 10 °C/min for both heating and cooling cycles. The second heating cycle was used to characterize the samples. A Q500 TGA from TA Instruments was used to study the thermal degradation behavior. Liquid samples were placed in the

sample pan and heated from 25 to 1000°C under N_2 at a heating rate of 20 °C min^{-1}. The measurements were conducted using 10–20 mg samples, and the weights were recorded as a function of temperature.

Epoxide equivalent weight (EEW, g/eq.) of the epoxy products was determined by epoxy titration according to ASTM D 1652. A solution of 0.1N HBr in glacial acetic acid was used as titrant, and 1 wt% crystal violet in acetic acid was used as the indicator solution. EEW value was calculated using the following equation (1), where W is the sample mass in gram, N is the normality of HBr solution, and V is volume of HBr solution used for titration in mL.

$$EEW = \frac{1000 \times W}{N \times V} \qquad (1)$$

Iodine values were determined according to ASTM D 5768-02. For sucrose esters, 0.15-0.20 g of sample was dissolved in 20 ml cylcohexane and then mixed with 25 ml Wij's solution. For epoxidized sucrose esters, 10-12 g of sample was dissolved in 20 ml cylcohexane and then mixed with 25 ml Wij's solution. After one minute of swirling, the mixture was then left in the dark for one hour. Next, 20 ml of 10% potassium iodide (KI) solution and 100 ml of deionized water was added. The solution was then titrated against 0.1 N sodium thiosulfate solution. A blank titration was used for each sample. Iodine value was calculated using the following equation (2), where V is $Na_2S_2O_3$ solution required for titration of the specimen in ml, B is $Na_2S_2O_3$ solution required for titration of the blank in ml, N is the normality of $Na_2S_2O_3$ solution, and S is the sample mass in gram.

$$IV = \frac{[(B-V) \times N \times 12.69]}{S} \qquad (2)$$

3.4. Results and Discussion

3.4.1. Epoxidation

The SEFOSE sucrose esters used in this study are initially amber liquids, and sucrose linseedate and sucrose soyate B6 are darker brownish-yellow. The abbreviated name of the epoxidized sucrose ester is defined by adding an E in front of the abbreviated name of the corresponding sucrose ester. In this study, four epoxidized sucrose esters have been synthesized: epoxidized sucrose linseedate (ESL), epoxidized sucrose safflowerate (ESSF), epoxidized sucrose soyate (ESS), and epoxidized sucrose soyate B6 (ESSB6). Due to the epoxidization of double bonds and the bleaching action of the peroxide, the epoxidized sucrose esters are all colorless. It is commonly observed that epoxidized vegetable oils tend to become hazy on standing due to crystallization during storage. However, the epoxidized sucrose esters remain transparent during storage with no haze formation observed after several months.

The conversion of double bonds, epoxide equivalent weights, and epoxide functionalities for the ESE resins synthesized are shown in Table 3.2. The iodine value (IV) can be used to determine the conversion of double bonds to epoxides using equation (3), where IV_0 is the iodine value of the starting sucrose ester, and IV_f is the iodine value of the epoxy product. The conversion of double bonds to epoxy groups for all resins was greater than 99 percent.

$$\%\ Conversion = 100 \times \frac{IV_0 - IV_f}{IV_0} \qquad (3)$$

The epoxide functionality (EF) of the epoxy products can be estimated using the epoxide equivalent weight (EEW) and MALDI-TOF molecular weight values using equation (4), where W_i is the average MW of epoxidized sucrose ester with the degree of substitution *i*. For fully substituted epoxidized sucrose esters, *i* equals 8. For epoxidized sucrose soyate B6, *i* equals 6.

$$EF = \frac{W_i}{EEW} \qquad (4)$$

The epoxide functionality is higher for those sucrose ester resins having higher amounts of double bonds, as would be expected. It is lowest for the partially substituted sucrose soyate resin, SSB6, since only six of the eight available hydroxyls on sucrose are substituted with the unsaturated soya fatty acid. The epoxide functionality is quite high for these resins; much higher than can be achieved through epoxidization of triglyceride oils such as soybean oil, where the epoxy functionality would be around 4.4.

Table 3.2. The conversions of epoxidation and epoxide functionalities of epoxidized sucrose esters of fatty acids (ESEFAs)

Epoxy product	IV_f	% Conversion	W_i (g/mol)	EEW (g/eq.)	Epoxide functionality
ESL	0.16	99.9	2,701	180	15.0
ESSF	0.32	99.8	2,651	228	11.6
ESS	0.44	99.6	2,623	248	10.6
ESSB6	0.73	99.4	2,048	256	8.0

3.4.2. Functional Groups and Molecular Structure

3.4.2.1.FTIR results

Epoxidation of fatty acids transforms the double bonds into epoxides. Figure 3.2 (a) displays the FTIR spectra of SL and ESL. The FTIR spectrum of SL shows the sp^2 C-H (double bond) adsorption band at 3010 cm^{-1}, which disappears in the FTIR spectrum of SL. The FTIR spectrum of ESL also shows the small epoxide C-O-C characteristic adsorption band at 826 cm^{-1}. In Figure 3.2 (b), the overlaid FTIR spectra of SSB6 and ESSB6 show the same observations, except that both spectra have a medium hydroxyl adsorption band at 3200-3730 cm^{-1}, because SSB6 is a partially esterified sucrose ester. All spectra also show a strong ester carbonyl band at1749 cm^{-1}, indicating that the ester groups are intact after epoxidation.

3.4.2.2.^{1}H-NMR results

Figure 3.3 displays the ^{1}H-NMR spectra of SSF and ESSF. The spectrum of SSF shows the characteristic peaks of protons on double bonds (–C**H**=C**H**-) at 5.21-5.50 ppm, the peaks of protons on the carbons between double bonds (-CH=CH-C**H$_2$**-CH=CH-) at 2.72-2.83 ppm, and the peaks of protons on the carbons next to double bonds (-C**H$_2$**-CH=C-) at 1.95-2.10 ppm. In the spectrum of ESSF, these proton peaks all disappear, but the characteristic peaks of protons on epoxides (-C**H**-C**H**O-) at 2.83-3.22 ppm, and the peaks of protons on the carbons next to epoxides (-C**H**-CH-CHO-) at 1.35-1.63 ppm are observed.

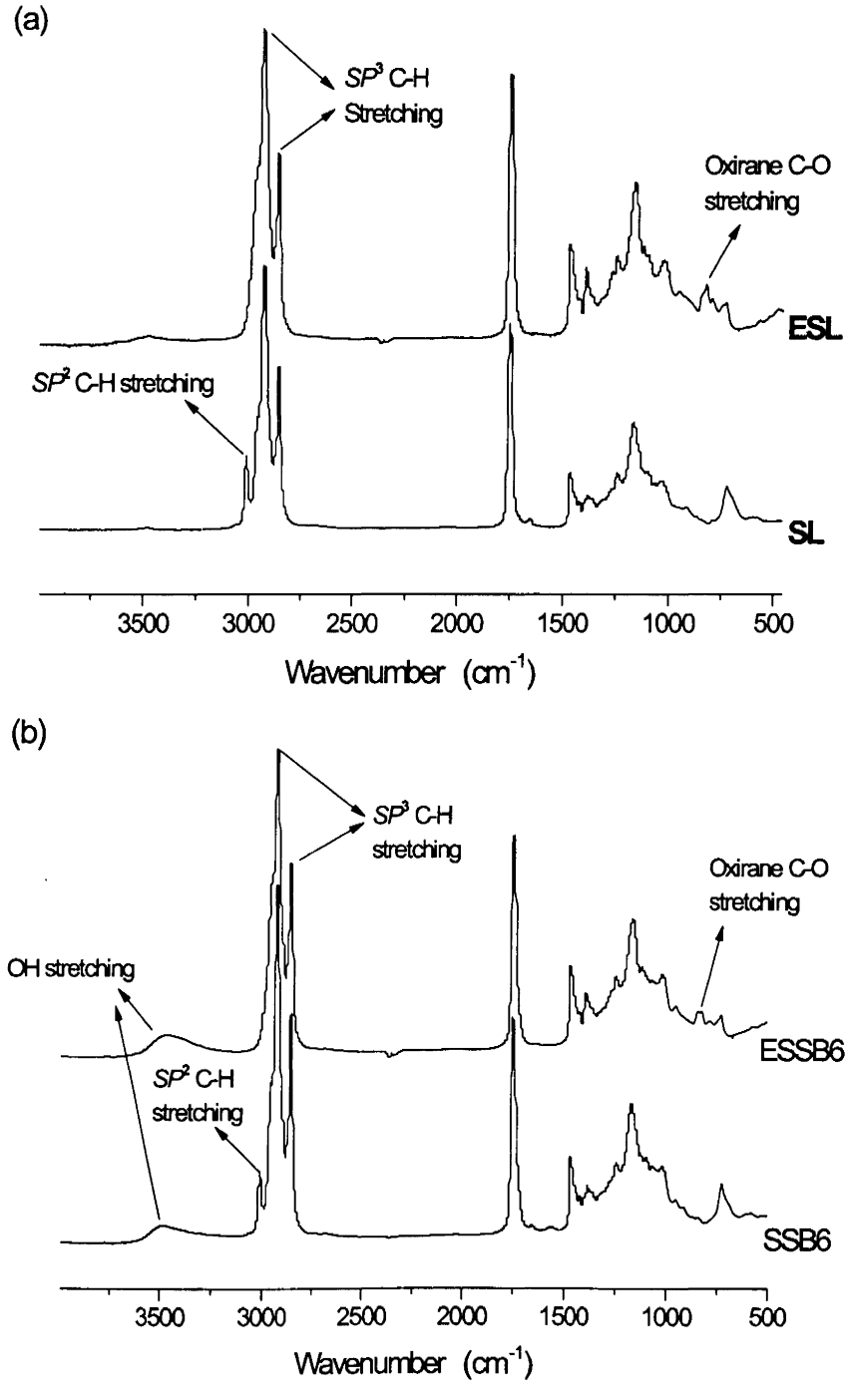

Figure 3.2. FT-IR spectra of (a) sucrose linseedate (SL) and epoxidized sucrose linseedate (ESL); (b) sucrose soyate B6 (SSB6) and epoxidized sucrose soyate B6 (ESSB6)

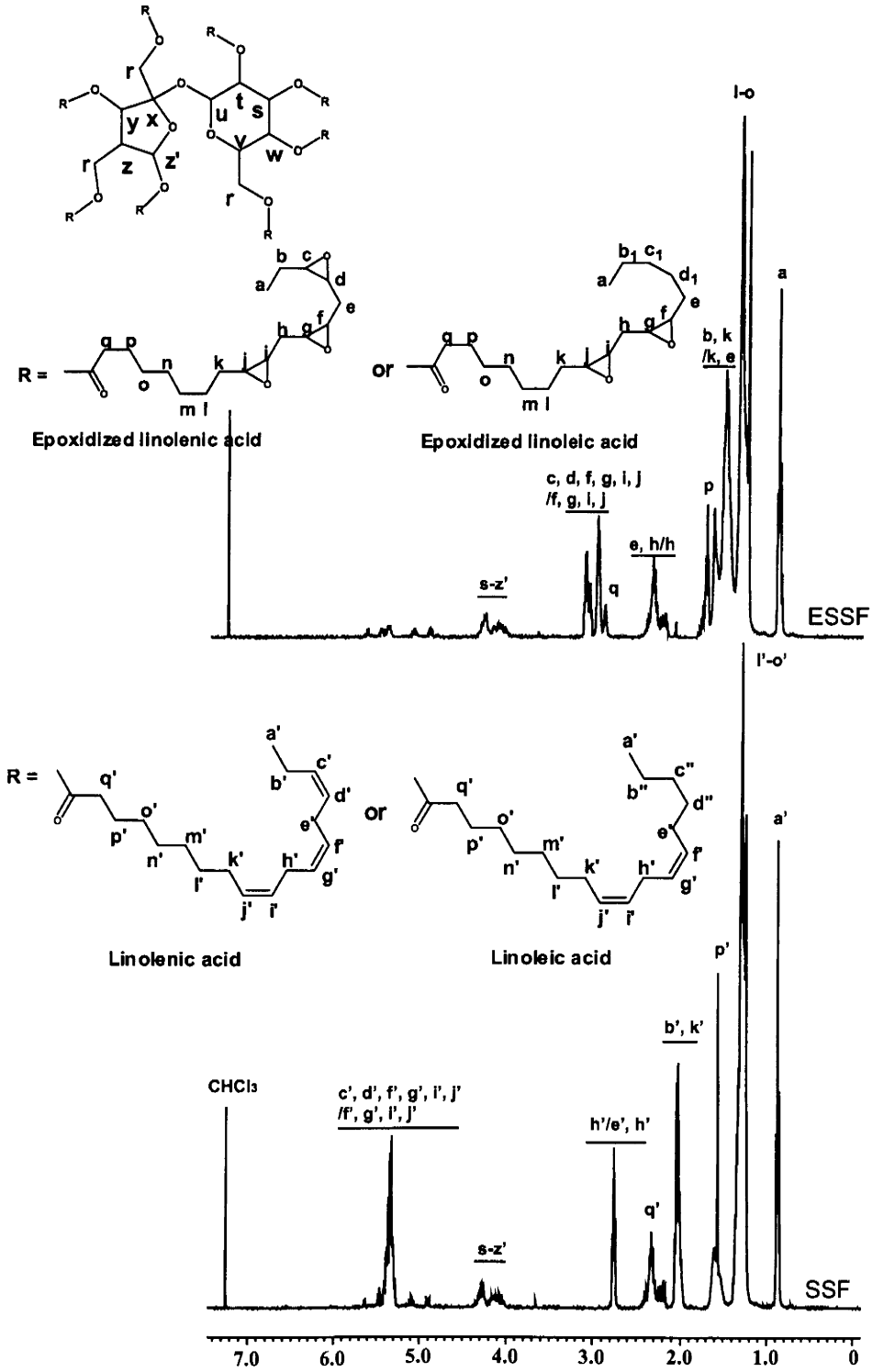

Figure 3.3. The ^{1}H-NMR spectra of sucrose safflowerate (SSF) and epoxidized sucrose safflowerate (ESSF)

3.4.2.3. ^{13}C-NMR results

Figure 3.4 displays the ^{13}C-NMR spectra of SSF and ESSF. The spectrum of SSF shows the characteristic peaks of ^{13}C carbons on the double bonds (-CH=CH-) at 128 and 131 ppm. The spectrum of ESSF shows the disappearance of double bonds and the appearance of ^{13}C carbons on epoxides (-CH-CHO-) at 54 and 56 ppm. The peaks at 172-173 ppm correspond to the ester C=O carbons in the ^{13}C-NMR spectra of both SSF and ESSF. The different chemical shifts of the ester C=O carbons are due to the different locations of the fatty acids on the sucrose molecule.

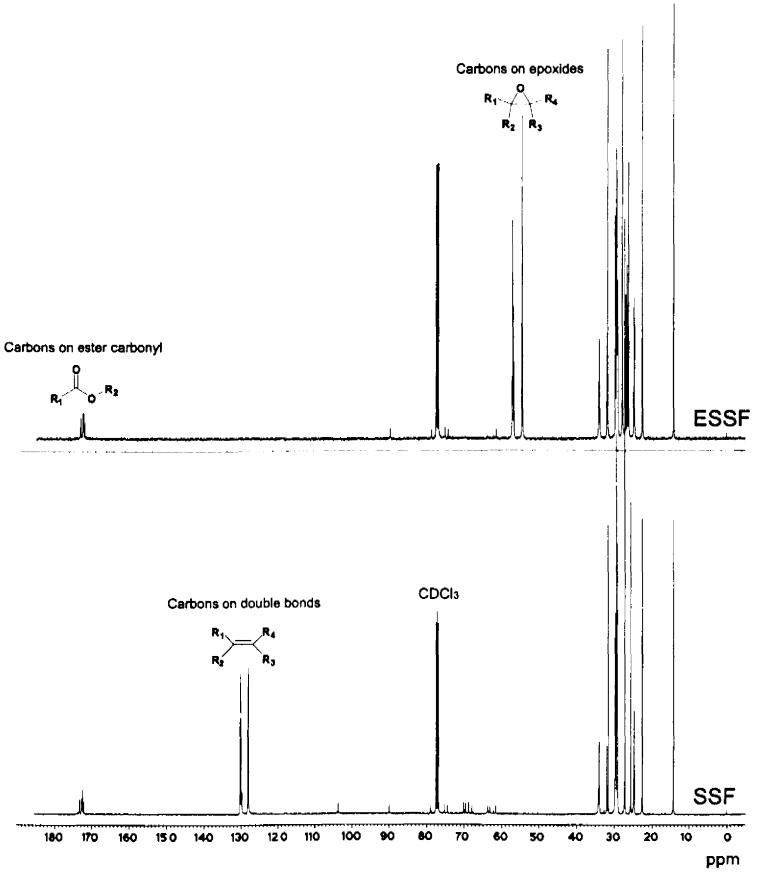

Figure 3.4. The ^{13}C-NMR spectra of sucrose safflowerate (SSF) and epoxidized sucrose safflowerate (ESSF)

3.4.3. Composition and Molecular Weight

Two key drivers of the differences between the sucrose esters are the degree of substitution and the type (composition) of fatty acids. This study involves sucrose esters with an average degree of substitution 7.7 (i.e. SL, SSF, and SS) and 6 (i.e. SSB6), and with fatty acids ranging from sixteen to eighteen carbon atoms with varying degrees of unsaturation.

Traditionally, analysis of triacylglycerols (TAGs) relied on methylation to form fatty acid methyl esters (FAME), which are then detected by GC mass spectrometry (GC-MS). This type of analysis does not allow detection of the individual TAGs, but it is useful to characterize the overall average composition of the fatty acids. Thus, this approach cannot be used to distinguish individual sucrose esters with the different degrees of substitution.

As one of the advanced "soft-ionization techniques", matrix-assisted laser desorption and ionization time-of-flight (MALDI-TOF) mass spectrometry has been widely used to give a highly detailed structural analysis on naturally occurring materials, such as proteins, carbohydrates, nucleic acids, lipids, phospholipids and others. As the simplest of lipids, TAGs can be studied by MALDI-TOF with very small amounts of fragmentation products, and the three fatty acids on the glycerol backbone are individually identified in mass spectra.[17] Jakab et al. could characterize the different TAGs by successfully combining MALDI-TOF mass spectrometry with statistical analysis.[18] Jürgen et al. analyzed the effects of oxidative modifications on the compositions of unsaturated vegetable oils by successfully combining MALDI-TOF with ^{1}H and ^{31}P NMR spectroscopy.[19] Asbury et al. reported the use of MALDI-TOF alone for the quantitative

and qualitative determination of TAG mixtures using TAG standards for calibration.[20] Ayorinde et al. developed a very simple and effective MALDI-TOF sample preparation method for TAGs, requiring no special cationization agent.[21]

In this study, MALDI-TOF MS analysis takes the challenges that the molecular weights of the sucrose esters are approximately three times that of TAGs and signal sensitivity decreases with increasing molecular weight. However, the challenges have been met by a successful selection of matrix and dopant leading to high quality MALDI-TOF MS spectra. Figure 3.5 displays the sodiated molecule peaks [M + Na^+] of ESEFA resins in positive ion MALDI-TOF mass spectra. The high resolution of the mass spectra is attributed to the fact that epoxides tend to form Na^+ adducts.[17] For the fully substituted epoxidized sucrose esters (i.e. ESL, ESSF, and ESS), three groups of peaks are observed in each mass spectrum. For the partially substituted ESSB6, five groups of peaks are observed in its mass spectrum. The m/z difference between each group of peaks is in the range of 274-284, which is approximately the mass of one fatty acid with an eighteen carbon length. Therefore, each group of peaks in the mass spectrum represents ESEFA molecules having the same degree of substitution. Thus, the presence of sucrose tetraester (DS=4), sucrose pentaester (DS=5), sucrose hexaester (DS=6), sucrose heptaester (DS=7), and sucrose octaester (DS=8) are confirmed based on the m/z values. Within each group, the m/z difference between two nearby peaks is around 14, which corresponds to the molecular weight of methylene (CH_2). It represents the mass difference between ESEFA molecules with different fatty acids at the same degree of substitution. The composition and molecular weight ranges for the epoxidized sucrose esters are shown in Table 3.3.

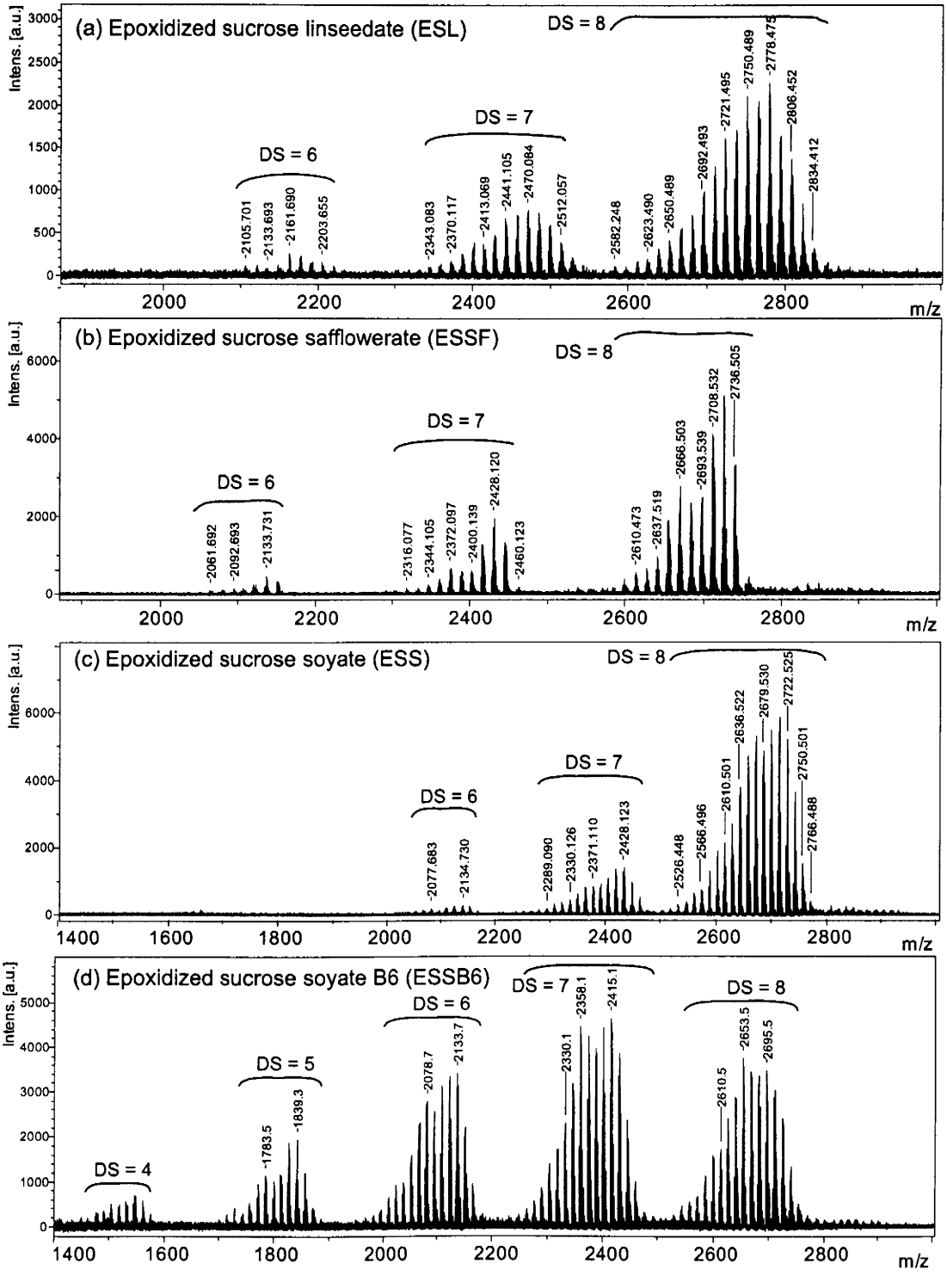

Figure 3.5. Positive ion MALDI-TOF mass spectra of epoxidized sucrose esters: (a) epoxidized sucrose linseedate (ESL); (b) epoxidized sucrose safflowerate (ESSF); (c) epoxidized sucrose soyate (ESS); (d) epoxidized sucrose soyate B6 (ESSB6)

Table 3.3. Compositions and molecular weights of epoxidized sucrose esters

Epoxy products	Composition and molecular weight (g/mol)				
	Tetraester	Pentaester	Hexaester	Heptaester	Octaester
ESL	-	-	2082-2195	2320-2503	2588-2814
ESSF	-	-	2038-2125	2293-2437	2573-2728
ESS	-	-	2040-2125	2266-2433	2503-2743
ESSB6	1464-1562	1705-1844	1957-2139	2237-2447	2503-2743

3.4.4. Density

Figure 3.6 displays the densities of the sucrose esters and their corresponding epoxidized products. It shows that the densities of the sucrose esters are below 1.0 g/cm^3, but that the densities of their epoxy products are above 1.0 g/cm^3. For fully substituted sucrose esters, Figure 3.6 (a) shows that the density of the sucrose ester increases with the amount of double bonds; Figure 3.6 (b) shows that the density of epoxidized sucrose ester increases with the amount of epoxide. Sucrose soyate B6 is a partially substituted sucrose ester. It has the highest density of the sucrose esters, due to its higher amount of sucrose (d=1.587 g/cm^3). After epoxidation, ESSB6 still has a higher density than ESS.

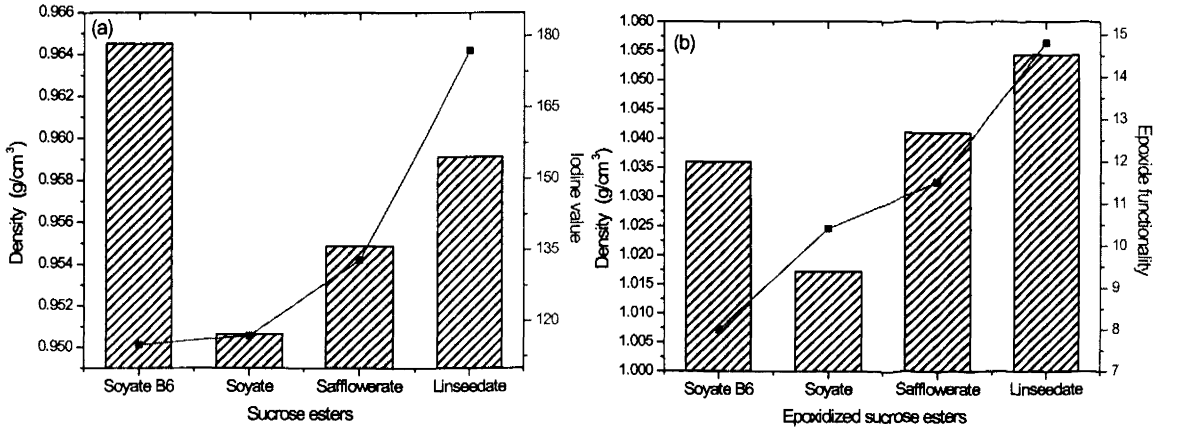

Figure 3.6. (a) Density of sucrose ester versus iodine value; (b) density of epoxidized sucrose ester versus epoxide functionality

3.4.5. Bulk Viscosity

Intermolecular forces between sucrose ester molecules, such as van der Waals dispersion forces and dipole-dipole interactions, will be increased in epoxidation. In addition, the trace hydroxyls in the fully substituted epoxidized sucrose esters and the hydroxyls in ESSB6 provide hydrogen atoms for hydrogen bonding. As the strongest intermolecular force, hydrogen bonding will be highly enhanced after epoxidation due to the role of incorporated oxygen atoms as hydrogen bond acceptors. Figure 3.7 displays the bulk viscosities of sucrose esters and their epoxy products. It shows that the viscosity of epoxidized sucrose ester is higher than that of its corresponding sucrose ester starting material. The viscosity of the fully substituted sucrose esters decreases with the amount of double bonds, but the viscosity of fully substituted epoxidized sucrose ester increases with the amount of epoxides. Due to the more hydroxyls for hydrogen bonding, SSB6 has the highest viscosity of the sucrose esters and its epoxy product ESSB6 has the second highest viscosity of the epoxidized sucrose esters.

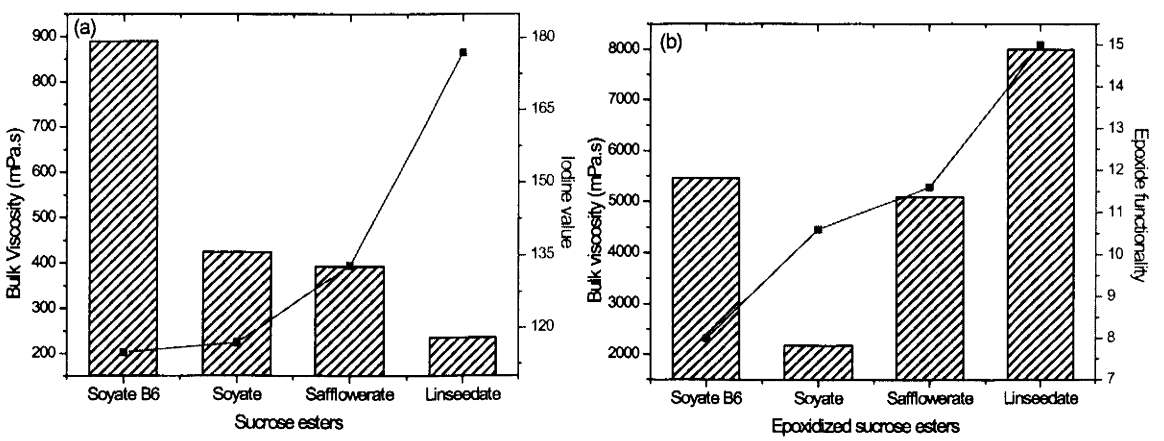

Figure 3.7. (a) Bulk viscosity and iodine value of sucrose ester; (b) bulk viscosity and epoxide functionality of epoxidized sucrose esters

3.4.6. Intrinsic Viscosity

The intrinsic viscosities of soybean oil, sucrose esters and their epoxy products in THF were measured, and the results are shown as a bar graph for comparison (Figure 3.8). It is observed that the intrinsic viscosity of each starting material possessing double bonds is lower than that of the corresponding epoxy product possessing epoxides. SSB6 and ESSB6 have the lowest intrinsic viscosity in sucrose esters due to their lower degree of substitution. The intrinsic viscosities of fully substituted sucrose esters are similar to each other. However, for fully substituted epoxidized sucrose esters, the higher content of epoxides leads to the higher value of intrinsic viscosity.

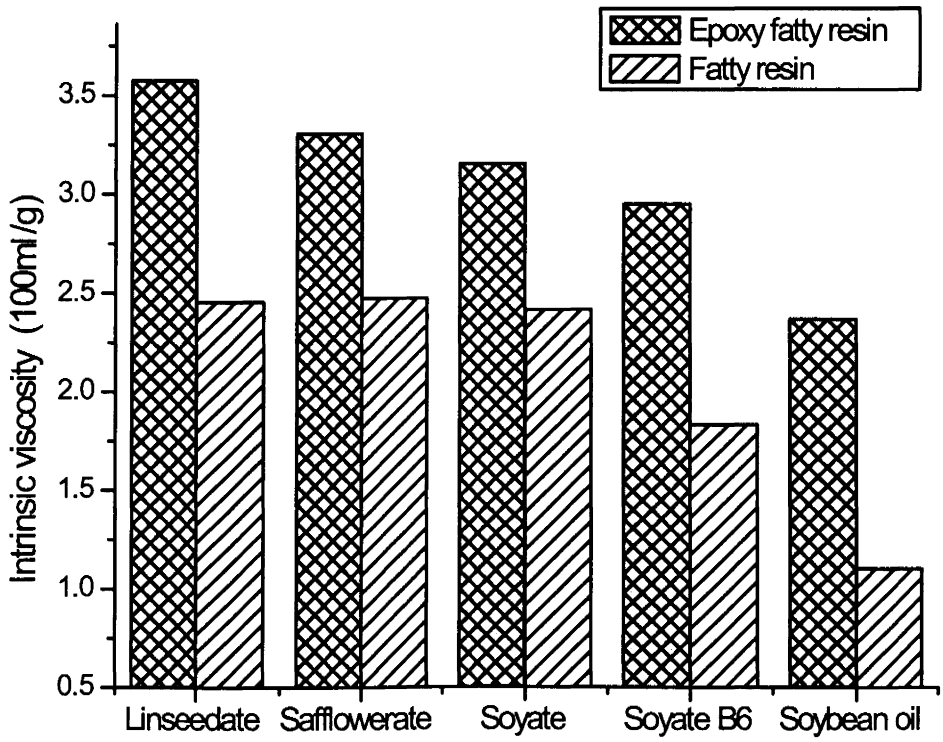

Figure 3.8. Intrinsic viscosities of soybean oil, sucrose esters, and their epoxy products in THF at 25°C

3.4.7. Thermal Properties

3.4.7.1.DSC results

Figure 3.9 displays the DSC curves of the sucrose esters and their corresponding epoxy products. The absence of crystalline melting transitions indicates that these compounds are amorphous and not prone to crystallize. Differential scanning calorimetry describes the thermal equilibrium thermodynamics studies dealing with the form of energy transfer—heat, throughout a process occurring at constant pressure. The jump in the $C_p = f(T)$ DSC curve indicates a second-order transition as the glass transition, in which there is no heat of transition. Thus, the glass transition is characterized by the heat capacity jump or heat capacity increase at the glass transition (ΔC_p). The incorporation of oxygen on the double bonds increases the mass of the sucrose ester molecule, which results in the increase of the heat capacity. Since the amplitude of the DSC curve is proportional to the heat capacity of the sample at constant pressure, epoxy products of sucrose esters show much clearer glass transitions than their corresponding starting materials.

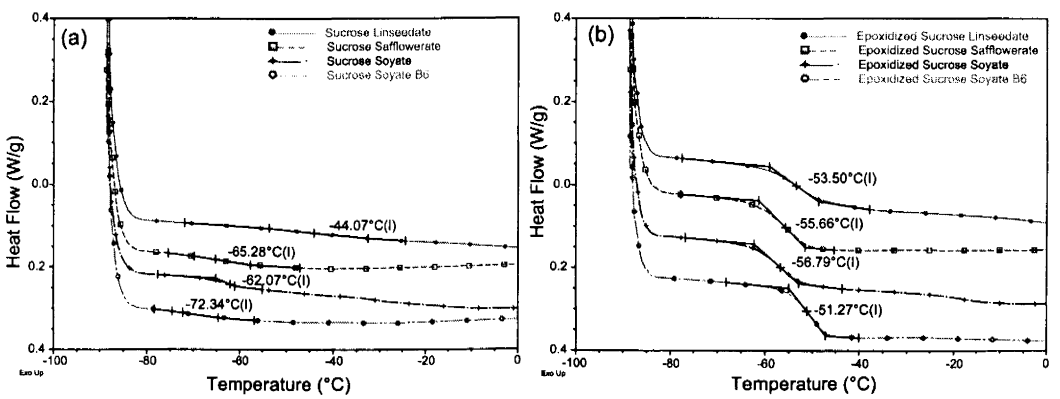

Figure 3.9. DSC curves indicating glass transition temperatures of (a) sucrose esters; (b) epoxidized sucrose esters

3.4.7.2.TGA results

The thermal stabilities of sucrose esters and their epoxy products were studied using thermogravimetric analysis in nitrogen. Figure 3.10 displays the plots of mass against temperature. Both sucrose esters and their epoxy products show one-step decomposition profiles, in which the broad stage of the mass loss is attributed to the random thermal decomposition of molecules. The mass loss starts through the loss of trace volatiles (0.1-1%) contained in samples in the 100-250°C range. Figure 3.10 (a) shows that the degradation (≥2%) of the fully substituted sucrose esters (SL, SSF, and SS) starts in the 320-332°C range. Figure 3.10 (b) shows that the degradation (≥2%) of the fully substituted epoxidized sucrose esters (ESL, ESSF, and ESS) starts in the 292-317°C range. Thus, the fully substituted sucrose esters have slightly better thermal stabilities than their epoxy products. Both of the partially substituted resins, SSB6 and ESSB6, show a lower onset decomposition temperature. This observation indicates that the thermal stability of sucrose esters can be impaired by decreasing the degree of substitution.

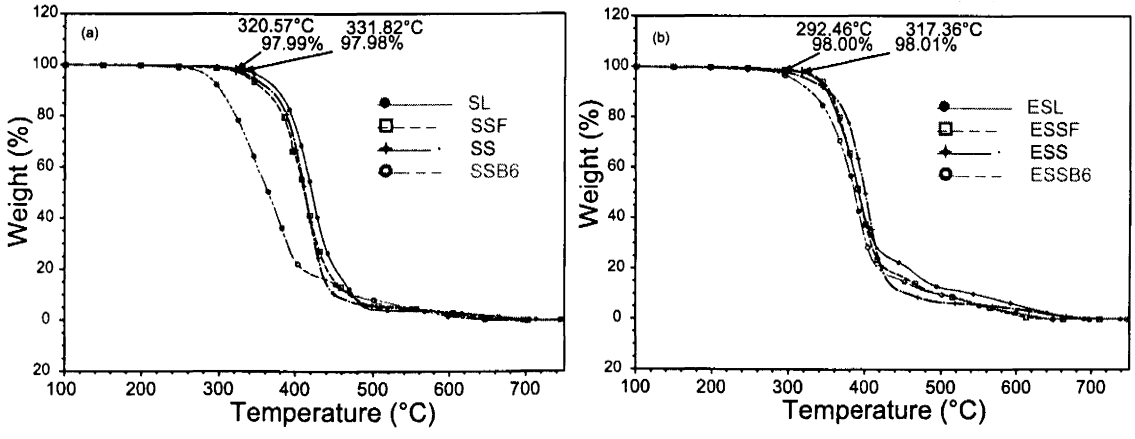

Figure 3.10. TGA thermograms of (a) sucrose esters; and (b) epoxized sucrose esters (Experiments were carried out in a nitrogen atmosphere)

3.4.8. Structure and Property Relationships

The geometry of the double bonds in naturally occurring plant oil fatty acids are in the *cis* configuration, in which the adjacent hydrogen atoms are on the same side of the double bond. One interesting feature of the double bond in these unsaturated fatty acid chains is that it puts a "kink" in the chain (Figure 3.11 a). For example, linolenic acid can be significantly bent by three "kinks" of three *cis* double bonds. Peroxyacids transfer oxygen to the double bonds with syn stereochemistry. The reaction is stereospecific, in which *cis* double bonds yield *cis* epoxides. The main effect of epoxidation on the alkene carbons is to transform their hybridization from sp^2 to sp^3 (Figure 3.11 b). The bond length of sp^2 C=C is extended from 1.33 Å to 1.47 Å; the bond angle of sp^2 C-C=C is slightly reduced from 120° to 116°, which is still higher than the typical alkane tetrahedron bond angle (109.5°) due to the nature of the strained epoxide ring.[22]

Sucrose esters have compact macromolecular structures, due to the compact structure of the sucrose core and the uniform distribution of fatty acids around the core. Since the presence of *cis* double bonds and epoxides can vary the extension of the fatty acid chains, the amount of double bonds and epoxides surely influences the overall dimension of sucrose ester macromolecules. Therefore, the morphology of sucrose esters is influenced by the morphology of its eight fatty acid chains.

A dilute solution of sucrose ester molecules can be thought of as their equivalent spheres. They are uniform, rigid, and noninteracting. The intrinsic viscosity of sucrose esters reflects the hydrodynamic volume of their equivalent spheres. For fully substituted sucrose esters, it was found that 1) epoxidized sucrose esters have higher intrinsic viscosities than their corresponding sucrose esters, and 2) higher amounts of epoxide result

in higher intrinsic viscosities. These observations indicate that the hydrodynamic volume of the sucrose ester molecules is increased by epoxidation and that the higher epoxide content results in larger dimension molecules.

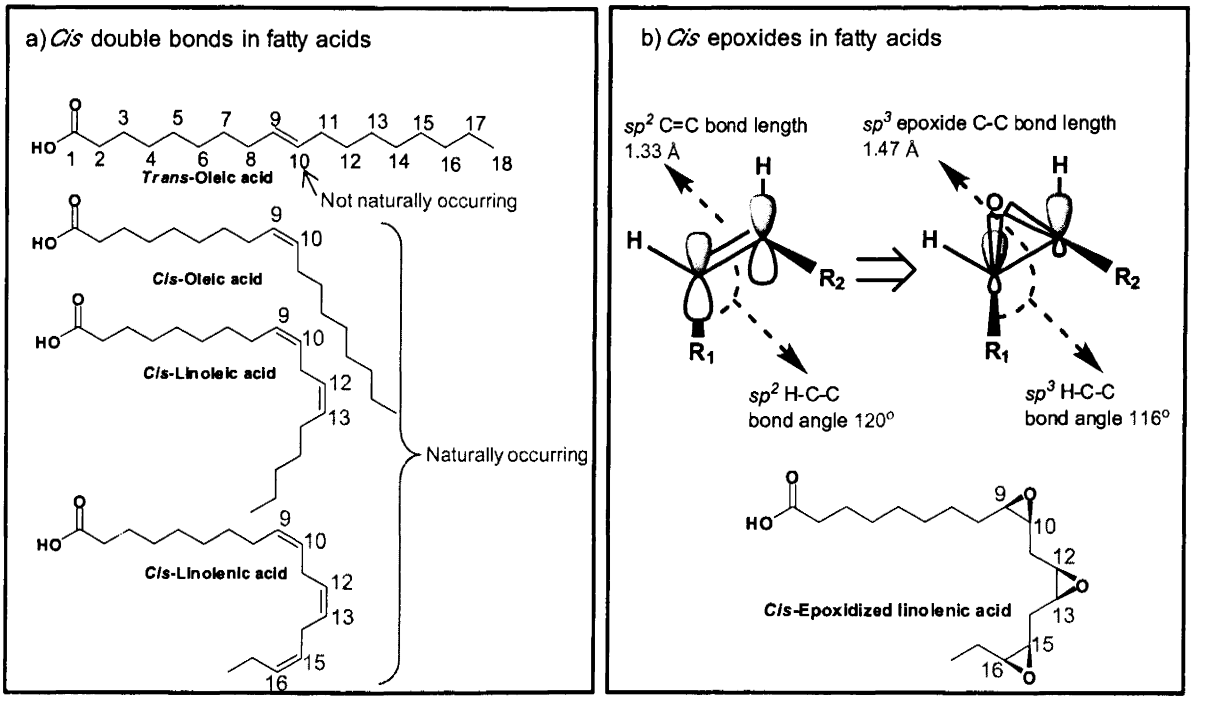

Figure 3.11. The effect of *cis* configuration of double bonds and epoxides on fatty acid morphology: a) naturally occurring *cis* double bonds bend fatty acid chains, with the assumption that the C-C single bonds are all in *trans*; b) *cis* double bonds produce *cis* epoxides with the bond length and bond angle slightly changed

In addition to the larger volume for the epoxidized sucrose esters, intermolecular forces, such as van der Waals forces and dipole-dipole interactions, can be invoked for understanding the observations of bulk viscosity and density of the sucrose esters. Not only does epoxidation increase the molecular weight of sucrose esters, the polarity of the sucrose esters also increases. Thus, the epoxidized sucrose ester molecules can interact more extensively, leading to a higher bulk viscosity and higher density. Since even in the

"fully substituted" sucrose esters there are some residual hydroxyls, hydrogen bonding may also occur between the molecules. Indeed, the bulk viscosity and density of the partially substituted epoxidized sucrose ester is higher than its fully substituted counterpart, due to the additional hydrogen bonding. This increase in polarity is also reflected in a more well-defined glassy state as is indicated by the sharp glass transitions observed in DSC.

The epoxidation of sucrose esters of unsaturated vegetable oil fatty acids has resulted in unique biobased resins having a high concentration of epoxy groups. As has been seen, functionalities of 8 to 15 epoxide groups per molecule can be achieved, depending on the composition of the fatty acid used and the degree of substitution of the fatty acids on the sucrose moiety. This is substantially higher than what can be achieved through epoxidation of triglycerides which range from about 4 for epoxidized soybean oil up to 6 for epoxidized linseed oil.

The high epoxide functionality of these resins coupled with the rigidity of the sucrose group has significant implications for the further use of these resins and their derivatives in applications such as thermosetting materials. The crosslinking of these materials through the epoxy groups and the synthesis of polyols from these resins are currently being explored and will be the subject of future publications. However, the results from these studies are indicating that crosslinked materials having an outstanding combination of properties can be achieved.

3.5. Conclusions

Novel biobased epoxy compounds, epoxidized sucrose esters of fatty acids (ESEFA) were successfully prepared from sucrose esters of fatty acids (SEFA). The

epoxidation of the fatty acids was carried out using peracetic acid generated *in situ* from hydrogen peroxide and acetic acid in the presence of an acidic ion exchange resin as catalyst. The product yield was up to 95%, and the conversion of double bonds to epoxides was greater than 99.0%. No side reactions were observed. Characterization using a range of analytical methods confirmed the structures of the epoxidized sucrose esters.

Both SEFAs and ESEFAs are macromolecular esters with well-defined compact structures, and thus they have unique structure-property relationships. Compared with the common fatty epoxy compound—epoxidized vegetable oils—ESEFAs have a rigid sucrose core which can impart hardness to their thermosets, as well as a much higher epoxide functionality which can lead to rapid gelation and high crosslink densities in crosslinking. We predict that the ESEFAs, made of vegetable oils and sugar, are much closer than any other epoxy fatty compound discovered so far to be competitive with the epoxy products derived from petrochemicals in a number of potential applications. Additionally, epoxidized sucrose esters are a highly tunable platform which can be used to develop a wide variety of polymeric resins having different properties.

3.6. References

1. Petrović, Z. S.; Guo, A.; Javni, I. *U.S. Pat. No. 6,107,433*, **2000**.
2. Petrović, Z. S.; Javni, I.; Guo, A.; Zhang, W. *U.S. Pat. No. 6,6867,435*, **2004**.
3. Zlatanić, A.; Lava, C.; Zhang, W.; Petrović, Z. S. *J. Polym. Sci., Part B: Polym. Phys.* **2004**, *42*, 809.
4. Scala, J. L.; Wool, R. P. *J. Am. Oil Chem. Soc.* **2002**, *79*, 59.
5. Scala, J. L.; Wool, R. P. *Polymer* **2005**, *46*, 61.

6. Pelletier, H.; Belgacem, N.; Gandini, A. *J. Appl. Polym. Sci.* **2006**, *99*, 3218.

7. Mungroo, R.; Pradhen, N. C.; Goud, V. V.; Dalai, A. K. *J. Am. Oil Chem. Soc.* **2008**, *85*, 887.

8. Petrović, Z. S.; Zlatanić, A.; Lava, C. C.; Sinadinović-Fišer, S. *Eur. J. Lipid Sci. Technol.* **2002**, *104*, 293.

9. Goud, V. V.; Patwardhan, A. V.; Dinda, S.; Pradhan, N. C. *Chem. Eng. Sci.* **2007**, *62*, 4065.

10. Karmalm, P.; Hjertberg, T.; Jansson, A.; Dahl R. *Polym. Degrad. Stab.* **2009**, *94*, 2275.

11. Fenollar, O.; García, D.; Sánchez, L.; López, J.; Balart, R. *Eur. Polym. J.* **2009**, *45*, 2674.

12. Bueno-Ferrer, C.; Garrigós, M.C.; Jiménez, A. *Polym. Degrad. Stab.* **2010**, *95*, 2207.

13. Miyagawa, H.; Misra, M.; Drzal, L. T. *Polym. Eng. Sci.* **2005**, *45*, 487.

14. Crivello, J. V.; Narayan, R. *Chem. Mater.* **1992**, *4*, 692.

15. Thames, S. F.; Yu, H. *Surf. Coat. Technol.* **1999**, *115*, 208.

16. Ortiz, R. A.; López, D. P.; Cisneros, M. d. L. G.; Valverde, J. C. R.; Crivello J. V. *Polymer* **2005**, *46*, 1535.

17. Schiller, J.; Süß, R.; Arnhold, J.; Fuchs, B.; Leßig, J.; Müller, M.; Petković, M.; Spalteholz, H.; Zschörnig, O.; Arnold, K. *Prog. Lipid Res.* **2004**, *43*, 449.

18. Jakab, A.; Nagy, K.; Héberger, K.; Vékey, K.; Forgaćs, E. *Rapid Commun. Mass Spectrom.* **2002**, *16*, 2291.

19. Schiller, J.; Süß, R.; Petković, M.; Arnold, K. *Eur. Food Res. Technol.* **2002**, *215*, 282.

20. Asbury, G. R.; Al-Saad, K.; Siems, W. F. *J. Am. Soc. Mass. Spectrom.* **1999**, *10*, 983.

21. Ayorinde, F. O.; Elhilo, E.; Hlongwane, C. *Rapid Commun. Mass Spectrom.* **1999**, *13*, 737.

22. Tanaka, Y.; In *Epoxy resins: chemistry and technology, 2nd ed.*, C. A. May, Marcel Dekker, Inc.: New York, **1988**, *Chapter 2*, 10.

CHAPTER 4. HIGH BIOBASED CONTENT EPOXY-ANHYDRIDE THERMOSETS FROM EPOXIDIZED SUCROSE ESTERS OF FATTY ACIDS

4.1. Abstract

Novel highly functional biobased epoxy compounds, epoxidized sucrose esters of fatty acids (ESEFAs), were crosslinked with a liquid cycloaliphatic anhydride to prepare polyester thermosets. The degrees of cure or conversions were studied using differential scanning calorimetry (DSC), and the sol contents of thermosets were studied using solvent extraction. The mechanical properties were studied using tensile testing to determine Young's modulus, tensile stress, and elongation at break. The dynamic mechanical properties were studied using dynamic mechanical analysis (DMA) to determine glass transition temperature, storage modulus, and crosslink density. The nanomechanical properties on surface were studied using nanoindentation to determine reduced modulus and indentation hardness. The properties of coatings on steel substrates were studied using ASTM methods to determine coating hardness, adhesion, solvent resistance, and mechanical durability. Compared with the control—epoxidized soybean oil, the anhydride-cured ESEFAs are high modulus, hard and ductile, high performance thermoset materials while maintaining a high biobased content (71-77% in theory). The exceptional performance of the ESEFAs is attributed to the unique structure of these macromolecules: well-defined compact structures with high epoxide functionality. These biobased thermosets have potential uses in applications such as composites, adhesives, and coatings.

4.2. Introduction

The applications of epoxy functional materials are extensive in coatings, adhesives, and composites. The most commonly used class of epoxy compounds are the bisphenol-A diglycidyl ether resins. The high reactivity of the petroleum-based epoxies is due to their external/terminal epoxides. Epoxides generated from the epoxidation of the double bonds of unsaturated fatty acids are internal epoxides—both carbons of the heterocyclic ring are substituted with another carbon. Since internal epoxides are much less reactive than external epoxides in most epoxy curing reactions, the roles currently assigned to epoxidized triglyceride oils are limited to uses such as stabilizers and plasticizers for halogen-containing polymers and reactive toughening agents for rigid thermoset plastics (i.e. phenolic resins).[1-4] Recently, Cádiz et al. prepared a biobased external epoxy using 10-undecenoic acid and successfully managed the epoxy-amine curing.[5-6] However, while 10-undecylenic acid is a derivative of naturally occurring castor oil, it is mainly used in pharmaceuticals and cosmetics and may not be suitable for the large scale production of resins.[7] Therefore, end users are still seeking for an economical biobased epoxy having internal epoxides that can be competitive with petroleum-based epoxies having external epoxides.

We have recently reported the discovery of novel biobased epoxy compounds—epoxidized sucrose esters of fatty acids (ESEFA).[8] It was observed that the ESEFA compounds have a compact structure, high density, and high internal epoxide functionality (Figure 4.1). When considering the use of ESEFAs to form crosslinked materials, the rigid core of sucrose and the compact structure can potentially impart hardness to the thermoset, and the high epoxide functionality can lead to rapid gelation and high crosslink density.

Thus, ESEFAs have the potential to be a significant advance in biobased epoxy resin technology.

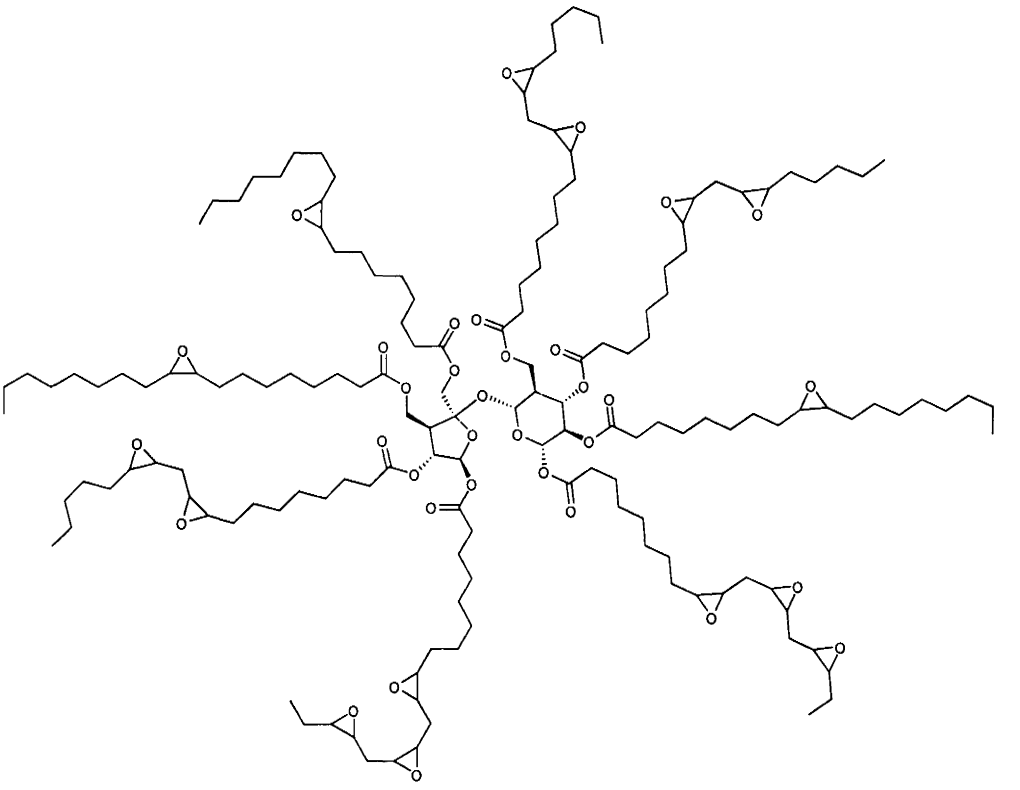

Figure 4.1. Epoxidized sucrose ester of fatty acids (ESEFAs)

Epoxy resins can be cured with a variety of mechanisms using various hardeners, catalysts, and crosslinking agents. Curing agents having active hydrogens reacting with epoxide groups are amines, alcohols, acids, and anhydrides. Epoxy-anhydride thermosets, using external epoxy compounds (e.g. diglycidyl ether of bisphenol-A (DGEBA), N, N, N', N'-tetraglycidyl-4,4'-diamino diphenylmethane (TGDDM)), have been widely used as electrically insulating materials. Tertiary amines, imidazoles and their derivatives are usually used as the catalyst.[9-10] The curing kinetics of external epoxies with anhydrides have been extensively studied using FT-Raman spectroscopy, differential scanning calorimetry (DSC), and dynamic mechanical analysis.[11-13] Boey et al. developed an

experimental model using DSC isothermal and non-isothermal methods to elucidate an accurate curing kinetics model.[14] The mechanism of epoxy-anhydride curing in the presence of amine catalysts has been explained by zwitterion formation[15-17] and carboxylate formation.[18-21] The presence of hydroxyls in epoxy-anhydride curing has been proposed to facilitate network formation through the fast reaction between hydroxyl and anhydride.[11, 15, 19, and 22]

The epoxy-anhydride curing of epoxidized soybean oil (ESO) with dicarboxylic acid anhydrides has been explored. Rösch et al. prepared a series of highly flexible rubbery materials with glass transition temperatures below room temperature by crosslinking ESO with the anhydrides of hexahydrophthalic acid, succinic acid, and norbornene dicarboxylic acid.[23] Thermosets with higher glass transition temperatures varying between 43 and 73°C could be obtained using the anhydrides of maleic and phthalic acid. Gerbase et al. studied in detail the dynamic mechanical properties of polyester thermosets prepared by curing ESO with various cyclic acid anhydrides.[24] With an epoxide/anhydride equivalent ratio of 1:1, the glass transition temperatures of the thermosets varied between -5 to 65°C and the storage moduli in the elastic region (T_g+40°C) were in the range of 2-23 MPa. Due to the flexible and semiflexible nature of ESO-anhydride thermosets, reinforcing fillers (e.g. cellulose fiber, organoclay) have been incorporated to form the composite materials.[25-26]

In this initial study, a series of ESEFAs derived from different vegetable oils (i.e. linseed, safflower, and soybean) and different substitutions were used to formulate epoxy-anhydride curing systems. 4-Methyl-1,2-cyclohexanedicarboxylic anhydride (MHHPA) was used as a cycloaliphatic anhydride crosslinker, and 1,8-Diazabicyclo[5.4.0]undec-7-

ene (DBU) was used as a tertiary amine (amidine) catalyst. A commercial ESO was used as a control for comparison with ESEFAs in anhydride curing. To maintain a high biobased content without compromising the properties of the thermosets, the epoxide/anhydride equivalent ratio in most formulations was 1:0.5. An epoxide/anhydride equivalent ratio of 1:0.75 was also used to study the effect of anhydride on the thermosetting properties.

4.3. Experimental

4.3.1. Raw Materials

Sucrose esters of fatty acids (SEFAs) were kindly supplied by Procter & Gamble Chemicals (Cincinnati, OH) and were the starting materials to prepare epoxidized sucrose esters of fatty acids (ESEFAs). Vikoflex 7170 epoxidized soybean oil (ESO) was supplied by Arkema Inc. (Philadelphia, PA). 4-Methyl-1,2-cyclohexanedicarboxylic anhydride (mixture of isomers, 98%), or 4-methyl hexahydrophthalic anhydride (MHHPA), was purchased from Alfa Aesar (Heysham, England). 1,8-Diazabicyclo[5.4.0]undec-7-ene (DBU) (≥99.0% GC) was purchased from Sigma-Aldrich Co. (St. Louis, MO). All materials were used as received without further purification.

4.3.2. Preparation of Epoxidized Sucrose Esters of Fatty Acids

As reported previously, SEFAs were epoxidized by peracetic acid generated *in situ* from hydrogen peroxide and acetic acid in the presence of an acidic ion exchange resin as a catalyst. High conversion of double bonds to epoxides was achieved at an acetic acid: hydrogen peroxide (50%): double bonds molar ratio of 0.5:2:1, and a catalyst concentration of 20 wt% (based on SEFA) at 60°C. There are four ESEFAs used in this study. They are

epoxidized sucrose linseedate (ESL), epoxidized sucrose safflowerate (ESSF), epoxidized sucrose soyate (ESS), and epoxidized sucrose soyate B6 (ESSB6).

4.3.3. Epoxy-anhydride Formulation and Curing

The equivalent ratio of epoxides to anhydrides was 1:0.5 or 1:0.75. DBU was used at 1.5 wt% (based on the total weight of resins). The effects of stoichiometric ratio on the thermosetting properties were studied using ESL and ESSB6. In ESL-anhydride curing, the equivalent ratios of epoxides to anhydrides were used as 1:0.5, 1:0.4 and 1:0.3. In ESSB6 anhydride curing, the equivalent ratios of epoxides to anhydrides were used as 1:0.625, 1:0.5 and 1:0.4. As an example, the formulation of ESL-anhydride curing in the equivalent ratio of epoxide to anhydride of 1:0.5 is as follows: 10 g of ESL (3.70 mmoles) containing 54.64 mmoles epoxide, 4.60 g of MHHPA (27.35 mmoles) containing 27.35 mmoles anhydride and 0.219 g of DBU (1.44 mmoles). ESEFA-anhydride curing was done for 12 hours at 85°C, but ESO-anhydride curing had to be done for 48 hours at 85°C. Thin films (coatings) were cast on cleaned steel QD panels and glass panels using a draw-down bar with a gap of 8 mils. The thermoset thin films (0.10-0.16 mm) on glass panels were used to make the specimens for DMA and tensile testing. Thick thermoset samples were prepared by curing in Teflon molds, and their thicknesses were controlled in 1.6-2.0 mm.

4.3.4. Characterization on Epoxy-anhydride Thermosets

4.3.4.1.Differential scanning calorimetry (DSC)

A DSC Q1000 from TA Instruments (New Castle, DE) with an autosampler was used to measure the exothermic heats (heat per mass of material, J/g) when samples were

subjected to a heat cycle from 0 to +250°C by ramping at 10°C/min. The degree of cure or conversion of epoxy-anhydride system is given by the Equation 1:

$$\alpha_t = \frac{\Delta H_{rxn} - \Delta H_{res}}{\Delta H_{rxn}} \equiv \frac{\Delta H_t}{\Delta H_{rxn}} \qquad (1)$$

Where α_t is denoted the degree of cure at curing time t (hr), ΔH_t is the liberated heat during time t, ΔH_{res} is the residual heat after time t, and ΔH_{rxn} is the total heat of reaction. Since ΔH_{rxn} is defined as the total liberated heat when the thermoset material is taken from 0% to 100% conversion, it is very important to start DSC running just after preparing the formulation. The residual heat, ΔH_{res}, was measured after isothermally curing in oven at 85°C for time t.

4.3.4.2.Soxhlet extraction

Solvent extraction of epoxy-anhydride thermoset was carried out in Soxhlet extraction using dichloromethane (CH_2Cl_2, b.p. =39.6°C) as the solvent. A 500 ml flask containing 300 ml CH_2Cl_2 was equipped with a Soxhlet extractor that is connected to a water condenser. Vacuum dried samples were weighed and packed into folded filter paper and inserted into the extractor. Samples were extracted for 24 hours by warm CH_2Cl_2 when CH_2Cl_2 was heated to reflux. One cycle of Soxhlet extraction took 8-10 minutes. The wet residual samples after extraction were dried in vacuum and weighed. The sol content (weight percentage) of epoxy-anhydride thermoset is given by the Equation 2:

$$\%\ Sol\ content = 100 \times \left(\frac{W_t - W_{gel}}{W_t}\right) = 100 \times \frac{W_{sol}}{W_t} \qquad (2)$$

Where W_t is the total weight of thermoset sample, W_{gel} is the weight of residue after extraction which refers to the gel fraction (crosslinked), and W_{sol} is the weight of loss during extraction which refers to the sol fraction. The sol content was determined as the average of 3 measurements and the uncertainty is the standard deviation.

4.3.4.3.Fourier transform infrared (FTIR) spectroscopy

FTIR measurements were done with a Thermo Scientific Nicolet 8700 FTIR spectrometer. The liquid samples were prepared in CH_2Cl_2 solution with the concentration of 5 mg/ml. Then, a 200 μL drop of the solution was deposited by micropipette on the center of a potassium bromide (KBr) salt crystal and the drop was naturally spread out. After the evaporation of CH_2Cl_2, a thin layer of sample film was formed on the KBr crystal. The solid samples were milled with the pure KBr power into a mixture of very fine power, and the weight percentage of sample in the mixture was in the range of 2-3 wt%. This powder was then compressed into a thin pellet which can be analyzed. Spectra acquisitions were based on 32 scans with data spacing of 2.0 cm^{-1}, and the data were set for autogain to monitor spectral ranges of 4000–450 cm^{-1}.

4.3.4.4.Tensile testing

The die-cut specimens were prepared from the thin films (0.10-0.16 mm) and thick samples (1.6-2.0 mm) according to ASTM D-638. The tensile tests were carried out at 25°C using an Instron 5542 (Norwood, MA). The grip separation distance of the tensile testing was 25.4 mm, and the effective gauge length was 20.4 mm. The crosshead speed was 0.1% elongation/sec. (0.0204 mm/sec.). The tensile properties of each sample were

reported as the average of 5 measurements taken using different specimens and the uncertainty was the standard deviation.

4.3.4.5.Dynamic mechanical analysis (DMA)

The dynamic mechanical properties of the thermosetting films were measured in tension mode using a Q800 DMA from TA Instruments (New Castle, DE). Rectangular specimens with dimensions of 20 mm length, 5 mm width, and 0.10-0.16 mm thickness were prepared. The measurements were performed from -110 to 200°C at a heating rate of 5°C/min and a frequency of 1 Hz. The glass transition temperature (T_g) was determined as the temperature at the maximum of the tan δ vs. temperature curve. The storage modulus (E') in the rubbery plateau region was determined at generally 60°C above the glass transition temperature. The crosslink density (ν_e) is calculated by the Equation 3, derived from the theory of rubber elasticity: where E' is the storage modulus of thermoset in the rubbery plateau region, R is the gas constant, and T is the absolute temperature.

$$E' = 3\nu_e RT \qquad (3)$$

4.3.4.6.Nanoindentation

The nanoindentation tests were carried out using a Hysitron TI900 TriboIndenter. A diamond Berkovich tip was used with a DMA transducer. An air indent was performed as the specific calibration before each testing; this calibrates the electrostatic force of the transducer which is required to measure the depth of indents correctly. Periodically, a compliance calibration was performed to make sure the instrument was reading the correct depth of displacement. The testing conditions were quasi-static, load-controlled indents

performed at a 200 μN peak load using a 5 second loading time (40 μN/s loading rate), 5 second hold time, and a 5 second unloading time. The thick thermoset samples were used.

4.3.4.7.Thermogravimetric analysis (TGA)

A TGA Q500 from TA Instruments (New Castle, DE) was used to study the thermal degradation of the thermosets. Samples were placed in the pans and heated from 25 to +900°C under N_2 at a heating rate of 20°C/min. The measurements were conducted using 5–15 mg samples, and the weights were recorded as a function of temperature.

4.3.4.8.Coating measurements

The thickness of the cured coatings was the average of 10 measurements taken using a Byko-Test 8500 coating thickness gauge at different locations on the film and the uncertainty is the standard deviation. König pendulum hardness and pencil hardness were measured using ASTM D 4366 and ASTM D 3363, respectively. The crosshatch adhesion of coatings on the steel substrate was evaluated using ASTM D 3359. Methyl ethyl ketone (MEK) double rub test was carried out following ASTM D 5402. Impact resistance was determined according to ASTM D 2794. Mandrel bend test was carried out using ASTM D 522, and the results were reported as the elongation of the coating at cracking.

4.4. Results and Discussion

4.4.1. Properties of The Epoxy Compounds

The properties of ESEFAs and the control ESO are shown in Table 4.1. Sucrose naturally contains 8 hydroxyls per molecule. ESL, ESSF, and ESS are "fully substituted"

epoxidized sucrose esters having an average degree of substitution of 7.7; they have 0.3 trace hydroxyls per molecule. ESSB6 is a partially substituted epoxidized sucrose soyate with an average degree of substitution of 6; it has 2 hydroxyls per molecule. There is no hydroxyl available in the ESO control. The molecular weights (MW) of ESEFAs are in the range of 2,000-2,700 g/mol, but the MW of ESO is around 1,000 g/mol. Epoxide functionalities per molecule of ESEFAs are 8-15, which are 2-3 times that of ESO. The densities of ESEFAs are all above 1.0 g/cm^3, but the density of ESO is below 1.0 g/cm^3.

Table 4.1. Properties of ESEFAs and ESO control used in this study

Epoxy compounds	The average degree of sucrose substitution	Average absolute molecular weight, MW (g/mol)	Epoxide equivalent weight, EEW (g/eq.)	Epoxide functionality per molecule	Density (g/cm^3)
ESL	7.7	2,700	183	15.0	1.05
ESSF	7.7	2,645	230	11.6	1.04
ESS	7.7	2,628	248	10.6	1.02
ESSB6	6	2,048	256	8.0	1.03
ESO (Control)	3	993	231	4.3	0.99

4.4.2. Curing Reaction Mechanism

The mechanism of epoxy-anhydride curing was illustrated mainly in two situations: (I) curing epoxide with anhydride in the presence of amine catalyst; (II) curing epoxide with anhydride in the presence of trace hydroxyls. In this study, the epoxy-anhydride curing formulation consists of epoxidized sucrose esters, anhydride crosslinker, and amine catalyst (Figure 4.2). The prior study showed that the fully substituted ESEFAs contain trace hydroxyls due to the presence of less than 30 wt% of hexaester and heptaester in the starting sucrose ester resins. Epoxidized sucrose soyate B6 (ESSB6) has additional hydroxyls available due to the partial substitution of the sucrose. Therefore, the presence of hydroxyls needs to be considered in the curing reaction. Additionally, there is trace diacid

available in the anhydride (98% purity) and the possibility of some newly formed diacid from adventitious atmospheric moisture during formulating and curing.

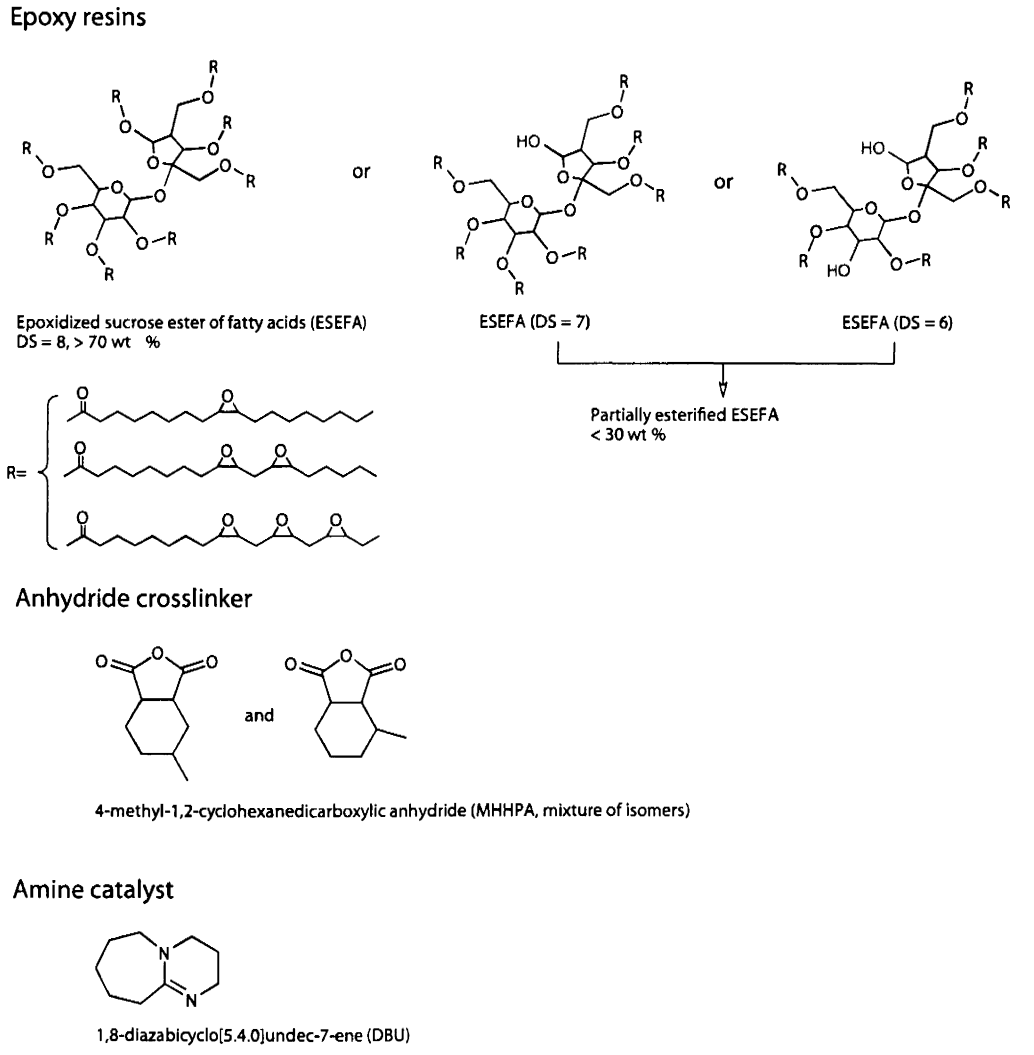

Figure 4.2. Chemical formulae of the reactants used for epoxy-anhydride

DBU is a tertiary amine compound, with a remarkably stronger basicity than normal tertiary amines (e.g. quinuclidine, triethylamine). DBU also belongs to amidine compounds with the characteristic amidino functional group, -HN=C-NH_2. Experimentally, we found that DBU reacts with MHHPA very rapidly to form a solid product with a strong

heat release. Thus, formulation preparation in the sequence of ESEFA→MHHPA→DBU unavoidably results in the formation of some tiny solid particles, even though MHHPA had been homogeneously dispersed into the ESEFA resin before adding DBU. These tiny solid particles could not be destroyed by mechanical stirring and sonication, and while they disappeared during curing, local brittle regions were formed in the thermoset. Thus, a preferred sequence for preparing the formulations is ESEFA→DBU→MHHPA: (a) homogeneously disperse DBU into ESEFA; (b) add and mix MHHPA later. It seems that DBU couples with the internal epoxides completely because no particle formation is observed while adding anhydride.

Based on this procedure, Figure 4.3 outlines the reactions that take place on curing internal epoxides with MHHPA in the presence of DBU catalyst and trace hydroxyls and possible diacids. Three reactions probably initiate the curing: (1) DBU reacts with an internal epoxide to form an alkoxide anion; (2) hydroxyl reacts with an anhydride to form a carboxylate; and (3) DBU reacts with an anhydride to form a carboxylic acid. There is some possibility that diacids have been involved in the curing by reacting with epoxides. The newly formed alkoxide anions are ready to react with anhydrides. The newly formed carboxylates and carboxylic acids are ready to react with epoxides. Subsequently, the polyester network is formed in a sequence of reactions alternatively consuming epoxides and anhydrides. The partially substituted epoxidized sucrose soyate, ESSB6, contains additional hydroxyls. It is an interesting epoxy compound for comparison with the fully substituted epoxidized sucrose soyate (i.e. ESS). Further studies will explore the character of hydroxyls in epoxy-anhydride curing system and their effects on the thermosetting properties. On the other hand, ESO has no available hydroxyl groups to react anhydrides.

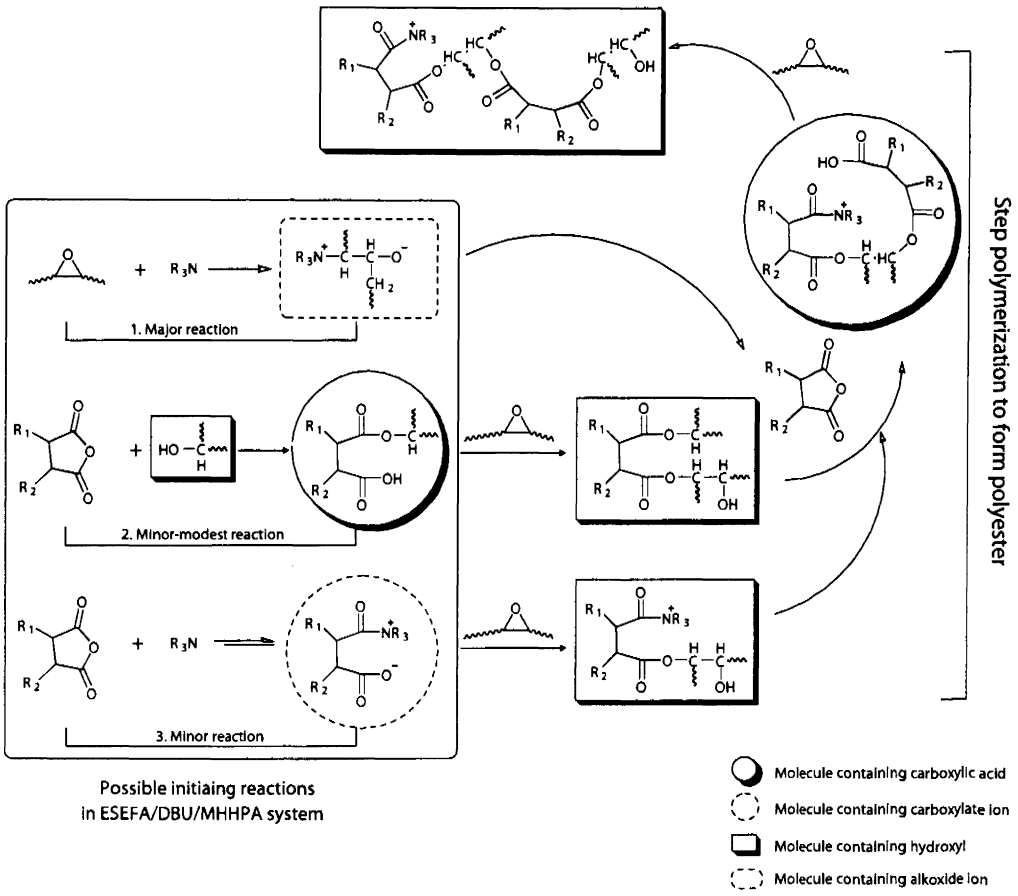

Figure 4.3. Reaction mechanism of epoxy-anhydride in the presence of DBU amidine catalyst and hydroxyls

4.4.3. The Degree of Cure or Conversion

The application of DSC to thermoset cure underlies the basic assumption that the measured heat flow is proportional to the rate of cure or conversion. Figure 4.4 shows the typical DSC temperature scans of ESO-anhydride and ESS-anhydride systems, which were uncured or isothermally cured at 85°C for 12 and 48 hours. The integrated area of the exothermic peak was determined as the liberated heat in the DSC scan. The total heat of

reaction, ΔH_{rxn}, and the residual heat after curing (ΔH_{res}) were obtained. Table 4.2 shows the degrees of cure that were calculated using Equation 2. With 12 hours of curing, the fully substituted ESEFAs and ESO achieved 91-94% curing, and ESSB6 achieved 84% curing. With 48 hours of curing, ESS and ESO had achieved 100% curing (Figure 4.4).

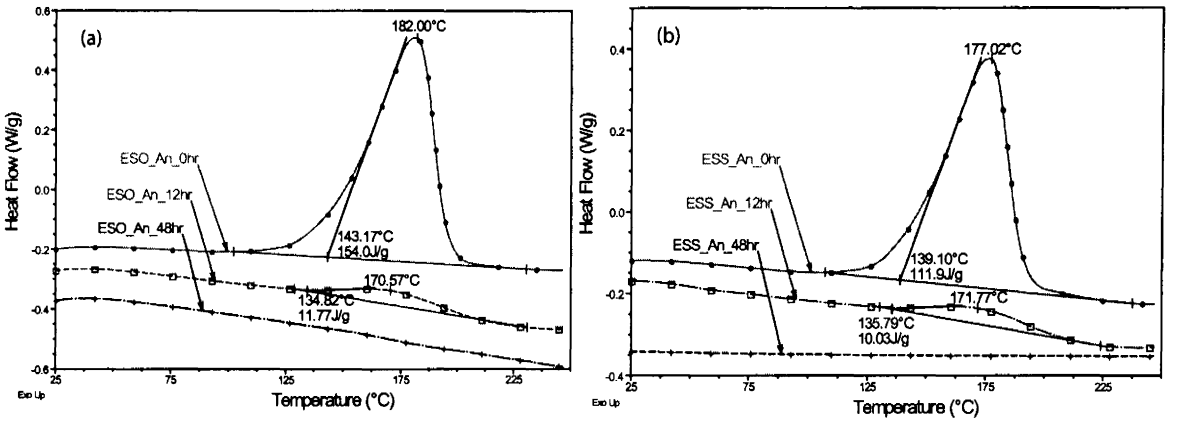

Figure 4.4. Typical DSC temperature scans at 10°C/min of ESO-anhydride curing system (a) and ESS-anhydride curing system (b) that have been cured at 85°C for 0 hour, 12 hours and 48 hours

Table 4.2 also reports the characteristic curing temperatures of the epoxy-anhydride systems. The values of T_{on} (onset initial curing temperature) and T_{en} (endset final curing temperature) are shown. The epoxy-anhydride systems using the fully substituted ESEFAs and ESO start the curing at 130-139°C and end at 184-198°C. However, the curing of ESSB6-anhydride spans a broader range of temperature from 120 to 215°C. The hydroxyls groups in the ESSB6 significantly contribute the polyester network formation in the initial stage of epoxy-anhydride curing, due to the fast reaction between hydroxyls and anhydrides. Since some of the anhydrides are consumed in reaction with the hydroxyls

groups, the amount of anhydride/acid remaining for reaction with epoxy groups is lower since the thermosets were formulated on the basis of an epoxide to anhydride ratio of 1:0.5.

Table 4.2. The degrees of cure or conversions of epoxy-anhydride thermosets with an equivalent ratio of epoxide to anhydride of 1:0.5

Epoxy compounds	Curing time, t (hr)	T_{on} (°C)	T_{en} (°C)	ΔH_{res} (J/g)	ΔH_{rxn} (J/g)	The degree of cure or conversion
ESL	12	131.6±0.23	183.5±0.42	14.1±0.45	183.4±5.3	92.3
ESSF	12	130.1±2.26	191.3±1.22	13.0±1.78	148.8±6.2	91.3
ESS	12	135.9±2.11	191.6±0.38	8.79±0.73	118.7±5.6	92.6
ESSB6	12	120.1±1.85	215.0±0.93	29.9±5.82	182.0±3.7	83.6
ESO (Control)	12	139.4±1.59	197.5±1.61	9.35±1.14	158.0±3.3	94.1

4.4.4. Sol Content

Figure 4.5 shows the sol contents, *S*, of epoxy-anhydride thermosets determined using Soxhlet extraction. For the thermosets which had been cured for 12 hours, the sol contents for the ESEFA-anhydride thermosets are low indicating a higher degree of cure. The sol contents are in the order of $S_{(ESL)} < S_{(ESSF)} < S_{(ESSB6)} < S_{(ESS)}$, and correlates to the epoxide functionality of the ESEFA resins. The sol content of the ESO-anhydride thermoset is much greater at 4-10 times the sol contents of the ESEFA-anhydride thermosets, which are in the range of 2-6%. While the ESO-anhydride and ESS-anhydride systems achieve 100% conversion in 48 hours curing at 85°C, they still contain a low level of sol fractions in the range of 1.3-1.6%.

FTIR spectroscopy was also employed to monitor the curing of epoxy-anhydride system. Figure 4.6 shows the overlaid spectra of ESS/MHHPA/DBU systems that have been isothermally cured at 85°C for 0, 12, and 48 hours, along with the uncured

formulation. The carbonyl adsorption bands observed from the FTIR spectrum of the uncured sample are: 1864 cm^{-1} (anhydride C=O, antisymmetric stretch), 1791 cm^{-1} (anhydride C=O, symmetric stretch), 1747 cm^{-1} (sucrose ester C=O, stretch), and 1648 cm^{-1} (tertiary amide C=O, stretch). The characteristic epoxy group is observed at 824 cm^{-1}. After 12 hours curing, the adsorption of ester carbonyl made of sucrose ester C=O and anhydride ester C=O is observed at 1744 cm^{-1}, and the adsorption of tertiary amide carbonyl has been enhanced at 1650 cm^{-1}. After 48 hours curing, the adsorption of ester carbonyl is observed at 1742 cm^{-1}, and the adsorption of tertiary amide carbonyl is observed at 1651 cm^{-1}. The adsorption of tertiary amide carbonyl proves the reaction between MHHPA and DBU, which starts from the mixing of the formulation and increases during curing. The broad adsorption bands centered at 2452 and 3506 cm^{-1} represent the newly formed hydroxyls from curing, since the epoxy/anhydride ratio of 1:0.5 has been designed to the equivalent reaction between epoxy and anhydride.

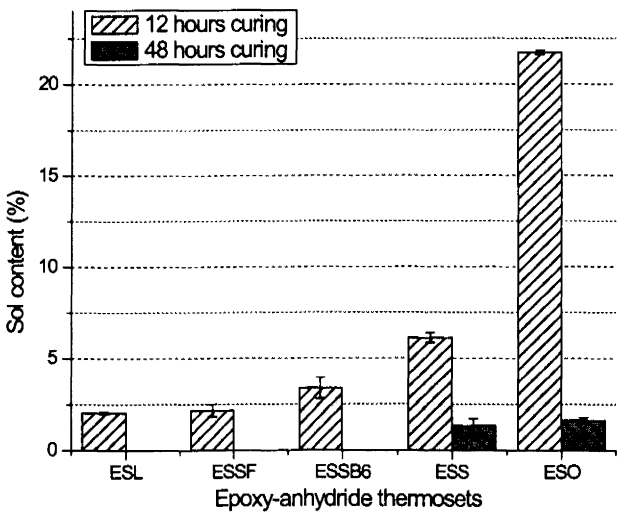

Figure 4.5. Sol content (wt %) of epoxy-anhydride thermosets that have been cured at 85°C for 12 and 48 hours

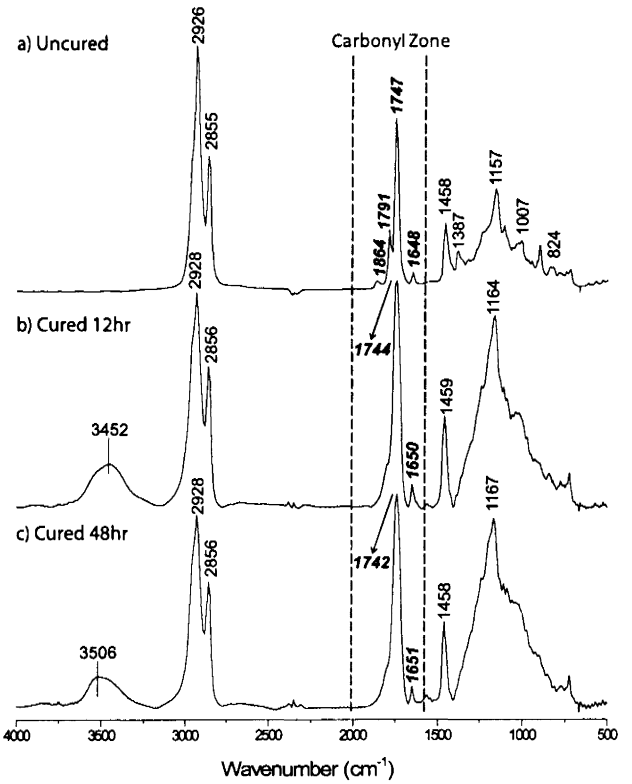

Figure 4.6. Overlaid FTIR spectra of samples from ESS/MHHPA/DBU system that has been cured at 85°C for 0, 12, and 48 hours

To characterize the composition of the sol fraction from Soxhelet extraction of the ESS-anhydride sample that has been cured for 12 hours, the sol fraction that is extracted by removing the solvent, and finally a viscous liquid with some tiny pieces of gel particles is obtained. The vacuum dried residual sample is solid. Figure 4.7 shows the overlaid FTIR spectra of the sol and gel samples. The carbonyl adsorption bands observed from the FTIR spectrum of the sol sample are: 1846 cm^{-1} (anhydride C=O, antisymmetric stretch), 1774 cm^{-1} (anhydride C=O, symmetric stretch), 1742 cm^{-1} (ester C=O, stretch), 1706 cm^{-1} (carboxylic acid C=O, stretch), and 1647 cm^{-1} (tertiary amide C=O, stretch). The broad adsorption band centered at 3193 cm^{-1} corresponds to the O-H stretching vibration of

carboxylic acids. The carbonyl adsorption bands observed from the FTIR spectrum of sol sample are: 1800 cm^{-1} (anhydride ester C=O, stretch), 1745 cm^{-1} (sucrose ester C=O, stretch), and 1648 cm^{-1} (tertiary amide C=O, stretch). The broad adsorption band centered at 3480 cm^{-1} corresponds to the O-H stretching vibration of hydroxyls. Therefore, the sol fraction contains unreacted anhydride and anhydride derived carboxylic acid, without the fatty acid chains that would also contain hydroxyls. Since the intensity of the tertiary amide carbonyl adsorption (1647 cm^{-1}) in the sol fraction is much larger than in the gel fraction, the sol fraction is mainly made of the oligomeric amides formed by MHHPA and DBU.

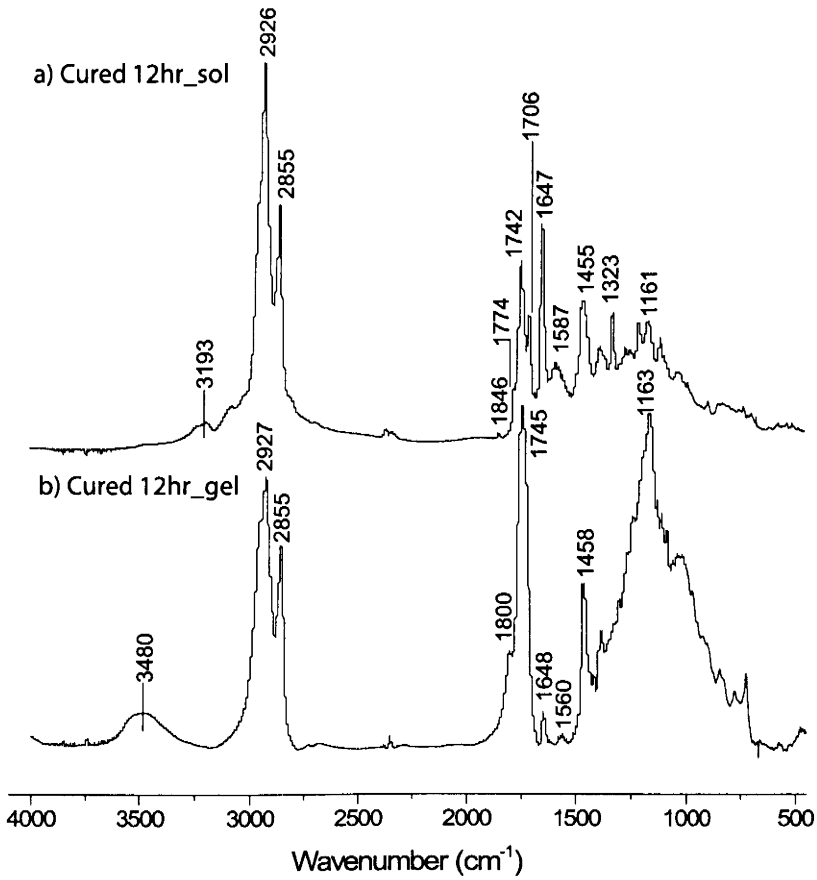

Figure 4.7. Overlaid FTIR spectra of sol and gel samples of ESS/MHHPA/DBU system that has been cured for 12 hours

4.4.5. Biobased Content

The US Department of Agriculture defined the biobased content of a product as the "amount of biobased carbon in the material or product as a percent of the weight (mass) of the total organic carbon in the product", and radiocarbon analysis in accordance with ASTM D 6866-05 is a reliable method for experimentally verifying the biobased content.[27]

The biobased content of the anhydride cured sucrose esters can be estimated from the definition given above. Sucrose esters are made of renewable raw materials—sugar and plant oil—but the MHHPA crosslinker and DBU catalyst are petrochemical-based products. Based on the above definition, ESEFAs are 100% biobased, and MHHPA and DBU are both 0% biobased. On a weight basis, an ESEFA is about 77.3% carbon, the MHHPA is 64.2% carbon, and the DBU is 70.9% carbon. A typical ESL/MHHPA/DBU system contains 10g of ESL, 4.6g of MHHPA, and 0.22g of DBU. Theoretically, when only carbon is considered in the system by weight, the biobased content is $\frac{10\times77.3\%}{10\times77.3\%+4.6\times64.2\%+0.22\times70.9\%}$, which comes out to and overall 71.3% biobased content. Using the same method of calculation, the biobased contents of epoxy-anhydride systems using ESSF, ESS, and ESSB6 theoretically are 75.6%, 77.2%, and 77.4%, respectively.

4.4.6. Tensile Properties

In general, the mechanical properties of epoxy-anhydride thermosets are dependent upon the structural nature of the anhydride,[20-23] the concentration of epoxides and anhydride,[20] and the type and concentration of catalyst.[9, 10, and 12] This study involves ESEFAs having an average degree of substitution of 7.7 (i.e. ESL, ESSF, and ESS) and 6 (i.e. ESSB6), and with different epoxidized fatty acids ranging from sixteen to eighteen

carbon atoms yielding varying epoxide content. The key difference among the fully substituted ESEFAs (i.e. ESL, ESSF, and ESS) is the epoxide content. However, ESSB6 differs from them not only in the epoxide content, but also in the hydroxyl content. ESEFAs differ from ESO in several important aspects: chemical structure, density, epoxide functionality, and the presence of hydroxyls.

Figure 4.8 shows the typical stress-strain curves of epoxy-anhydride thermoset thin films (0.1-0.16 mm) and the data of all samples is compiled in Table 4.3. The tensile properties of the ESEFA materials are significantly different than that of the ESO thermoset, with the ESEFA materials having a significantly higher modulus and tensile strength. The ESL thermoset is a brittle material, because it fails while the deformation is elastic. ESSF and ESSB6 thermosets are more flexible than the ESL thermoset, because each shows a well-defined yield point after the linear elastic portion and fails in plastic deformation. The ESS thermoset is more plastic and shows a lower modulus than both ESSB6 and ESSF thermosets. The ESO control thermoset exhibits rubbery behavior with the lowest modulus and tensile strength, and an extremely high elongation at break. There is no linear portion on its stress-strain curve to represent elastic deformation. Additionally, the tensile properties are proportional to the concentration of epoxides in ESEFAs, with the exception of ESSB6, which contains hydroxyls. Comparing the soyate based systems, it is seen that the modulus and tensile strength of ESS are greater than that of the ESO control by factors of 7 and 2, respectively. The properties of the ESL thermoset are even higher with a modulus 21 times greater and a tensile strength 4.5 times greater than that of the ESO thermoset.

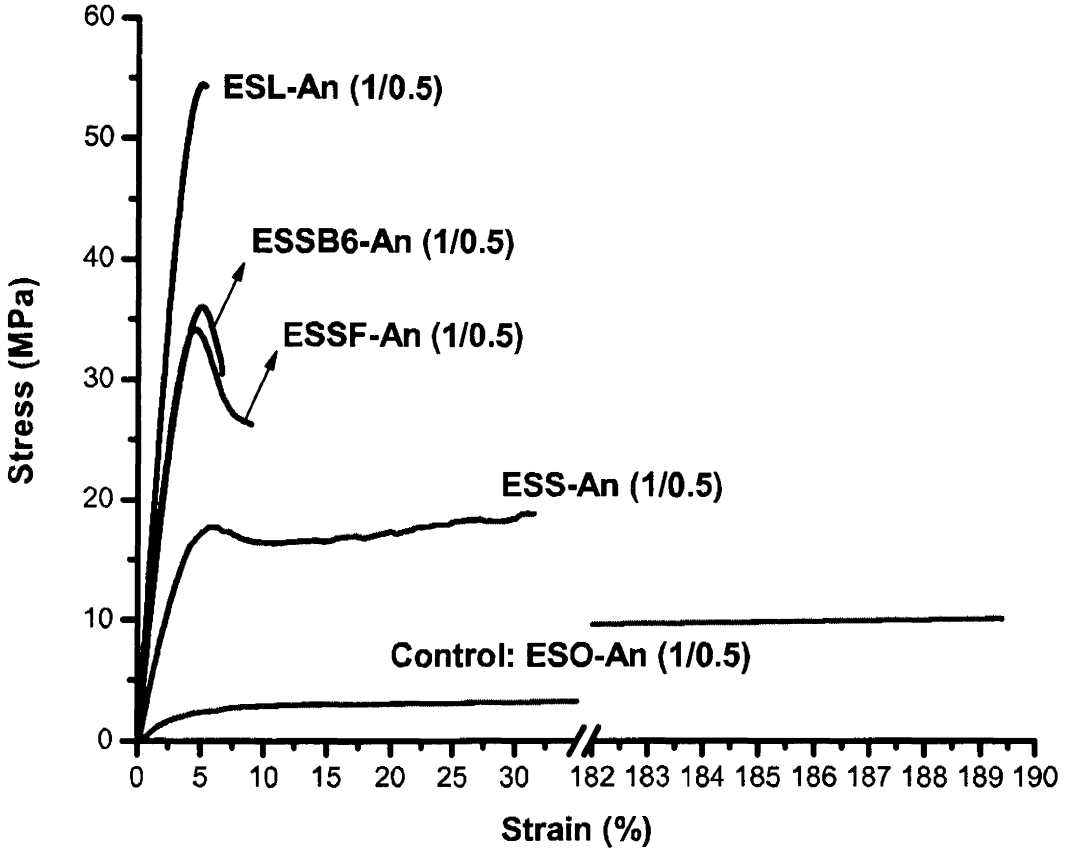

Figure 4.8. Typical stress-strain curves of epoxy-anhydride thermosetting thin films with an equivalent ratio of epoxide to anhydride of 1:0.5

Table 4.3. The tensile properties of epoxy-anhydride thermosetting thin films with an equivalent ratio of epoxide to anhydride of 1:0.5

Epoxy compounds	Modulus (MPa)	Tensile strength (MPa)	Elongation at break (%)	Tensile toughness (J) X 10^3
ESL	1395 ± 191	45.8 ± 5.4	5.7 ± 2.6	8.44 ± 3.5
ESSF	909 ± 179	31.5 ± 3.2	8.5 ± 2.7	11.5 ± 6.3
ESS	497 ± 38	20.3 ± 4.3	21.7 ± 7.8	29.4 ± 9.2
ESSB6	1002 ± 52	35.1 ± 3.6	5.4 ± 0.7	9.1 ± 3.8
ESO (Control)	65 ± 10	10.2 ± 2.5	167 ± 19	97 ± 13.8

Figure 4.9 shows the typical stress-strain curves of a series of soyate-based epoxy-anhydride thermoset thick samples (1.6-2.0 mm) with the data summarized in Table 4.4. It is observed that the epoxidized sucrose soyate thermosets have higher tensile strength and modulus than the ESO thermosets. Two different epoxide/anhydride ratios were explored and the change in stoichiometric ratio in the formulations demonstrates that the tensile properties of thermosets are proportional to the anhydride concentration. Higher amounts of anhydride result in higher modulus, higher tensile strength, and lower elongation at break.

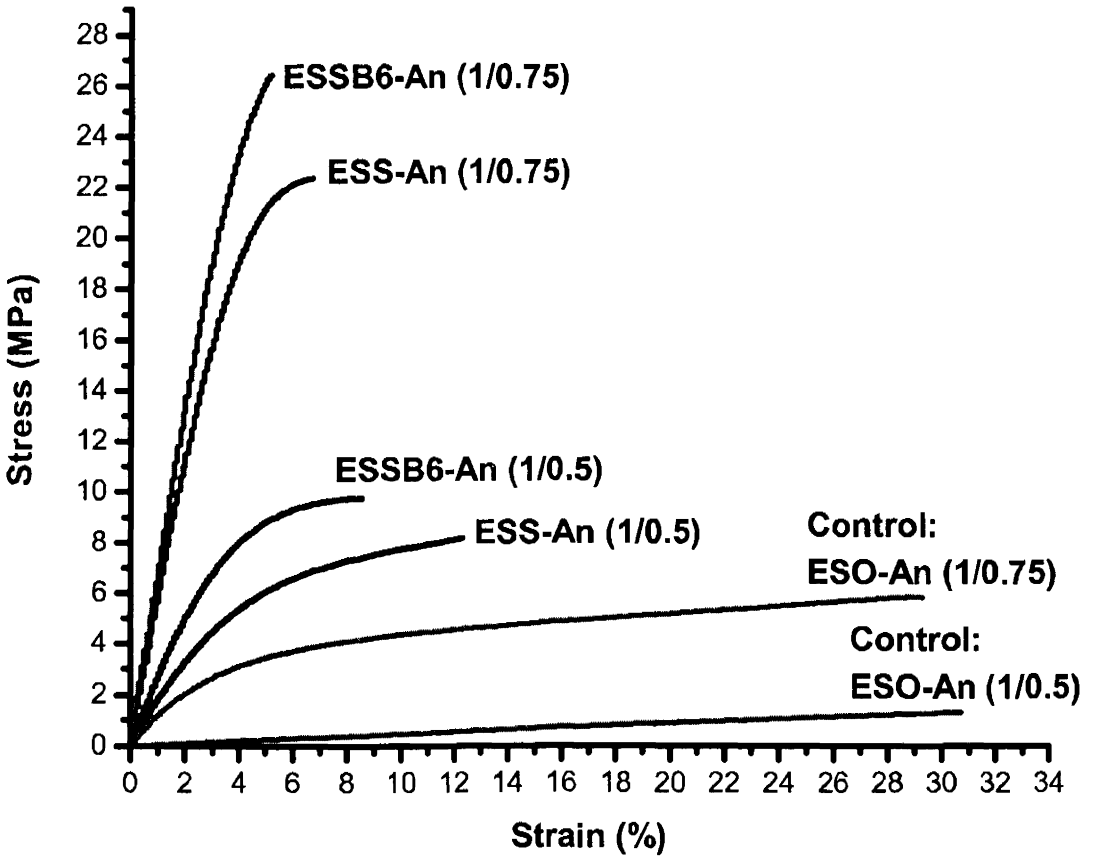

Figure 4.9. Typical stress-strain curves of epoxy-anhydride thermosetting thick samples with an equivalent ratio of epoxide to anhydride of 1:0.75 and 1:0.5

Table 4.4. The tensile properties of epoxy-anhydride thermosetting thick samples with an equivalent ratio of epoxide to anhydride of 1:0.75 and 1:0.5

Epoxy compounds	Epoxide/anhydride (equivalent ratio)	Modulus (MPa)	Tensile strength (MPa)	Elongation at break (%)
ESS	1:0.5	170.8 ± 12.8	7.8 ± 0.4	11.0 ± 1.8
ESS	1:0.75	595.1 ± 8.2	21.8 ± 1.4	6.2 ± 1.0
ESSB6	1:0.5	231.8 ± 40.5	8.9 ± 1.6	10.4 ± 2.2
ESSB6	1:0.75	643.9 ± 26.1	19.6 ± 5.7	4.5 ± 0.7
ESO (Control)	1:0.5	5.0 ± 0.16	1.2 ± 0.1	27.9 ± 3.6
ESO (Control)	1:0.75	97.7 ± 28.7	6.0 ± 0.5	28.7± 5.6

4.4.7. Dynamic Mechanical Properties

The DMA data is tabulated in Table 4.5. The glass transition temperatures (T_g) were determined as the temperatures at the maximum of the tan δ curves. The storage modulus E' in the rubbery plateau region, which is 60°C above T_g, is used to calculate crosslink density (ν_e) using $E' = 3\nu_e RT$: where E' is the storage modulus of thermoset in the rubbery plateau region at T_g+60 °C, R is the gas constant, and T is the absolute temperature.

Table 4.5. Dynamic mechanical properties and crosslink densities of epoxy-anhydride thermosets

Epoxy compounds	Epoxide/anhydride (equivalent ratio)	T_g (°C)	E' (MPa) at 20 °C	E' (MPa) at T_g+60 °C	ν_e (X 10^3 mol/mm^3)
ESL	1:0.5	103.7	1,500	20.7	1.84
ESL	1:0.4	78.5	619	9.5	0.85
ESL	1:0.3	46.9	141	6.6	0.59
ESSF	1:0.5	71.3	1,103	7.7	0.69
ESS	1:0.5	48.4	103	5.6	0.50
ESSB6	1:0.5	79.6	368	13.8	1.23
ESO (Control)	1:0.5	24.8	36	3.1	0.28

Figure 4.10 shows the temperature dependence of loss factor (tan δ) and storage modulus (E') of ESEFA thermosets formulated with an equivalent ratio of epoxide to anhydride of 1:0.5. For the fully substituted ESEFAs, Figure 4.10 (a) shows that the glass

transition temperatures span a range of 48 to almost 104°C and are in the order of $T_{g(ESL)} > T_{g(ESSF)} > T_{g(ESS)}$. A glass transition temperature as high as 104°C for a crosslinked epoxidized vegetable oil based material appears to be unprecedented. For the fully substituted ESEFAs, the epoxide equivalent weight (EEW) values are in the order of $EEW_{(ESL)} < EEW_{(ESSF)} < EEW_{(ESS)}$, thus the concentrations of epoxides are in the order of $[e]_{(ESL)} > [e]_{(ESSF)} > [e]_{(ESS)}$. Increasing epoxide concentration leads to increased crosslink density and an increase in the T_g. In addition, an increase in the amount of cycloaliphatic anhydride crosslinker used can also contribute to an increase in T_g. Figure 4.10 (b) shows that the storage moduli in the rubbery plateau region, and the calculated crosslink density values (Table 4.5), are in the order of $E'_{(ESL)} > E'_{(ESSF)} > E'_{(ESS)}$. While ESSB6 has the lowest epoxide content, the ESSB6 thermoset shows a higher T_g and E' than the ESSF and ESS thermosets. Therefore, the hydroxyl groups present in the ESSB6 contribute significantly to the polyester network formation in epoxy-anhydride curing.

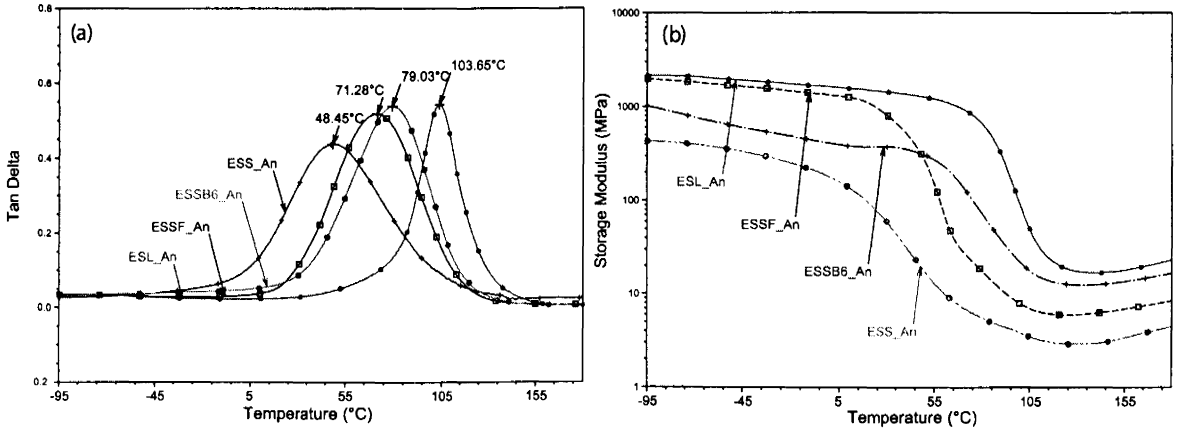

Figure 4.10. Temperature dependence of loss factor tan δ (a) and storage modulus E' (b) of epoxy-anhydride thermosets using ESEFAs (The equivalent ratio of epoxide to anhydride is 1:0.5)

Figure 4.11 shows the temperature dependence of tan δ and *E'* in a series of ESL thermosets formulated with equivalent ratios of epoxide to anhydride of 1:0.5, 1:0.4, and 1:0.3. Figure 4.11 (a) shows that the glass transition temperatures decrease as the amount of anhydride crosslinker decreases. Figure 4.11 (b) and Table 4 shows that the crosslink density decreases with decreasing anhydride crosslinker.

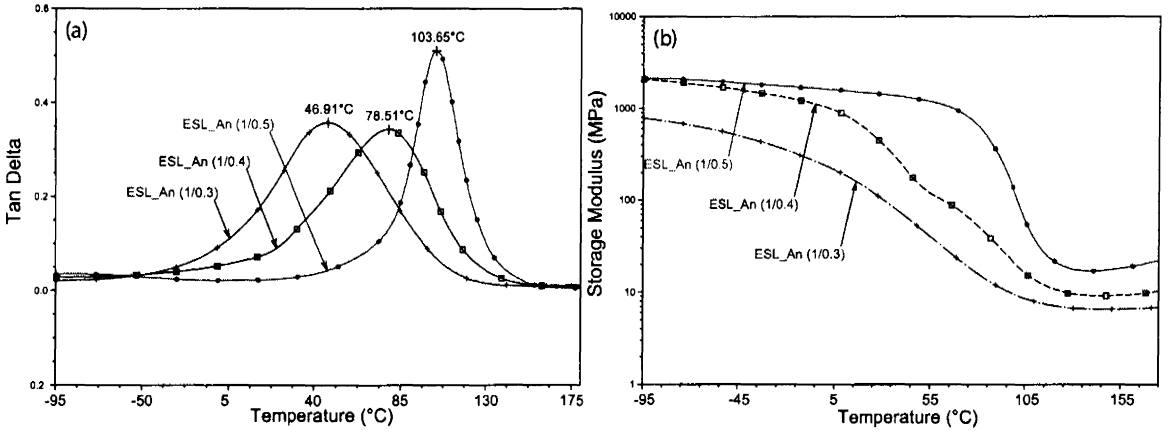

Figure 4.11. Temperature dependence of loss factor tan δ (a) and storage modulus *E'* (b) of ESL thermosets (The equivalent ratios of epoxide to anhydride are 1:0.5, 1:0.4, and 1:0.3)

Figure 4.12 shows a comparison of tan δ and *E'* for the soyate epoxy-anhydride thermosets from ESS, ESSB6, and the control ESO. The equivalent ratio of epoxides to anhydrides is 1:0.5. Figure 4.12 (a) shows that the glass transition temperatures are in the order of $T_{g(ESSB6)} > T_{g(ESS)} > T_{g(ESO)}$. Figure 4.12 (b) shows that the storage moduli in the rubbery plateau region are in the order of $E'_{(ESSB6)} > E'_{(ESS)} > E'_{(ESO)}$. The data in Figure 4.10 above demonstrated that the dynamic mechanical properties are proportional to the concentration of epoxides for the sucrose based epoxides. However, Figure 4.12 appears to show the opposite result and, although the ESO control has the highest epoxide content in

terms of EEW, it has the lowest epoxide functionality. Thus, the compact structure and high epoxide functionality of ESEFAs is shown to lead to a higher crosslink density, significantly impacting the mechanical properties of the resulting thermosets.

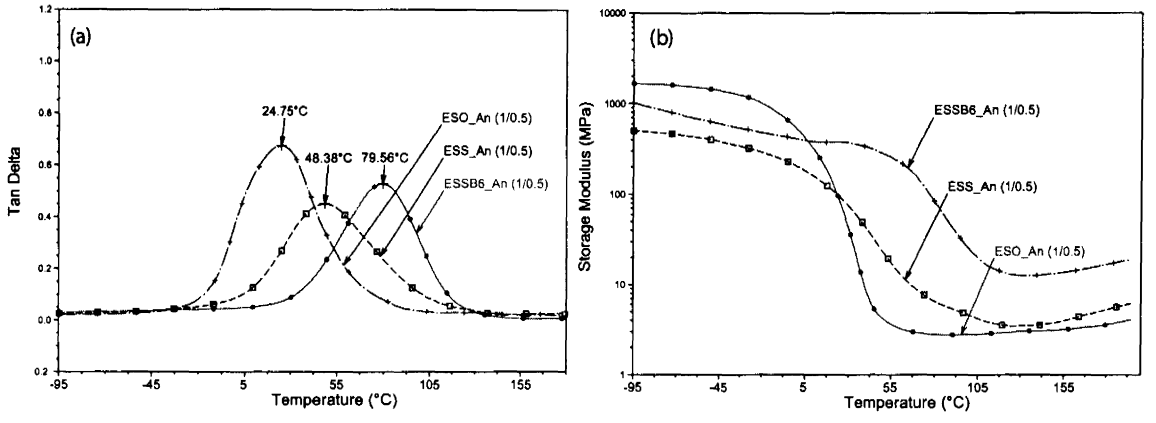

Figure 4.12. Temperature dependence of loss factor tan δ (a) and storage modulus *E'* (b) of soyate epoxy (i.e. ESS, ESSB6, and ESO) thermosets (The equivalent ratio of epoxide to anhydride is 1:0.5)

4.4.8. Nanomechanical Properties

The thick soyate epoxy thermosetting samples (1.6-2.0 mm) were nanoindented with the depth of penetration on the surface in the range of 0.5-5 μm. The slope of the load-displacement curve, *dP/dh*, upon unloading is indicative of the stiffness of the contact. The stiffness of the contact in this nanoindentation test is used to calculate the *reduced Young's modulus*, E_r. The *reduced modulus*, E_r, is related to *Young's modulus*, E_s, of the test sample through the following relationship from contact mechanics, where ν is the Poisson ratio and *i* and *s* refer to the indenter and sample, respectively:

$$\frac{1}{E_r} = \frac{(1 - v_i^2)}{E_i} + \frac{(1 - v_s^2)}{E_s}$$

Herein, for a diamond Berkovich indenter tip, E_i is 1140 GPa and ν_i is 0.07. Poisson's ratio of the sample, ν_s, generally varies between 0.3 and 0.5 for most polymeric materials. Therefore, the *reduced modulus*, E_r, is proportional to *Young's modulus*, E_s.

Indentation hardness is tested and given by the equation below, relating the maximum load to the indentation. The geometry of the indenter tip is used to calculate the indentation area, A_r. Thus, the tip-area calibration has been done periodically to check that whether the tip shows wear and gets deformed. A quartz standard has been indented to make sure that the reduced modulus is within specifications of 69.6 GPa.

$$H = \frac{P_{max}}{A_r}$$

The typical load-displacement curves of soyate epoxy thermosets in nanoindentation are shown in Figure 4.13. The equivalent ratio of epoxide to anhydride is 1:0.5. A comparison of the sample modulus and indentation hardness values of soyate epoxy thermosets are shown in Figure 4.14. The sample modulus values have been calculated from the testing results of reduced modulus values, assuming 0.34 as the Poisson's ratio of these materials. For the same epoxide/anhydride ratio, it is observed that the trends of nanomechanical properties observed herein agree with the results in the tensile tests. The sample moduli are in the order of $E_{s(ESSB6)} > E_{s(ESS)} > E_{s(ESO)}$.The indentation hardness are also in the order of $H_{(ESSB6)} > H_{(ESS)} > H_{(ESO)}$. However, the nanoindentation modulus and hardness of ESO thermoset with an equivalent ratio of epoxide to anhydride of 1:0.75 are higher than those of ESS and ESSB6 thermosets with an

equivalent ratio of epoxide to anhydride of 1:0.5. In the tensile tests, the ESO thermosets are softer and more rubbery than ESS and ESSB6 thermosets at both equivalent ratios. It should also be noted that the variation in the nanoindentation properties of the ESO sample at the equivalent ratio of epoxide to anhydride of 1:0.75 is high, possibly indicating inhomogeneity of the sample.

Tensile tests consider the bulk of thick samples (1.6-2.0 mm). Nanoindentation tests determine the nanomechanical properties on the surface with the depth of penetration 0.5-5 μm. Therefore, the depth of penetration is only about one thousandth of a sample's whole thickness. It is possible that the surface composition differs than the bulk composition due to preferential migration of one component to the surface during curing, resulting in different surface and bulk mechanical properties.

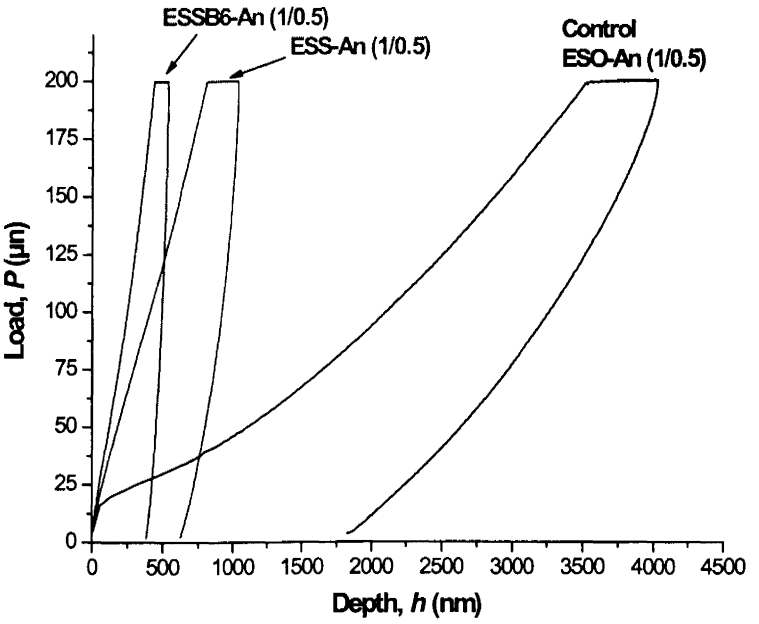

Figure 4.13. Typical load-displacement curves of soyate epoxy thermosets in nanoindentation tests (The equivalent ratio of epoxide to anhydride is 1:0.5)

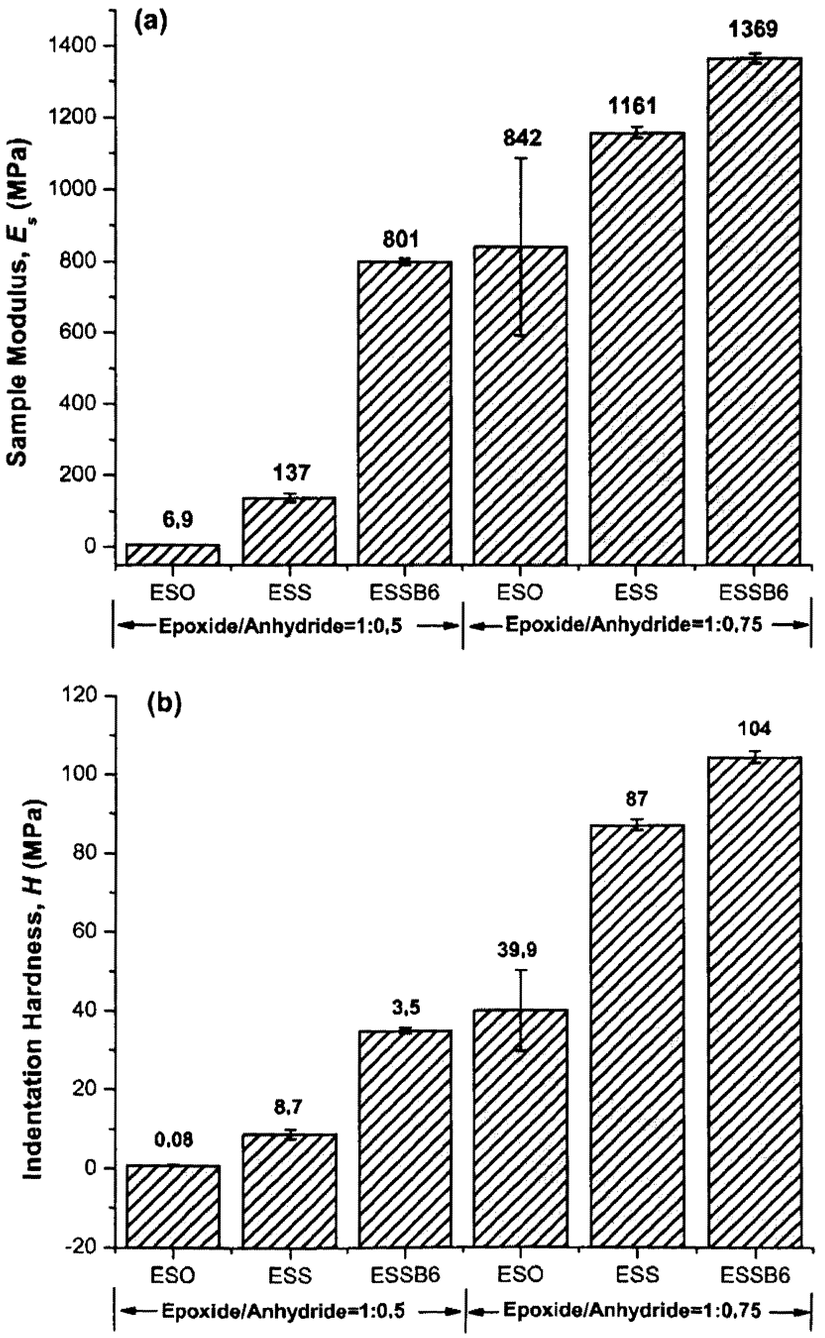

Figure 4.14. The sample modulus E_s (a) and indentation hardness H (b) of soyate epoxy thermosets in nanoindentation tests (The equivalent ratios of epoxide to anhydride are 1:0.5 and 1:0.75)

4.4.9. Thermal Stability

The thermal stabilities of the epoxy-anhydride thermosets were studied using TGA in nitrogen. Figure 4.15 displays the TGA thermograms as a function of temperature at a heating rate of 20°C/min. All of the epoxy-anhydride thermosets exhibit a one-step decomposition profile.

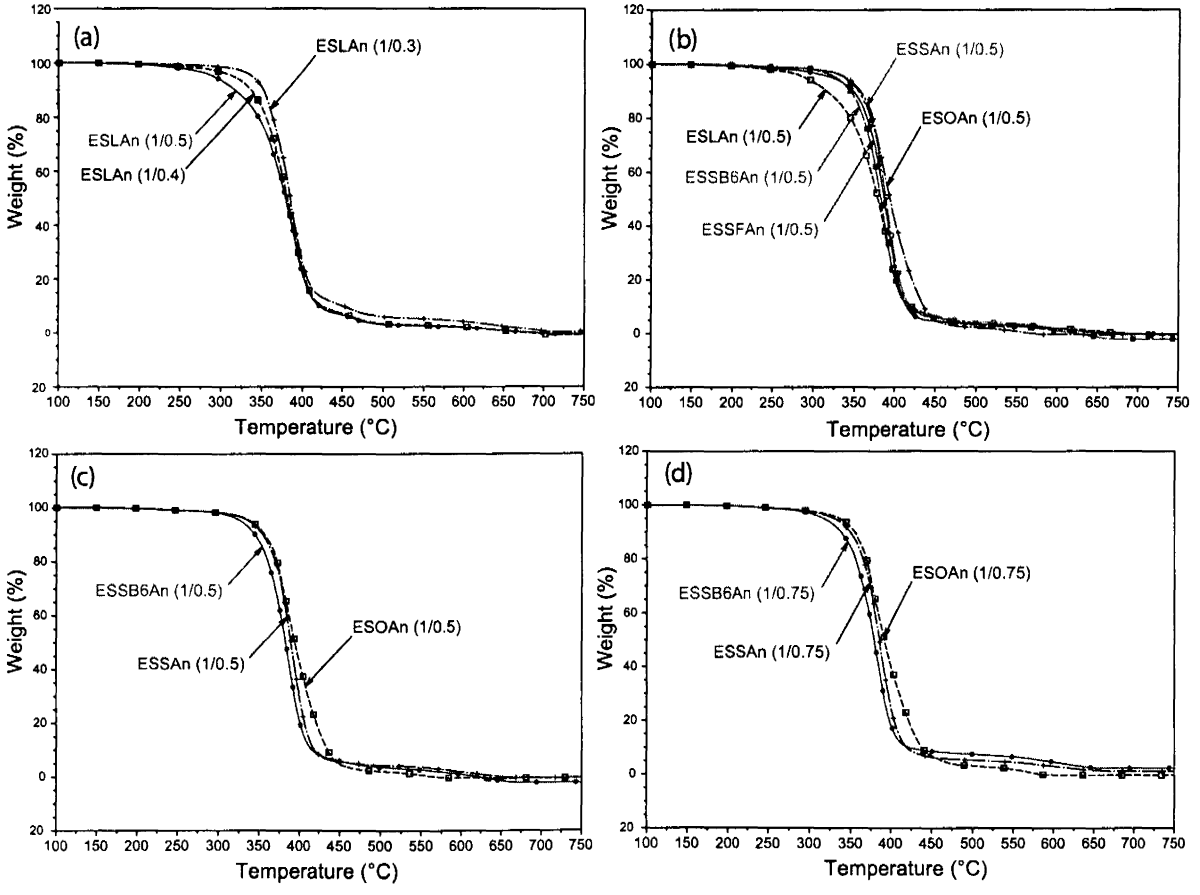

Figure 4.15. TGA curves of epoxy-anhydride thermosets in nitrogen at a heating rate of 20°C/min: (a) ESL thermosets in different epoxide/anhydride molar ratios; (b) ESEFAs thermosets with epoxide:anhydride=1:0.5; (c) Soyate epoxy thermosets with epoxide:anhydride=1:0.5; (d) Soyate epoxy thermosets with epoxide:anhydride=1:0.75

Figure 4.16 shows a comparison of the onset decomposition temperatures of the thermosets. In the ESL thermosets, the lower equivalent ratio of epoxides to anhydrides results in better thermal stability. In fully substituted ESEFA thermosets using epoxides:anhydride =1:0.5, the lower epoxide functionality results in better thermal stability. In the soyate epoxy thermosets, the thermal stability of thermoset using epoxides:anhydrides =1:0.5 is better than that of thermoset using epoxides: anhydrides =1:0.75. Thus, it is observed that the higher degree of polyester network formation results in poorer thermal stability. Thus, the thermal decomposition of epoxy-anhydride thermosets is mainly contributed by the decomposition of ester bonds.[28-29]

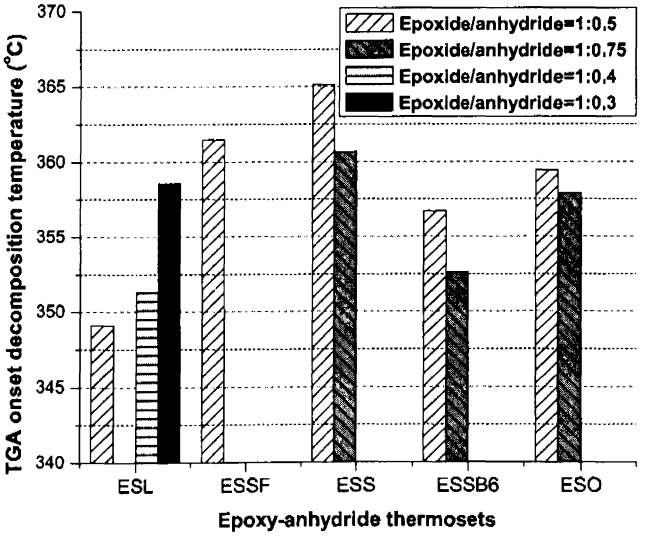

Figure 4.16. The onset decomposition temperatures of epoxy-anhydride thermosets

4.4.10. Coating Properties

Thermally cured coatings are used as factory applied finishes for a variety of products including metal furniture and fixtures, appliances, and food and beverage

containers. Thus, it was of interest to obtain an initial assessment of the coatings properties of the anhydride cured epoxy resins. Table 4.6 shows the properties of a series of epoxy-anhydride coatings. The ESL and ESSB6 coatings clearly show the effects of the stoichiometric ratio on the coating properties. The lower amount of anhydride results in more flexible and less hard coatings. ESSB6 coatings show similar hardness, flexibility and solvent resistance compared to the ESSF coatings. In summary, it is observed that the ESEFAs coatings show good hardness, good adhesion, good-to-excellent mechanical durability, and excellent solvent resistance. However, the ESO coating shows much lower hardness and solvent resistance, but higher flexibility due to its rubbery nature. Thus epoxidized soybean oil cannot be used as a suitable coating resin with this epoxy-anhydride curing method since they cure very slowly and the films are tacky.

Table 4.6. Properties of epoxy-anhydride coatings

Epoxy compounds	Epoxide/ anhydride (Eq. ratio)	Thickness (μm)	König pendulum hardness (sec.)	Pencil hardness (gouge)	Cross-hatch adhesion	MEK double rub resistance	Reverse impact (in-lb)	Mandrel bend (elongation -at-break)
ESL	1:0.5	110 ± 7.0	183	H	4B	>400	28	<2.5%
ESL	1:0.4	120 ± 17.7	90	F	5B	>400	>172	>28%
ESL	1:0.3	94.4 ± 5.4	47	B	5B	330	>172	>28%
ESSF	1:0.5	113 ± 3.3	118	F	5B	>400	32	4-4.5%
ESS	1:0.5	102 ± 8.4	63	2B	5B	>400	72	>28%
ESSB6	1:0.625	99.8 ± 2.5	123	HB	3B	>400	100	>28%
ESSB6	1:0.5	112 ± 4.5	115	B	5B	>400	80	>28%
ESSB6	1:0.4	99.5 ± 4.4	39	2B	2B	320	>172	>28%
ESO (Control)	1:0.5	108 ± 4.8	22	<EE	5B	25	>172	>28%

4.4.11. Structure-property Relationships

In this study, epoxidized sucrose esters show much better performance than epoxidized soybean oil in epoxy-anhydride curing. The thermosets using epoxidized sucrose esters are hard and ductile with high modulus, and exhibit excellent coating performance. However, thermosets using ESO are highly flexible and rubbery with low modulus, and exhibit poor coating performance.

ESO has the same epoxide content as ESSF that has the second highest epoxide content in ESEFAs. However, the epoxide functionalities of the fully substituted ESEFAs per molecule are 11-15, and the functionality of ESO per molecule is 4.3. The high epoxide functionality of the ESEFAs can lead to rapid gelation and high crosslink densities in crosslinking. The sol contents of ESEFA thermosets are also much lower than that of the ESO thermoset, with the equivalent ratio of epoxides to anhydrides as 1:0.5 and curing at 85°C for 12 hours.

ESEFAs have higher densities than ESO, due to the fact that the density of sucrose (d=1.587 g/cm^3) is higher than that of glycerol (d=1.261 g/cm^3). While there is no simple correlation between the density and the hardness of an organic material, the mass density of a polyester thermoset material made of carbon, hydrogen and oxygen atoms definitely contributes to the hardness. The rigid core of the sucrose and the compact structure of ESEFA impart hardness to the thermoset and this factor will be further explored in the following chapter.

Within soyate-based epoxy compounds, both ESSB6 and ESS thermosets are much better than the ESO thermoset, and the ESSB6 thermoset is not only better than the ESS thermoset, but also as good as the ESSF thermoset. In DSC, it has been observed that the

ESSB6-anhydride curing starts 15°C earlier, but ends 24°C later than the ESS-anhydride curing, and the total heat of reaction of the ESSB6-anhydride curing is 70 J/g higher than that of the ESS-anhydride curing. Although the degree of cure of the ESSB6-anhydride curing is 9% lower than that of the ESS-anhydride curing, the sol content of the ESSB6 thermoset is only 2.7% lower than that of the ESS thermoset. The FTIR spectrum of the sol fraction from Soxhlet extraction of the ESS thermoset demonstrates that the sol content is mainly from the anhydride. Due to the faster rate of reaction in the polyester formation, the hydroxyls of ESSB6 enable faster incorporation of the anhydrides than the alkoxide anions of ESS, which improves the incorporation of anhydrides.

4.5. Conclusions

A series of novel biobased polyester thermosets were developed using epoxidized sucrose esters of fatty acids (ESEFAs) as the epoxy compounds, MHHPA as the hardener, and DBU as the amidine catalyst. Polyester thermosets with high biobased content (71-77% in theory) were obtained having excellent properties, in the equivalent ratio of epoxides to anhydrides of 1:0.5. ESEFAs are novel highly functional biobased epoxy compounds. They have the potential to provide a revolutionary impact in some applications replacing petrochemical-based epoxy compounds having external epoxides. The compact structure of ESEFAs contributes to the hardness of thermoset. The high epoxide functionality leads to rapid gelation and crosslinking in curing. ESEFAs also benefit from the presence of sucrose hydroxyls in anhydride curing. Due to the impressive performance of ESSB6, we discovered a method for using soyate-based sucrose esters with a lower degree of substitution. Due to the high performance achieved, this technology may have wide-

ranging applications in areas where thermally cured materials are used such as in protective coatings, structural adhesives, and composites.

4.6. References

1. Karmalm, P.; Hjertberg, T.; Jansson, A.; Dahl, R. *Polym. Degrad. Stab.* **2009**, *94*, 2275.
2. Fenollar, O.; García, D.; Sánchez, L.; López, J.; Balart, R., *Eur. Polym. J.* **2009**, *45*, 2674.
3. Bueno-Ferrer, C.; Garrigós, M. C.; Jiménez, A. *Polym. Degrad. Stab.* **2010**, *95*, 2207.
4. Miyagawa, H.; Misra, M.; Drzal, L. T.; Mohanty, A. K. *Polym. Eng. Sci.* **2005**, *45*, 487.
5. Lligadas, G.; Ronda, J. C.; Galià, M.; Cádiz, V. *J. Polym. Sci., Part A: Polym. Chem.* **2006**, *44*, 5630.
6. Lligadas, G.; Ronda, J. C.; Galià, M.; Cádiz, V. *J. Polym. Sci., Part A: Polym. Chem.* **2006**, *44*, 6717.
7. Ereaux, L. P.; Craig, G. E. *Canad. M. A. J.* **1949**, *61*, 361.
8. Pan, X.; Sengupta, P.; Webster, D. C. *Green Chem.* **2011**, *13*, 965.
9. Heise, M. S.; Martin, G. C. *Macromolecules* **1989**, *22*, 99.
10. Fedoseev, M. S.; Zvereva, I .V. *Russ. J. Appl. Chem.* **2008**, *81*, 836.
11. Rocks, J.; Rintoul, L.; Vohwinkel, F.; George, G. *Polymer* **2004**, *45*, 6799.
12. Montserrat, S.; Flaque, C.; Calafell, M.; Andreu, G.; Málek, J. *Thermochim. Acta* **1995**, *269/270*, 213.

13. Musto, P.; Abbate, M.; Ragosta, G.; Scarinzi, G. *Polymer* **2007**, *48*, 3703.

14. Boey, F .Y. C.; Qiang, W. *Polymer* **2000**, *41*, 2081.

15. Trappe, V.; Burchard, W. *Macromolecules* **1991**, *24*, 4738.

16. Park, W. H.; Lee, J. K.; Kwon, K. J. *Polym. J.* **1996**, *28*, 407.

17. Fisch, W.; Hofmann, W.; Koskikallio, J. *J. Appl. Polym. Sci.* **1956**, *6*, 429.

18. Matějka, L.; Lövy, J.; Pokorný, S.; Bouchal, K.; Dušek, K. *J. Polym. Sci.: Polym. Chem. Ed.* **1983**, *21*, 2873.

19. Foix, D.; Yu, Y.; Serra, A.; Ramis, X.; Salla, J. M. *Eur. Polym. J.* **2009**, *45*, 1454.

20. Komata, M.; Watanabe, S. *Kobunshi Ronbunshu* ***1992***, *49*, 601.

21. Komata, M.; Watanabe, S. *Kobunshi Ronbunshu* ***1992***, *49*, 609.

22. Mauri, A. N.; Riccardi, C. C. *J. Appl. Polym. Sci.* **2002**, *85*, 2342.

23. Rösch, J.; Mülhaupt, R. *Polym. Bull.* **1993**, *31*, 679.

24. Gerbase, A. E.; Petzhold, C. L.; Costa, A. P. O. *J. Am. Oil Chem. Soc.* **2002**, *79*, 797.

25. Takahashi, T.; Hirayama, K.; Teramoto, N.; Shibata, M. *J. Appl. Polym. Sci.* **2008**, *108*, 1596.

26. Tanrattanakul, V.; Saithai, P. *J. Appl. Polym. Sci.* **2009**, *114*, 3057.

27. Norton, G. A.; Devlin, S. L. *Bioresour. Technol.* **2006**, *97*, 2084.

28. Pohl, H. A. *J. Am. Chem. Soc.* **1951**, *73*, 5660.

29. Gupta, A. P.; Ahmad, S.; Dev, A. *Polym.Plast. Tech. Engr.* **2010**, *49*, 657.

CHAPTER 5. IMPACT OF STRUCTURE & FUNCTIONALITY OF CORE POLYOL IN HIGHLY FUNCTIONAL BIOBASED EPOXY RESINS

5.1. Abstract

Highly functional epoxy resins were prepared using dipentaerythritol (DPE), tripentaerythritol (TPE), and sucrose as core polyols that were highly substituted with epoxidized soybean oil fatty acids, and the impact of structure and functionality of core polyol on the properties of macromolecular resins and their epoxy-anhydride thermosets was explored. The chemical structures, functional groups, molecular weights and compositions of epoxies were characterized using nuclear magnetic resonance (NMR) spectroscopy, Fourier-transform infrared (FTIR) spectroscopy, gel permeation chromatography (GPC), and matrix-assisted laser desorption/ionization mass spectrometry (MALDI MS). The physical properties of epoxies were studied in bulk viscosity, intrinsic viscosity, and density measurements. Crosslinked with dodecenyl succinic anhydride (DDSA), epoxy-anhydride thermosets were evaluated in differential scanning calorimetry (DSC), dynamic mechanical analysis (DMA), tensile tests, and tests of coating properties. Epoxidized soybean oil (ESO) was used as a control. Overall, sucrose based thermosets exhibited the highest moduli, most rigid and ductile performance while maintaining the highest biobased content. DPE/TPE based thermosets showed modestly better thermosetting performance than the control ESO thermoset.

5.2. Introduction

Drying oils (e.g. linseed oil), naturally occurring glycerol triesters of unsaturated fatty acids, have been used as a key component of coating binder systems for centuries. By concerning with the different concepts relating to the drying properties, a considerable volume of research was undertaken to improve and modify drying oils in the early 20th century, including bodied oils, brown oils, maleic anhydride-treated oils, and copolymer-type oils (e.g. styrenation), etc.[1] As one of the methodologies, reconstituted oils were prepared by substituting glycerol with a new polyol having more hydroxyls. This method of re-esterification was a logical development based on Carothers' theory of functionality.[2] Bradley further developed this theory in the drying mechanism of drying oils and resins, and experimentally proposed that drying oils were improved based upon the functionality concept that the number of double bonds per molecule in new ester is higher than the corresponding natural glycerol triester.[3-4]

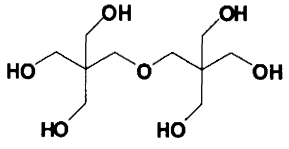

Dipentaerythritol (d=1.373 g/cm^3)

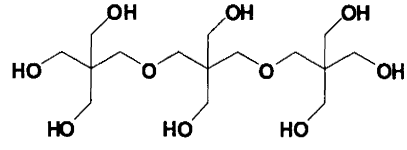

Tripentaerythritol(d=1.301 g/cm^3)

Figure 5.1. Molecular structures of dipentaerythritol (DPE) and tripentaerythritol (TPE)

Pentaerythritol (PE) and ethers of PE (i.e. dipentaerythritol (DPE), and tripentaerythritol (TPE)) once received a significant attention as high functionality polyols (Figure 5.1). In the 1940s, PE-type esters of unsaturated fatty acids had been prepared and

documented as new esters that crosslinked more easily than the corresponding glycerol triesters.[5] During the 1930s to 1960s, a variety of chemical pathways had been explored to prepare DPE and TPE, but they were mainly produced as the byproducts of condensation reaction of formaldehyde with acetaldehyde to prepare PE.[6, 7] Therefore, although DPE/TPE esters provided protective coatings with definitely superior properties, the small volumes available had discouraged interest in large-scale production. Currently, catalytic dehydration of PE has been employed as a new synthetic strategy to facilitate the preparation of DPE and TPE.[8] Today DPE has been widely used in high-solid solventborne alkyd coating resins as a branching agent, or as the core of hyperbranched polyesters.[9-11]

Glucose, fructose, and sucrose are naturally-occurring high functionality polyols. However, esters using the mono-/di-saccharides didn't have practical value before the 1960s, because this family of natural polyols caramelize and char at the high temperatures used in esterification. Sucrose esters of unsaturated fatty acids were first explored as coating vehicles in the 1960s, and they were prepared using base-catalyzed transesterification between fatty acid methyl esters (FAME) and sucrose.[12-13] While these early studies indicated that the highly substituted sucrose esters had a low viscosity, rapid air-drying time and good coating properties, obtaining a high degree of substitution of fatty acids on the sucrose proved to be challenging. In the 1970s, sucrose esters with a full substitution had been developed by Procter & Gamble (P&G) Chemicals as a fat substitute, called Olestra or known as the brand name Olean. In the late 1990s, Olestra became infamous in the U.S for its unpleasant side effects. In 2002, sucrose esters under the brand name Sefose were commercialized by P&G Chemicals with a focus on marketing to the lubricant and paint industry. Due to the viscosities of Sefose sucrose esters (300-400

mPa·s), Sefose-based alkyd resin technology won the 2009 Presidential Green Chemistry Award from the U.S. Environmental Protection Agency (EPA), due to the formulation of coatings having less than half the VOCs (Volatile Organic Compounds) of traditional solventborne alkyd coatings.[14] In our group, research has been carried out to develop sucrose esters as binders in coating systems. The alkyd use of sucrose esters had been extended using acetoacetate chemistry.[15] The use of sucrose esters have been expanded beyond their use as alkyds by epoxidation.[16] Epoxidized sucrose esters (ESEs) have been used as the resins for cationic UV-curable coatings.[17] The epoxy-anhydride curing of ESEs has been studied, and the performance of ESE based thermosets has been shown to be exceptional in comparison with epoxidized soybean oil (ESO).[18]

Instead of serving as stabilizers and plasticizers for poly(vinyl chloride), ESO has been explored to prepare biobased thermosets in epoxy-anhydride curing with dicarboxylic acid anhydrides.[19-20] However, the ESO-anhydride thermosets prepared using the anhydrides of hexahydrophthalic acid, succinic acid, and norbornene dicarboxylic acid were highly flexible and rubbery materials with glass transition temperatures (T_g) below room temperature. The aromatic anhydrides (e.g. maleic anhydride, phthalic anhydride) could produce the hard and ductile thermoset materials with the T_g values higher than room temperature. Due to the softness, ESO-anhydride system has to fit in the new roles, either as reactive toughening agents for rigid thermoset plastics (i.e. phenolic resins)[21], or composite binders that incorporates with reinforcing fillers (e.g. fibers, organoclay).[22-23]

The properties of the epoxidized sucrose esters have been initially compared to the corresponding glycerol triester.[18] However, the two large differences between sucrose and glycerol—notably, their chemical structure and hydroxyl functionality—makes it

challenging to distinguish the impact of these two variables on the epoxidized polyol esters and their thermoset products. The gap between sucrose and glycerol polyols can be filled using the polyols DPE and TPE, having functionalities of six and eight hydroxyls. For example, the difference between the fully substituted sucrose ester and the corresponding TPE ester is mainly in the structure of core polyol, since they have the same number of hydroxyls. In this study, epoxidized polyol ester resins have been prepared using sucrose, DPE, and TPE as the core polyols, and the average degree of substitution of fatty acids on polyols have been well controlled (Figure 5.2). The impact of the structure and functionality of the core polyols on the properties of epoxy resins and their epoxy-anhydride thermosets have been studied. To the best of our knowledge, epoxidation of reconstituted oils has not been reported and no one has explored these resins in an epoxy-anhydride curing system.

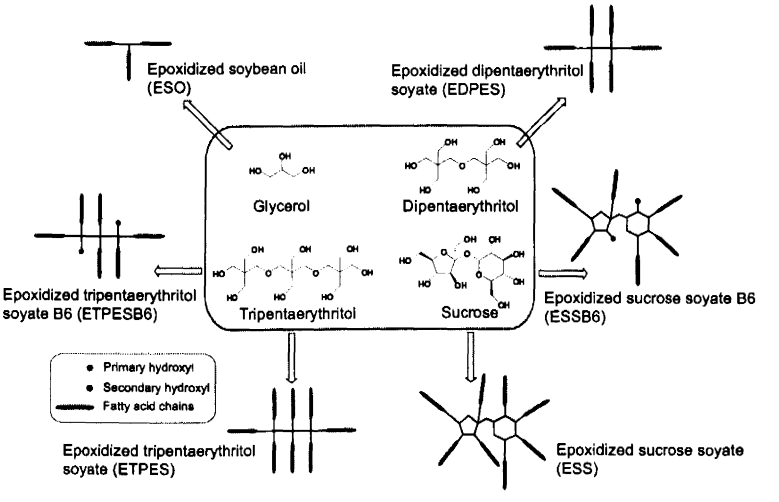

Figure 5.2. Glycerol, dipentaerythritol, tripentaerythritol, and sucrose were used as core polyols in the polyol esters of epoxidized soybean oil fatty acids

5.3. Experimental

5.3.1. Raw Materials

Vikoflex 7170 epoxidized soybean oil was supplied by Arkema Inc. (Philadelphia, PA). Sucrose esters of soybean oil fatty acids, sucrose soyate, were provided by Procter & Gamble Chemicals (Cincinnati, OH). Soybean oil was provided by Cargill Industrial Oils & Lubricants (Chicago, IL). Methanol (ACS grade, ≥99.8%) was purchased from VWR International (West Chester, PA). Potassium hydroxide (technical grade) was purchased from Mallinckrodt Baker, Inc. (Phillipsburg, NJ). Dipentaerythritol (technical grade), tripentaerythritol (technical grade), dibutyltin oxide (98%), dibutyltin dilaurate (95%), dodecenylsuccinic anhydride (DDSA, mixture of isomers), and 1,8-Diazabicyclo[5.4.0]undec-7-ene (≥99.0% GC) were purchased from Sigma-Aldrich Inc. (St. Louis, MO). Acetic acid (ACS reagent, ≥99.7%), diethyl ether (ACS reagent, ≥99.0%), hydrogen peroxide (50 wt% solution in water), Amberlite IR-120H ion-exchange resin, sodium carbonate (ACS reagent), and anhydrous magnesium sulfate (reagent grade, ≥97%) were also purchased from Sigma-Aldrich, Inc. (St. Louis, MO). All materials were used as received without further purification.

5.3.2. Preparation of DPE/TPE Esters of Soybean Oil Fatty Acids

The synthesis of fatty acid methyl ester (FAME) was carried out in a 500 mL four-neck flask equipped with a mechanical stirrer, nitrogen inlet, thermocouple, and reflux condenser. Soybean oil (200 g, 0.230 mol), and potassium hydroxide (9.3 g, 0.166 mol) in methanol (110g, 3.45 mol) solution were charged into the flask, and stirred and heated at 65°C in nitrogen purge. The reaction was allowed to run for 3 hours, and finally a

transparent brownish red solution was obtained. After it was cooled down to room temperature, the solution was transferred into a separatory funnel. A large amount of distilled water was charged into the funnel, and the reaction mixture was separated into two phases. The upper phase consisted of FAME, and the lower phase contained the glycerol, monoglyceride, possible diglyceride, potassium hydroxide, and the excess of methanol. The upper FAME layer was successively purified by washing with distilled water until the water layer was clear. The residual water inside of FAME was eliminated by treatment with anhydrous magnesium sulfate, followed by filtration. Finally, FAME were obtained as a light yellow liquid. The recovered yield was 65-70% due to the loss of monoglyceride and diglyceride in water purification.

DPE/TPE soyate, DPE/TPE ester of soybean oil fatty acids, were prepared via transesterification between DPE/TPE and FAME, using organotin catalyst. The degree of substitution was controlled by the feed ratio of FAME to DPE/TPE. Herein, the synthesis of fully substituted tri-pentaerythritol soyate (TPES) was used as an example. The synthesis is carried out in a 250 mL four-neck flask equipped with a mechanical stirrer, nitrogen inlet, thermocouple, condenser, and Dean-Stark trap.TPE (25 g, 0.067 mol), FAME (157 g, 0.537 mole), dibutyltin dilaurate (0.091g, 0.144 mmol) and dibutyltin oxide (0.091g, 0.366mmol) were charged into the flask, and stirred and heated at 225°C in nitrogen purge. As the byproduct of the transesterification, methanol was collected in the Dean-Stark trap. The reaction was allowed to run for 7 hours, and finally tripentaerythritol soyate was obtained as a yellow liquid resin.

5.3.3. Preparation of Epoxidized Soyate Compounds

Epoxidation reactions were carried out in a 500 mL four-neck flask, equipped with a mechanical stirrer, nitrogen inlet, thermocouple and addition funnel. Unsaturated soyate compounds were epoxidized using peracetic acid generated *in situ* from hydrogen peroxide and acetic acid, in the presence of Amberlite IR 120H as catalyst. As reported previously, good conversion of double bonds to internal epoxides was achieved in the molar ratio of acetic acid: hydrogen peroxide (H_2O_2): double bond of 0.5:2:1, catalyst concentration of 20 wt% (based on resin) at 60°C.[16] Herein, epoxidization of the fully substituted tripentaerythritol soyate (TPES) is shown as an example. The mixture of TPES (200 g, 81.51mmol) containing 0.984 mol double bonds, acetic acid (29.5g, 0.492 mol), and Amberlite IR 120H (40 g) were stirred and heated at 60°C under nitrogen purge protection. Hydrogen peroxide (50 wt% aqueous solution, 134g, 1.97 mol) was added dropwise using an addition funnels at a rate so that the reaction temperature was controlled in the range of 60-65°C. After the completion of the hydrogen peroxide addition, the reaction was stirred at 60°C for 30 minutes. The product was purified through the steps of extraction, water removal, filtration, and rotavapping.[16] Finally, a transparent viscous liquid was obtained as the epoxidized tripentaerythritol soyate (ETPES). Recovered yields were all about 97 percent.

5.3.4. Characterization on Epoxidized Soyate Compounds

Molecular weight was determined using a Waters 2410 gel permeation chromatograph equipped with refractive index detector. Polystyrene standards were used for calibration. A 1.5% sample solution in THF using a flow rate of 1 ml/min was used.

MALDI-TOF mass spectra were recorded on a Bruker Ultraflex II spectrometer equipped with a 1.85 m linear flight tube and a Smart beam laser. All mass spectra were obtained in positive ion and linear mode. Samples were dissolved in THF (1 mg/mL), and α-cyano-4-hydroxycinnamic acid (10 mg/mL in THF) was used as matrix, and trifluoroacetic acid (0.1 wt% in water) was used as the dopant. A mixture of 10 μL of the matrix solution, 2 μL of the dopant, and 2 μL of the polymer solution was prepared and a 2 μL sample was spotted on the target plate. All data were processed using Flex analysis and PolyTools software package. FTIR measurements were done with a Thermo Nicolet 8700 FTIR spectrometer. Samples were prepared in THF solution with the concentration of 4 mg/ml. Then, a 200 μL drop of the solution was deposited by micropipette on the center of the potassium bromide salt crystal and the drop was naturally spread out. After the evaporation of the THF, a thin layer of sample film was formed on the KBr crystal. Spectra acquisitions were based on 32 scans with data spacing of 4.0 cm^{-1} in the range of 4000–500 cm^{-1}. NMR measurements were done at 23°C using a JEOL-ECA (400 MHz) NMR spectrometer with an autosampler accessory. All measurements were made using $CDCl_3$ as solvent. The data was processed using the Delta software package. The bulk viscosities of samples were measured using a Brookfield Viscometer (DV-II+ Pro) at 21°C. Intrinsic viscosity [η] of the materials was measured in THF with a Cannon-Fenske viscometer (size 50) at 25°C. The concentration of solution was 3.7-9.0 g/100 mL, and the relative viscosity η_r was controlled in the range of 1.1-1.6. The extrapolations of reduced viscosity and inherent viscosity were averaged to yield the intrinsic viscosity. The densities of samples were measured using a BYK-Gardner Weight Per Gallon Cup at 25°C, referring to ASTM D 1475. The Midget Cup having a capacity of 8.32 grams of water at 25°C was used. The net weight of the fluid

sample in grams equals the sample's density in pounds per U.S. gallon, which is converted into grams/mL. Iodine values were determined according to ASTM D 5768. Epoxide equivalent weight (EEW, g/eq.) of the epoxy products was determined by epoxy titration according to ASTM D 1652.

5.3.5. Epoxy-anhydride Formulation and Curing

The equivalent ratio of epoxides to anhydrides was 1:0.5 and 1:0.75. DBU was used at 1.5 wt% (based on the total weight of resins). Herein, EPETS in the epoxide/anhydride equivalent ratio of 1:0.5 was used as an example. EPETS (20 g, 7.52 mmol) containing 76.6 mmol epoxides was mixed with DBU (0.45 g, 2.95 mmol) amidine catalyst firstly, and DDSA (10.3 g, 3.83 mmol) was added secondly.

Coatings were cast on cleaned steel panels (QD panels from Q-panel) and glass panels using a draw-down bar with a gap of 8 mils. Anhydride curing was done for 5 hours at 120°C. The thermosetting thin films (0.08-0.12 mm) on glass panels were carefully peeled off to make the specimens for DMA and tensile testing.

5.3.6. Characterization on Epoxy-anhydride Thermosets

A DSC Q1000 from TA Instruments (New Castle, DE) with an autosampler was used to determine the glass transition temperature (T_g). Samples were subjected to a heat–cool–heat cycle from -90 to +200°C by ramping at 10 °C/min for both heating and cooling cycles. The second heating cycle was used to characterize the samples. Dynamic mechanical properties of thermosetting films were measured in tension mode using Q800 DMA from TA Instruments (New Castle, DE). Rectangular specimens with dimensions of

20 mm length, 5 mm width, and 0.08-0.12 mm thickness were prepared. The measurements were performed from -110 to +200°C at a heating rate of 10°C/min and frequency of 1 Hz. The glass transition temperature (T_g) was determined as the temperature at the maximum of tan δ vs. temperature curve. The storage modulus (E') in the rubbery plateau region was determined at 60°C above the glass transition temperature. The rectangular specimens were also used in tensile tests. The tensile tests were carried out at 25°C using Instron 5542 (Norwood, MA). The grip separation distance of the tensile testing was 25.4 mm, and the effective gauge length was 20.4 mm. The crosshead speed was 0.1% elongation/sec. (0.0204 mm/sec.). The tensile properties were reported as the average of 5 measurements taken at different specimens and the uncertainty was the standard deviation. Pencil hardness was measured using ASTM D 3363, and gauge hardness was recorded as the pencil hardness of coating. MEK (Methyl ethyl ketone) double rubs test was carried out following ASTM D 5402 modified with hammer to assess the solvent resistance of the cured coatings. A 1.65 lb hammer covered with four layers of folded cheesecloth on the hammerhead was soaked in MEK for rubbing. The cheesecloth was re-wetted with MEK after every 100 double rubs. The number of MEK double rubs was recorded as the mar (scratch) resistance.

5.4. Results and Discussion

5.4.1. Synthesis of Epoxidized Soyate Compounds

DPE/TPE esters of soybean oil were synthesized using transesterification, from soybean methyl ester and the DPE/TPE polyols. These unsaturated polyol esters along with sucrose esters were epoxidized using the method reported previously.[16]

5.4.1.1.GPC results

Figure 5.3 (a) displays the GPC plots of polyol esters of soybean oil fatty acids. DEP/TPE esters are prepared via transesterification between DPE/TPE polyol and FAME, which is produced via transesterification between glycerol triester and methanol. The symmetric GPC peaks of DEP/TPE esters and the absence of unreacted FAME prove that the degree of fatty acid substitution on DEP/TPE has been well controlled. Based on the retention times, it seems that the sequence of molecular weights (MWs) is TPES> TPESB6≈ DPES> SO> FAME. The GPC plots of epoxidized polyol esters are shown in Figure 5.3 (b), the sequence of MWs is ETPES> ETPESB6≈ EDPES> ESO.

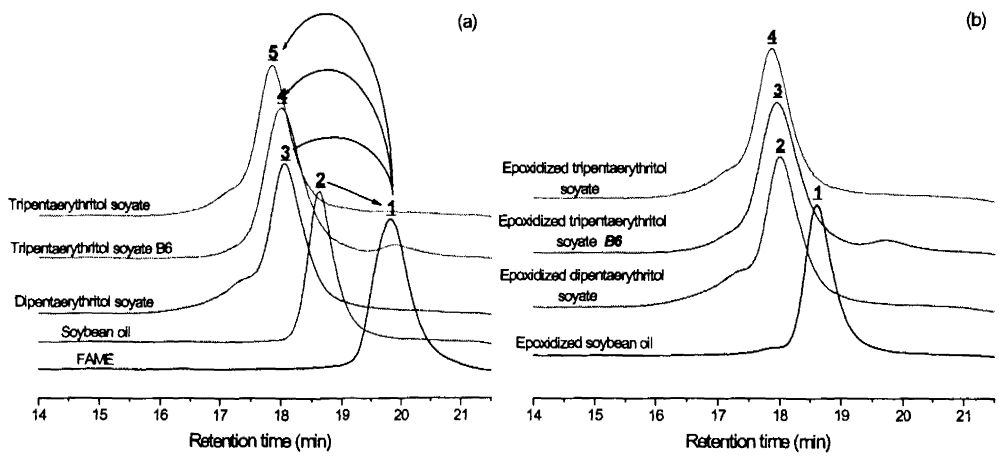

Figure 5.3. GPC plots of polyol esters of soybean oil fatty acids before and after epoxidation. (a) Unsaturated polyol esters: FAME, soybean oil, dipentaerythritol soyate, tripentaerythritol soyate B6, and tripentaerythritol soyate; (b) Epoxidized polyol esters: epoxidized soybean oil, epoxidized dipentaerythritol soyate, epoxidized tripentaerythritol soyate B6, and epoxidized tripentaerythritol soyate

5.4.1.2.FTIR results

Infrared (IR) spectroscopy has been used to identify the characteristic functional groups that present in the polyol esters before and after epoxidization. Figure 5.4 displays the overlaid FTIR spectra of polyol esters and their epoxy products. For unsaturated esters, the sp^2 hybridized C-H stretching adsorption shows peak at 3012 cm^{-1}. After epoxidization, the sp^2 hybridized C-H adsorption peak disappears, but the epoxide C-O-C adsorption peak appears at 826-832 cm^{-1}. Since tripentaerythritol soyate B6 is designed to substitute six of eight hydroxyls, its FTIR (Figure 5.4 (c)) spectra before and after epoxidation have a small hydroxyl adsorption band at 3500 cm^{-1}.

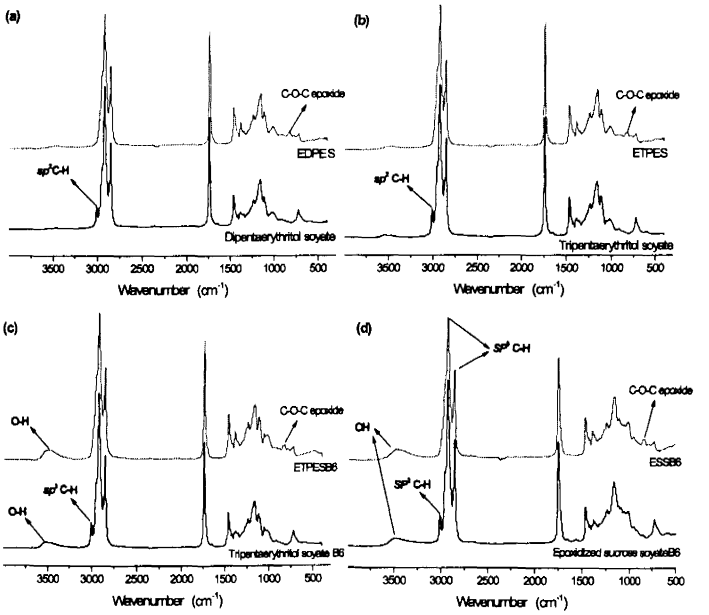

Figure 5.4. Overlaid FTIR spectra of polyol esters of soybean oil fatty acids before and after epoxidation. (a) DPES and EDPES; (b) TPES and ETPES; (c) ETPES and ETPESB6; SSB6 and ESSB6

5.4.1.3. ^{1}H-NMR results

As the method of structure determination, proton nuclear magnetic resonance (^{1}H-NMR) spectroscopy is used here to complement MALDI MS, GPC, and FTIR by providing a "map" of the carbon-hydrogen framework of each polyol ester before and after epoxidation. Figure 5.5 (a) shows the overlaid ^{1}H-NMR spectra of unsaturated polyol esters; Figure 5.5 (b) shows the overlaid ^{1}H-NMR spectra of epoxidized polyol esters. Before epoxidation, the chemical shifts of protons on double bonds are at 5.25-5.44 ppm, and the chemical shifts of protons on the carbons between double bonds are at around 2.76 ppm. After epoxidation, the above characteristic peaks related to double bonds all disappear, and the protons on epoxides appear at 2.84-3.20 ppm.

The structural difference between these polyol esters of soybean oil fatty acids are the core polyol, whose chemical shifts of protons mainly are located between 3.0 and 5.0 ppm and are labeled with Arabic number. The chemical shift of methine (CH) glycerol proton is at 5.25 ppm, and two methylene (CH_2) glycerol protons are at 4.26-4.30 ppm and 4.11-4.16 ppm, respectively. The chemical shift of methyl (CH_3) methanol protons is at 3.66 ppm. The chemical shifts of pentaerythritol external methylene protons for DPE/TPE esters are at 4.07 ppm, and the interal methylene protons are at 3.38 ppm.

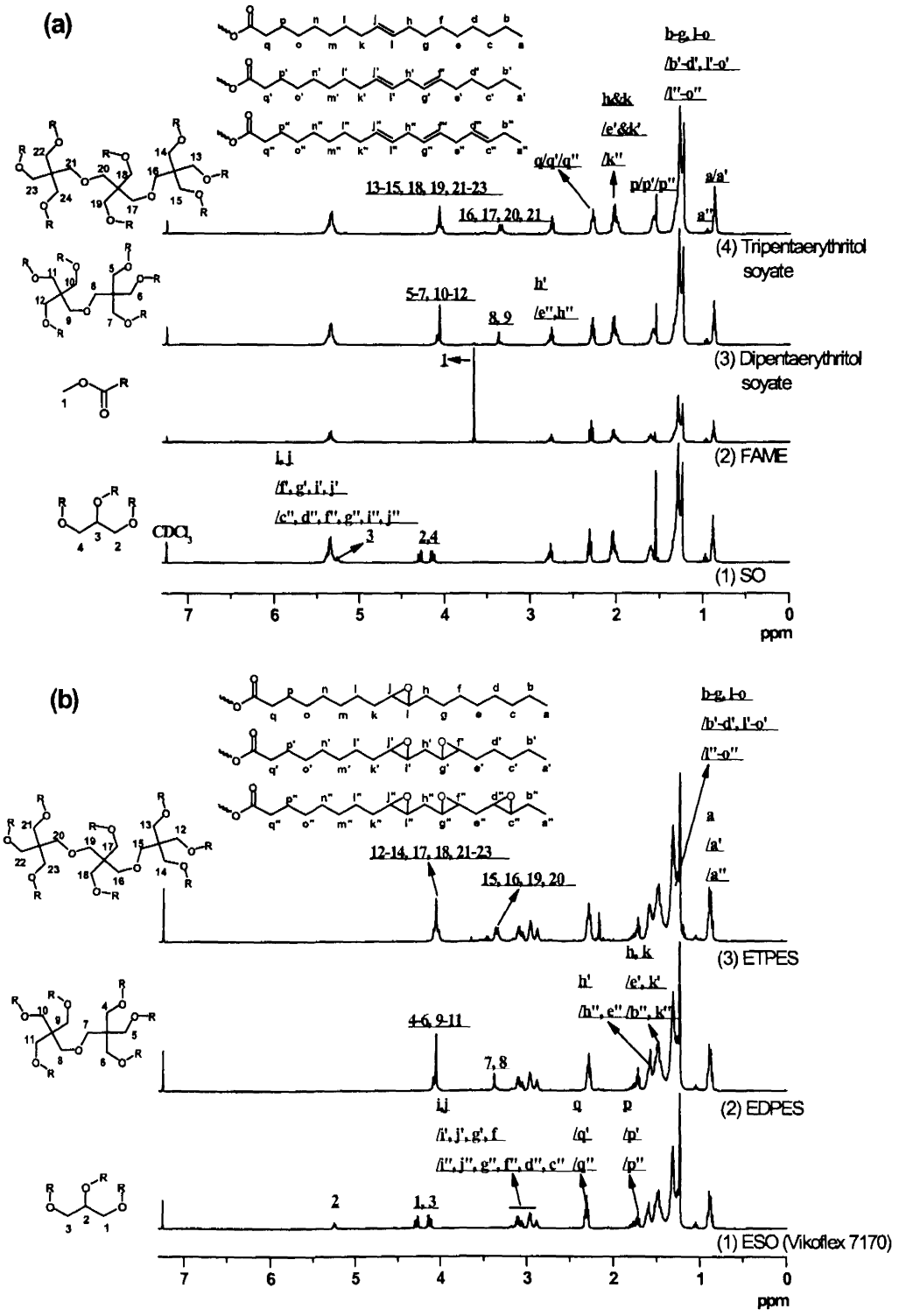

Figure 5.5. Overlaid ^{1}H-NMR spectra of (a) polyol esters of soybean oil fatty acids and (b) their epoxy products

5.4.2. Structure-property Relationships in Epoxy Compounds

The chemical and physical properties of these polyol esters before and after epoxidation were characterized using NMR, FTIR, GPC, iodine value and epoxy equivalent weight titrations, as well as bulk viscosity, intrinsic viscosity, and density measurements (in Table 5.1). The conversions of double bonds to epoxides of these polyol esters in epoxidation are close to 99%, due to the sharp decrease of the iodine values (IVs) from 115-125 to 0.44-1.36. However, sucrose esters show a higher completion of epoxidation than the other polyol esters. The lowest epoxy equivalent weight (EEW) of ESO reflects its highest epoxide content (wt %). ESO has the lower epoxide functionality EF than the other epoxy resins by 2-3 factors. Instead of using the MWs in GPC that are determined based on "size", the MWs in Mass spectrometry that are determined based on "mass-to-charge ratios" should be used.

Table 5.1. The properties of polyester esters of soybean oil fatty acids before and after epoxidation

Resin	Epoxidation	EEW (g/eq.)	IV	Viscosity (mPa·s)	Density (g/cm^3) at 25 °C	*[η]* (100ml/g), 25 °C in THF	GPC	
							Mn (g/mol)	*PDI*
Soybean oil	Cargill™	-	136	79	0.920	1.10	1,290	1.10
ESO	Vikoflex™ 7170	231	-	588	0.996	2.36	1,320	1.14
Dipentaerythritol soyate	Before	-	124	341	0.939	2.92	2,350	1.26
	After	268	1.25	1,192	1.000	3.27	2,480	1.28
Tripentaerythritol soyate	Before	-	124	415	0.943	3.32	2,810	1.15
	After	261	1.36	1,368	1.001	3.58	2,770	1.18
Tripentaerythritol soyate B6	Before	-	125	365	0.946	2.98	2,350	1.11
	After	270	1.05	1,824	1.011	3.21	2,510	1.13
Sucrose soyate	Before	-	117	425	0.945	2.41	2,380	1.08
	After	248	0.44	2,160	1.017	3.15	2,630	1.08
Sucrose soyate B6	Before	-	115	890	0.965	1.83	2,200	1.09
	After	256	0.73	5,460	1.036	2.94	2,480	1.20

Two key drivers of the differences among the polyol esters are: (a) the structure of the core polyol, and (b) the average degree of substitution (DS) of the fatty acids on the polyol. DPE, TPE, sucrose, and glycerol are different in chemical structure, hydroxyl functionality, content of primary/secondary hydroxyl, and density. Sucrose is made of glucose and fructose rings equipped with five secondary and three primary hydroxyls. DPE and TPE are linear ethers equipped with six and eight primary hydroxyls, respectively. Therefore, sucrose has a more rigid structure than DPE and TPE.

To study the impact of functionality of core polyol, the DS of fatty acids on polyol must be well controlled. MALDI MS was employed to give a highly detailed compositional analysis (Figure 5.6) that proves the well-defined structures of epoxy resins. As reported previously, the fully substituted epoxidized sucrose soyate (ESS) is defined as a mixture of sucrose hexa, hepta, and mainly octaesters, with an average DS of at least 7.7 of the 8 total hydroxyls, and the partially substituted epoxidized sucrose soyate B6 (ESSB6) is a mixture of sucrose esters with DS from 4 to 8 and an average DS of 6. The DS values of PE-type esters have been designed by precisely controlling the feed ratio of FAME to PE-type polyol, as well as GPC is used to determine the unreacted or excess FAME, and FTIR is used to determine the unesterified hydroxyls. While MALDI MS spectra display two DS values of 5 and 6 in epoxidized dipentaerythritol soyate (EDPES), three DS values of 6, 7 and 8 in epoxidized tripentaerythritol soyate (ETPES), and three DS values of 5, 6 and 7 in epoxidized tripentaerythritol soyate B6 (ETPESB6), the average DS values of these PE-type esters should be very close to the design.

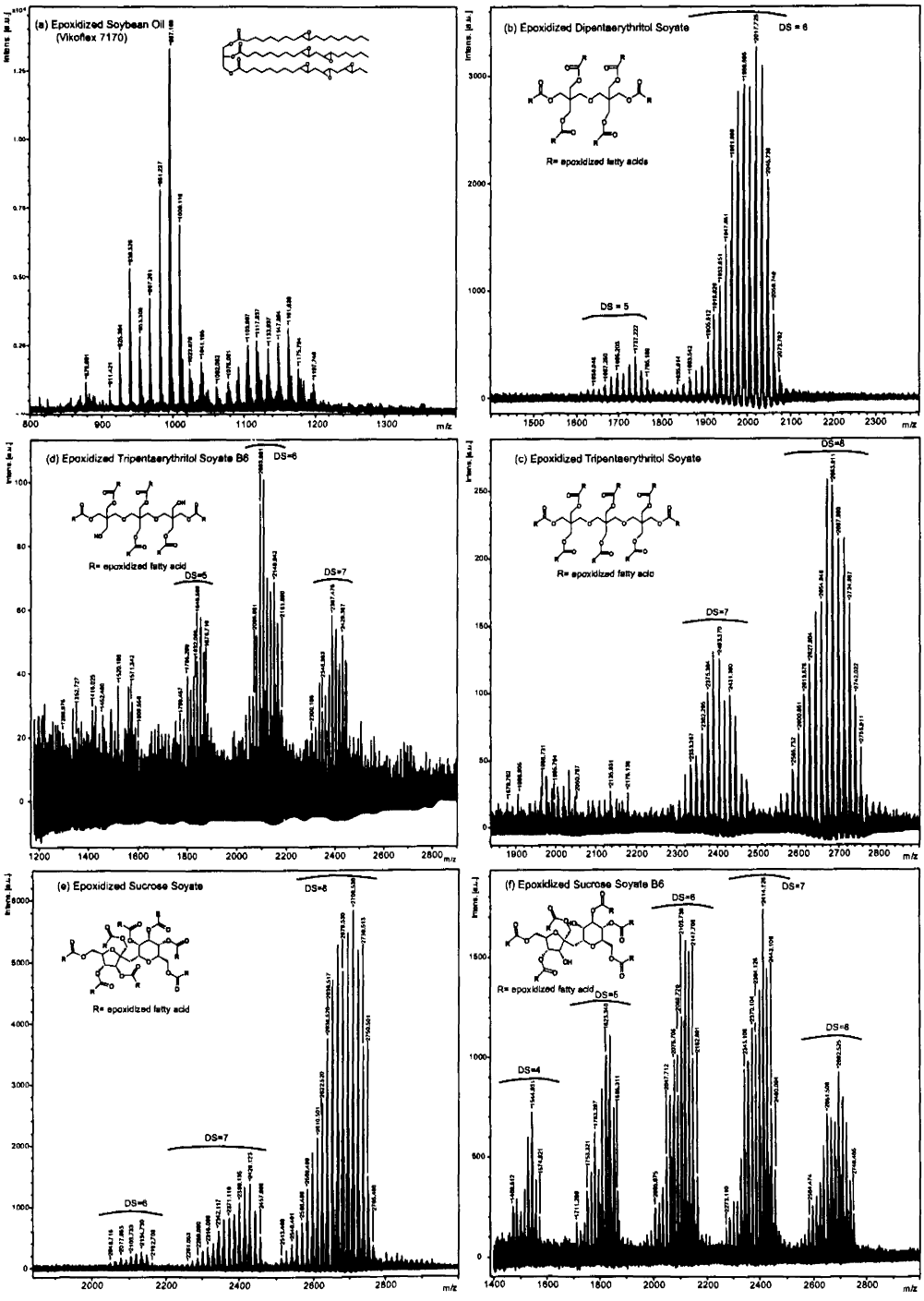

Figure 5.6. Positive ion MALDI mass spectra of epoxidized polyol esters of soybean oil fatty acids: (a) ESO; (b) EDPES; (c) ETPESB6; (d) ETPES; (e) ESS; (f) ESSB6. Sodiated peaks are labeled according to the m/z ratios

Figure 5.7 displays the effects of structure and functionality of core polyol on the properties of the resins. Sucrose esters have the highest densities since sucrose has the highest density among the polyols. ESSB6 and EDPESB6 have higher densities than their corresponding fully substituted epoxies due to the higher content of core polyol. Sucrose esters have the highest viscosities in part because of their highest densities among the polyol esters. Secondly, sucrose esters have a more rigid sucrose structure compared to the more flexible ether structure of the DPE and TPE polyols. ESSB6 and EDPESB6 have higher viscosities than their corresponding fully substituted epoxies, due to the hydrogen bonding effects from the unreacted hydroxyls. Polyol ester macromolecules in a dilute solution are the equivalent spheres that are uniform, rigid, and noninteracting. The intrinsic viscosity reflects the hydrodynamic volume of these spheres. The size of core polyol determines the size of its fatty acid ester. It is observed that TPE has a larger size than DPE, and DPE is slightly larger than sucrose ester. The results in intrinsic viscosity are showing the same trend as in GPC MWs, due to the same measurement principle.

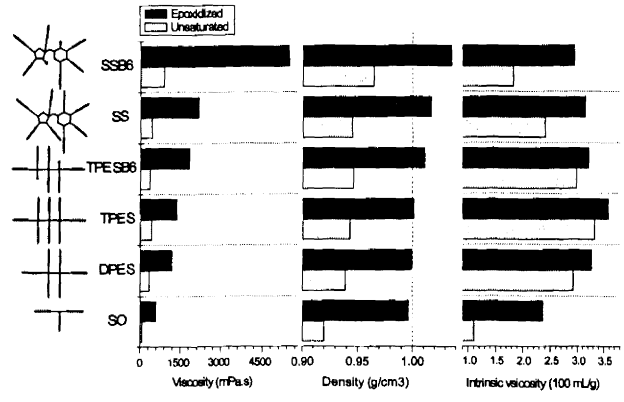

Figure 5.7. Comparison of the physical properties of polyol esters of fatty acids before and after epoxidation

5.4.3. Structure-property Relationships in Epoxy-anhydride Thermosets

Epoxy-anhydride thermosets were prepared using dodecenylsuccinic anhydride (Figure 5.8) with two different epoxide/anhydride equivalent ratios of 1:0.5 and 1:0.75. DBU, 1,8-Diazabicyclo[5.4.0]undec-7-ene, was used as the tertiary amine catalyst. The epoxy-anhydride curing system consists of internal epoxides, anhydrides, and tertiary amine. However, EDPES, ETPES, and ESS all contain trace hydroxyls, and ETPESB6 and ESSB6 have more hydroxyls available. The presence of hydroxyls in epoxy-anhydride curing has been proposed to facilitate polyester network formation through the fast reaction between hydroxyl and anhydride.[24-25] The advantages of hydroxyls in ESSB6-anhydride curing have been shown in the previous study.[18]

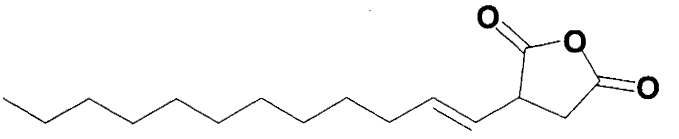

Figure 5.8. Molecular structure of dodecenylsuccinic anhydride (3-(dodec-1-enyl)oxolane-2,5-dione)

The tensile, dynamic mechanical and thermal properties of the thermosets are summarized in Table 5.2. The tensile properties include Young's modulus, tensile strength at maximum, and elongation at break. DSC and DMA measure the glass transition temperature (T_g) using different principles, but they show the same trend of T_g values relating to epoxide/anhydride equivalent ratios. In the same epoxy resin, the T_g of the thermoset using a ratio of 1:0.75 is always higher than that of the thermoset using 1:0.5. The storage modulus E' in the rubbery plateau region, which is 60°C above T_g, is used to

calculate crosslink density (ν_e) using Equation 1, derived from the theory of rubber elasticity: where E' is the storage modulus of thermoset in the rubbery plateau region at T_g+60 °C, R is the gas constant, and T is the absolute temperature.[26-27]

$$E' = 3\nu_e RT \qquad (1)$$

Table 5.2. The tensile, dynamic mechanical and thermal properties of epoxy-anhydride thermosets

Epoxy	Epoxy/ anhydride (molar ratio)	Tensile strength (MPa)	Young's modulus (MPa)	Elongation at break (%)	T_g, DSC (°C)	T_g, DMA (°C)	E' at 20 °C (MPa)	E' at T_g+60 °C (MPa)	ν_e (X 10^3 mol/m^3)
ESO	1:0.5	0.22 ± 0.07	2.01 ± 0.32	16.5 ± 3.3	-36	-20	1.98	1.93	0.17
	1:0.75	1.38 ± 0.54	4.83 ± 0.19	33.8 ± 10.1	-3.1	-4.2	4.46	3.25	0.29
EDPES	1:0.5	0.93 ± 0.40	5.72 ± 1.90	20.3 ± 4.1	-13	7.8	15.5	3.05	0.27
	1:0.75	1.73 ± 0.32	10.2 ± 1.42	22.2 ± 2.2	15	23	91.0	7.1	0.66
ETPES	1:0.5	0.64 ± 0.20	5.31 ± 0.96	15.3 ± 2.7	-28	1.8	6.79	3.43	0.31
	1:0.75	3.57 ± 1.29	17.2 ± 3.57	26.6 ± 5.1	-7.5	9.1	14.1	5.73	0.51
ETPESB6	1:0.5	1.97 ± 0.40	9.58 ± 0.95	24.5 ± 3.7	-1.4	4.1	4.15	2.05	0.18
	1:0.75	11.8 ± 1.56	163 ± 57.5	28.4 ± 6.6	6.3	15	13.6	3.10	0.28
ESS	1:0.5	8.87 ± 0.74	119 ± 14.5	39.5 ± 4.1	27	33	39.5	5.56	0.50
	1:0.75	13.2 ± 1.91	392 ± 27.7	8.0 ± 2.7	40	51	120	8.42	0.75
ESSB6	1:0.5	8.50 ± 1.54	154 ± 36.1	30 ± 9.0	35	35	148	8.65	0.77
	1:0.75	18.3 ± 1.63	591 ± 50.3	6.5 ± 0.9	48	58	280	9.60	0.86

Figure 5.9 displays the Young's modulus and tensile strength data in addition to the DSC T_g values for the thermosets. In general, the thermosets having a higher T_g possess higher Young's modulus and tensile strength. Focusing on the series of thermosets made with an epoxy/anhydride ration of 1.0:0.5, it can be seen that all of the thermosets from the

PE polyols as well as the ESO have T_g values below 0°C, while those based on the sucrose ester resins have T_g values above room temperature. The modulus and tensile strengths of the PE polyols and the ESO thermosets are somewhat similar; however, the mechanical properties of the sucrose-based thermosets are significantly higher. It can be seen that the rigid structure of the sucrose contributes significantly to the mechanical properties of the thermosets. The thermosets from the partially substituted polyol esters (i.e. ETPESB6 and ESSB6) have higher T_g values and mechanical properties than the corresponding thermosets using the fully substituted polyol esters, because of the higher densities of the partially substituted epoxies and the contribution of the polyol hydroxyls to polyester network formation.

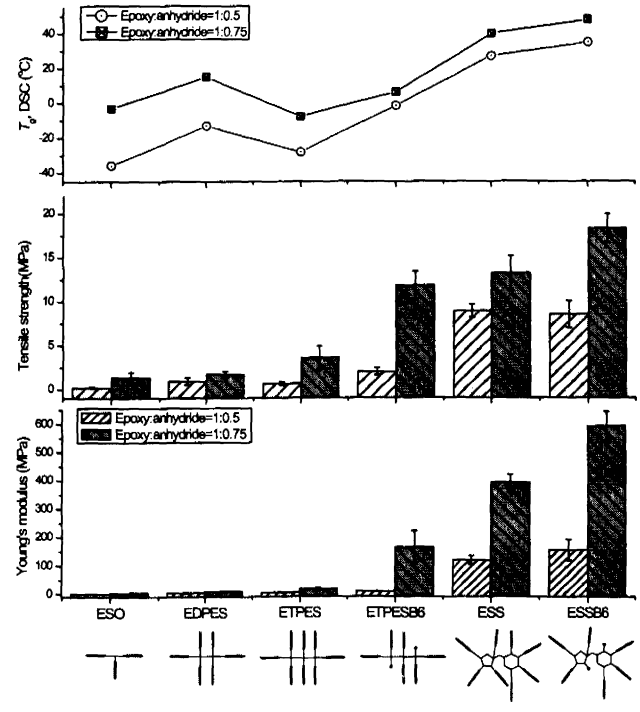

Figure 5.9. Comparison of the properties of epoxy-anhydride thermosets using different epoxidized polyol esters

Figure 5.10 displays the several coatings properties. Coating hardness is determined using gouge hardness, which is defined as the hardest pencil that cuts through the films (80-100 μm). We observe that sucrose-based thermosets have higher pencil hardness than the DPE/TPE-based thermosets, which in turn have higher pencil hardness than the thermosets using the glycerol trimester (ESO). MEK double rubs is a method commonly used to evaluate solvent resistance of thermosetting coatings, which highly relates to its crosslink density. Crosslink density (ν_e) of each thermoset has been obtained from DMA. Besides of the correlation of the solvent resistance with the crosslink densities, we also believe that the difference of solvent resistance between the sucrose-based thermosets and the DPE/TPE-based thermosets is due to the cyclic structure of sucrose and the linear structure of DPE/TPE. Also, the secondary hydroxyls in sucrose somehow result in a lower solubility of the thermoset in MEK and are taken into account into the explanations.

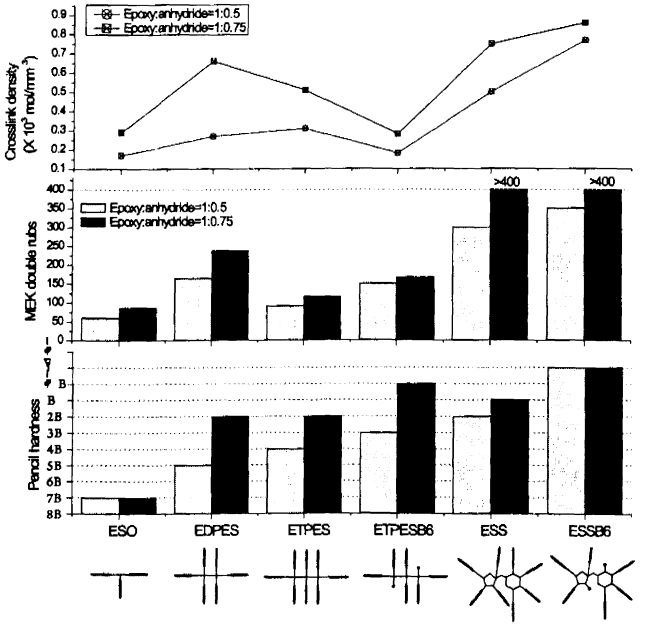

Figure 5.10. Comparison of the properties of epoxy-anhydride coatings using different epoxidized polyol esters

5.5. Conclusions

Soybean oil, glycerol triesters, has been reconstituted using DPE, TPE, and sucrose as core polyols with a high degree of substitution of fatty acids on the polyols, and their epoxidized products have been synthesized and then cured in an epoxy-anhydride curing system to form thermosets. The impact of the structure and functionality of the core polyol (i.e. glycerol, DPE, TPE, and sucrose) on the properties of the epoxy resins and their thermosets has been well interpreted in comparison. Although both structure and functionality of sucrose contribute to the remarkable performance of sucrose-based thermosets, from this study we can conclude that the structure of sucrose outweighs its functionality by evaluation of properties obtained in comparison with the TPE ester.

Today what we are witnessing is that interest in biofeedstock-based chemistry is rapidly increasing in both academic and industrial fields, but there is a significant history in the use petrochemicals in the preparation of high performance organic polymeric materials. Markets are not willing to give up the cost and properties currently achieved only for the sake of green chemistry. Sucrose-based highly functional epoxy fatty compounds appear to be an attractive technology to overcome the traditional deficiencies (e.g. highly flexible and low modulus) of vegetable oil-based materials, since thermosets made from these epoxy compounds exhibit high modulus, hard and ductile thermosetting properties while maintaining a high biobased content. Thus, sucrose, a core polyol of the esters of fatty acids, is not just "green" but also contributes significantly to the properties of the thermosets.

5.6. References

1. Rheineck, A. E. *J. Oil Colour Chem. Assoc.* **1958**, *41*, 474.
2. Carothers, W. H. *J. Am. Chem. Soc.* **1929**, *51*, 2548.
3. Bradley, T. F. *J. Ind. Eng. Chem.* **1937**, *29*, 440.
4. Bradley, T. F. *J. Ind. Eng. Chem.* **1938**, *30*, 689.
5. Burrell, H. *J. Ind. Eng. Chem.* **1945**, *37*, 86.
6. Trevoy, L. W.; Myers, M. E. *Can. J. Chem.* **1963**, *41*, 770.
7. Jaffe, J.; Pinchas, S. *Anal. Chem.* **1951**, *23*, 1164.
8. Li, L.; Kamiya, Y.; Okuhara, T. *Appl. Catal., A* **2003**, *253*, 29.
9. Haseebuddin, S.; Parmar, R.; Waghoo, G.; Ghosh, S. K. *Prog. Org. Coat.* **2009**, *64*, 446.
10. Bat, E.; Gündüz, G.; Kisakürek, D.; Akhmedov, Ï. M. *Prog. Org. Coat.* **2006**, *55*, 330.
11. Karakaya, C.; Gündüz, G.; Aras, L.; Mecidoğlu, Ï. A. *Prog. Org. Coat.* **2007**, *59*, 265.
12. Bobalek, E. G.; Walsh, T. J.; Ciang, H. *Official Digest* **1961**, 453.
13. Walsh, T. J.; Bobalek, E. G.; Hall, D. R. *Div. Org. Coatings Plastic Chem.* **1961**, *21*, 125.
14. Chempol® MPS wins the 2009 Presidential Green Chemistry Challenge Awards. http://www.pgsefose.com/sefose-in-the-news.html. (Accessed on February 15, 2011).
15. Pan, X.; Nelson, T. J.; Webster, D. C. *Prog. Org. Coat.*, DOI: 10.1016/j.porgcoat.2010.11.020.

16. Pan, X.; Sengupta, P.; Webster, D. C. *Green Chem.* **2011**, *13*, 965.

17. Sengupta, P. P.; Pan, X.; Nelson, T. J.; Paramarta, A.; Webster, D. C., *PMSE Preprints* **2010**, *102*, 888.

18. Pan, X.; Sengupta, P.; Webster, D. C. *Biomacromolecules*, submitted. Pan, X.; Sengupta, P.; Webster, D. C. *PMSE Preprints* **2010**, *103*, 268.

19. Rösch, J.; Mülhaupt, R. *Polym. Bull.* **1993**, *31*, 679.

20. Gerbase, A. E.; Petzhold, C. L.; Costa, A. P. O. *J. Am. Oil Chem. Soc.* **2002**, *79*, 797.

21. Miyagawa, H.; Misra, M.; Drzal, L. T.; Mohanty, A. K. *Polym. Eng. Sci.* **2005**, *45*, 487.

22. Takahashi, T.; Hirayama, K.; Teramoto, N.; Shibata, M. *J. Appl. Polym. Sci.* **2008**, *108*, 1596.

23. Tanrattanakul, V.; Saithai, P. *J. Appl. Polym. Sci.* **2009**, *114*, 3057.

24. Rocks, J.; Rintoul, L.; Vohwinkel, F.; George, G. *Polymer* **2004**, *45*, 6799.

25. Foix, D.; Yu, Y.; Serra, A.; Ramis, X.; Salla, J. M. *Eur. Polym. J.* **2009**, *45*, 1454.

26. Hill, L. W. *Prog. Org. Coat.* **1997**, *31*, 235.

27. Hill, L.W., in J.V. Koleske (ed.), Paint and Coating Testing Manual, Fourteenth Edition of the Gardner-Sward Handbook, ASTM, Philadelphia, PA, **1995**, 534.

CHAPTER 6. NOVEL BIOBASED HIGH FUNCTIONALITY POLYOLS AND THEIR USE IN POLYURETHANE COATINGS

6.1. Abstract

High functionality polyols for application in polyurethanes (PUs) were prepared by epoxide ring-opening reactions from epoxidized sucrose esters of soybean oil—epoxidized sucrose soyates (ESSs) —in which secondary hydroxyls were generated from epoxides on fatty acid chains. Ester-polyols were prepared using a base-catalyzed acid-epoxy reaction with carboxylic acids (e.g. acetic acid); ether-polyols were prepared using an acid-catalyzed alcohol-epoxy reaction with monoalcohols (e.g. methanol). The polyols were characterized by gel permeation chromatography (GPC), Fourier transform infrared (FTIR) spectroscopy, proton nuclear magnetic resonance (^{1}H-NMR) spectroscopy, differential scanning calorimetry (DSC), and viscosity measurements. Polyurethane thermosets were prepared using aliphatic polyisocyanates based on isophorone diisocyanate (IPDI) and hexamethylene diisocyanate (HDI). The properties of the PUs were studied using tensile testing, dynamic mechanical analysis (DMA), DSC and thermogravimetric analysis (TGA). The properties of PU coatings on steel substrates were evaluated using ASTM methods to determine coating hardness, adhesion, solvent resistance, and ductility. Compared with soy triglyceride polyol, sucrose soyate polyols provide greater hardness and a range of crosslink density to PU thermosets, due to the unique structure of these macromolecules: well-defined compact structures having a rigid sucrose core coupled with high hydroxyl functionality.

6.2. Introduction

Polyurethanes (PUs) have ubiquitous applications in coatings and other fields. Traditional plant oil-based PUs have been prepared by reacting diisocyanates with castor oil that naturally possesses hydroxyl groups.[1] Castor oil-based PUs have a broad application in PU foams, interpenetrating polymer networks (IPNs), and PU coatings.[2-6] In addition, plant oil-based urethane varnishes, urethane alkyds (uralkyds), typically prepared using diisocyanate, monoglyceride, and phthalic anhydride, have been used for decades.[7] Plant oil-based aqueous polyurethane dispersions (PUDs) can be achieved by incorporating dimethylol propionic acid (DMPA) into the reaction with diisocyanate, diol, and monoglyceride.[8] Through the subsequent neutralization reaction with triethylamine, the carboxylic ion of DMPA in the PU backbone is rendered hydrophilic and serves as an anionic center as well as internal emulsifier. Instead of using DMPA, maleinization of fatty acids on monoglycerides using maleic anhydride is also able to provide the acid groups needed for neutralization and water dispersion.[9]

Petrochemical-based polyester, polyether, and acrylic polyols are the main types of polyols used in PUs, but interest in plant oil-based polyols is growing.[10] The double bonds are reactive sites in plant oils. Epoxidation is one of the most important functionalization reactions of double bonds, and epoxide ring-opening reactions can lead to numerous products.[11] Secondary hydroxyls on fatty acids can be created from the reactions between epoxides and compounds containing active hydrogens such as alcohols, amines and carboxylic acids (Figure 6.1 (a)).[12] As another approach, primary hydroxyls on fatty acids may be made from the hydrogenation of aldehydes, which are created from the hydroformylation of double bonds (Figure 6.1 (b)).[13] As a further approach to plant oil-

based polyols for PUs, oligomeric polyether polyols are produced using epoxy polymerization of epoxidized methyl esters of fatty acids.[14-15]

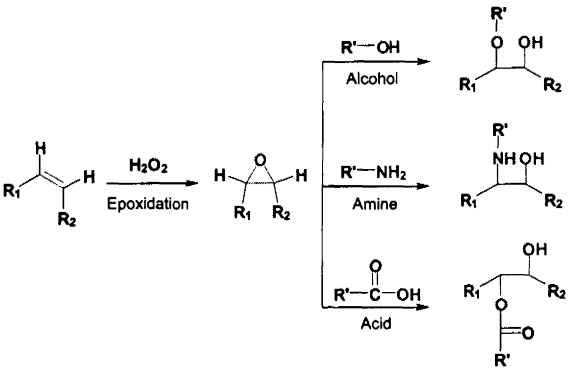

(a) Reactions of epoxides with active hydrogen containing compounds

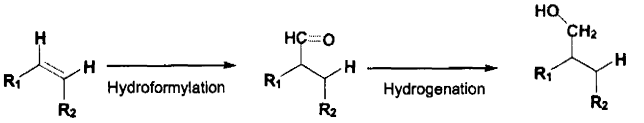

(b) Hydroformylation of double bonds followed by hydrogenation

Figure 6.1. Reaction strategies of producing triglyceride polyols by transforming double bonds to hydroxyls

Petrovic and coworkers have carried out many studies to prepare soy triglyceride polyols using the route of epoxide ring-opening and they have explored their use in PUs.[16-21] The composition of the triglyceride polyols has been varied by varying the nature of the side group (e.g. Br-, Cl-, CH_3O-, and H-) on the carbon atom adjacent to hydroxyl group.[15] The invention of reacting epoxidized soybean oils (ESOs) with methanol via an acid-catalyzed alcohol-epoxy reaction must be highlighted.[22-23] The effects of NCO/OH ratio and the type of diisocyanate on the properties of PUs have been studied.[17-18] The PU thermosets span a broad range from soft and rubbery to hard and glassy materials, in which ductile PUs with high moduli were obtained using aromatic diisocyanates (e.g. 4, 4'-

diphenylmethane diisocyanate (MDI), and 2, 4, 6-toluene diisocyanate (TDI)) in an NCO/OH ratio of 1:1.

Sucrose esters of soybean oil—sucrose soyates—are the most attractive and promising sucrose esters due to the fact that soybean oil is the most economic and readily available plant oil in the world, as well as the fact that the U.S. is the top soy producer. In this study, epoxidized sucrose soyates (ESSs) having different degrees of substitution (DS) on the sucrose were used as starting materials to prepare high functionality sucrose soyate polyols by epoxide ring-opening reactions. The fully substituted ESS is abbreviated as f-ESS and has an average DS of 7.7. The partially substituted ESS is epoxidized sucrose soyate B6 (ESSB6) having an average DS of 6. The epoxide functionality per molecule of f-ESS and ESSB6 is 11 and 8, respectively. Acid-epoxy reactions using a carboxylic acid were used to produce ester-polyols, and an alcohol-epoxy reaction using a monoalcohol was used to produce an ether-polyol. The obtained ester/ether-polyols were then reacted with polyisocyanates to yield PU thermosets. The tensile, dynamic mechanical, thermal and coating properties of PU thermosets were evaluated considering the hydroxyl functionality of polyol, the type of polyisocyanate, and the NCO/OH ratio in the formulation.

6.3. Experimental

6.3.1. Raw Materials

Fully substituted sucrose soyate (Sefose 1618U) and partially substituted sucrose soyate (Sefose 1618U B6) were kindly provided by Procter & Gamble Chemicals (Cincinnati, OH). Acetic acid (ACS reagent, ≥99.7%), propionic acid (reagent grade, ~99%), 2-ethylhexanoic acid (99%), and 1, 8-Diazabicyclo [5.4.0] undec-7-ene (≥99.0%

GC) were purchased from Sigma-Aldrich, Co. (St. Louis, MO). BDH™ Methanol (ACS grade, ≥99.8%) and 2-propanol (ACS grade, ≥99.5%) were purchased from VWR International (West Chester, PA). Tetrafluoroboric acid (48 wt% solution in water), sodium carbonate (ACS reagent), and anhydrous magnesium sulfate (reagent grade, ≥97%) were purchased from Sigma-Aldrich, Co. (St. Louis, MO). Tolonate IDT 70B (NCO equivalent weight=342 g/eq., 70% solids in butylacetate), an aliphatic polyisocyanate (trimer) of isophorone diisocyanate, was provided by Perstorp Group (Cranbury, NJ). Desmodur N 3600 (NCO equivalent weight=183 g/eq., solvent-free), an aliphatic polyisocyanate (trimer) of hexamethylene diisocyanate, was provided by Bayer MaterialScience (Pittsburgh, PA). All materials were used as received without further purification.

6.3.2. Synthesis of Sucrose Soyate Polyols

6.3.2.1.Acid-epoxy reaction

Acetic acid, propionic acid, and 2-ethylhexanoic acid were individually used to react with f-ESS to produce the ester-polyols in the presence of 1, 8-diazabicyclo [5.4.0] undec-7-ene (DBU) catalyst. The reactions were carried out at 125-130°C. Acid number titration was used to monitor the reaction which was stopped when the acid number was lower than 15. Herein, 2-ethylhexanoic acid (EHA) is used as an example for the synthesis of the ester-polyol in an acid/epoxide molar ratio of 0.8:1. The reaction was carried out in a 250 mL three-neck flask, equipped with mechanical stirrer, thermocouple and reflux condenser. 77.38 g of f-ESS (0.029 mol) containing 0.312 mol epoxides and 35.99 g of EHA (0.250 mol) containing 0.250 mol carboxylic acids were added to the flask at room temperature. 1.13g of DBU (0.007 mol) was used at 1 wt% of the total weight of f-ESS and

EHA. With mechanical stirring, the mixture of reactants and catalyst was heated to 130°C. After three and quarter hours, the reaction was stopped when the acid number approached 12. A light reddish-yellow viscous liquid resin was the product. Since DBU can also function as a PU curing catalyst, there was no further purification after the reaction.

6.3.2.2.Alcohol-epoxy reaction

Both f-ESS and ESSB6 were used in alcohol-epoxy reactions to produce the ether-polyols. Herein, f-ESS is used as an example having a methanol/epoxide molar ratio of 3:1. The reaction was carried out in a 500 mL four-neck flask, equipped with a mechanical stirrer, thermocouple, reflux condenser and 250 mL addition funnel. 100 g of f-ESS (0.037 mol) containing 0.403 mol epoxides dissolved into 150 ml of isopropanol and the solution was transferred into an addition funnel. 150 ml of isopropanol, 10 g of water, 40 g of methanol (1.25 mol), and 4 g of tetrafluoroboric acid (48 wt% solution in water, 0.022 mol) were charged into the flask and mixed well at room temperature. After the mixture in the flask was heated to 45°C, the f-ESS isopropanol solution was added dropwise at a rate of 1 ml/min. The reaction temperature was controlled at 50°C. After the addition of the f-ESS isopropanol solution was complete, the reaction was held at 50°C for 20 minutes. 5 g of sodium carbonate (0.047 mol) was added to decompose the tetrafluoroboric acid. The product solution was transferred into a beaker and dried with anhydrous magnesium sulfate overnight to remove the water. The hydrated magnesium sulfate was removed by filtration, and the excess alcohols were removed by distillation at reduced pressure.

6.3.3. Characterization on Polyols

Molecular weight was determined using a Waters 2410 gel permeation chromatograph equipped with refractive index detector. Polystyrene standards were used for calibration. A 1.5% sample solution in THF using a flow rate of 1 ml/min was used. FTIR measurements were done with a Thermo Scientific Nicolet 8700 FTIR spectrometer. Spectra acquisitions were based on 32 scans with data spacing of 2.0 cm^{-1}. NMR measurements were done at 23°C using a JOEL-ECA (400 MHz) NMR spectrometer with an autosampler accessory. All measurements were made using $CDCl_3$ as solvent. The data was processed using the Delta software package. The viscosities of polyols were measured using a Brookfield Viscometer (DV-II+ Pro) at 25°C at 100 RPM. A Q1000 DSC from TA Instruments (New Castle, DE) with an autosampler was used for measuring the thermal properties of polyols. Samples were subjected to a heat–cool–heat cycle from -90 to +80°C by ramping at 10 °C/min for both heating and cooling. The second heating cycle was used to determine the glass transition temperature.

6.3.4. Polyurethane (PU) Formulation and Curing

The ester-polyols were formulated with polyisocyanate in an NCO/OH ratio of 1.1:1. The formulations were prepared at 80% solids content using xylene. The ether-polyols were formulated with polyisocyanate in NCO/OH ratios of 1.1:1, 0.8:1, and 0.6:1. The formulations were prepared at 80% solids content using xylene. Additionally, 1 wt% of DBU (based on the total weight of solids) was used as the curing catalyst. PU coatings were cast on cleaned QD-36 steel panels and glass panels using a draw-down bar with a gap of 8 mils. The coatings were kept at ambient for three hours and then were further

cured in an oven at 80°C for one hour. PU coatings on steel panels were used for the ASTM tests to evaluate the coating properties. PU films on glass panels were removed and used for tensile testing and DMA.

6.3.5. Characterization on PU Thermosets

The thickness of the PU coatings on the steel substrates was the average of 10 measurements using a Byko-Test 8500 coating thickness gauge at different locations on the film and the uncertainty is the standard deviation. König pendulum hardness and pencil hardness were measured using ASTM D 4366 and ASTM D 3363, respectively. The adhesion of coatings on the steel substrate was evaluated using the ASTM D 3359 crosshatch adhesion method. The methyl ethyl ketone (MEK) double rub test was carried out following ASTM D 5402 which was modified with a 26 ounce hammer that was wrapped with four layers of cheesecloth and soaked in MEK for rubbing. The cheesecloth was rewet with MEK after 100 double rubs. The number of double rubs was reported as the point when mar appeared on the film surface, or a maximum of 400 double rubs was reached without damage. Reverse impact resistance was determined using ASTM D 2794. Mandrel bend test was carried out based on ASTM D 522, and the results were reported as the elongation of the coating at cracking. Rectangular specimens with dimensions of 20 mm length, 5 mm width, and 0.07-0.11 mm thickness were prepared for tensile testing. The tensile tests were carried out at 25°C using an Instron 5542 (Norwood, MA). The grip separation distance of the tensile testing was 25.4 mm, and the effective gauge length was 20.4 mm. The crosshead speed was 0.1% elongation/sec. (0.0204 mm/sec.). The tensile properties were reported as the average of 5 measurements with different specimens and

the uncertainty was the standard deviation. A Q1000 DSC from TA Instruments was used for measuring the thermal properties of the PUs. Samples were subjected to a heat–cool–heat cycle from -90 to +200°C by ramping at 10 °C/min for both heating and cooling. The second heating cycle was used to determine the glass transition temperature. A Q800 DMA from TA Instruments was used to study dynamic mechanical properties of the PU films in tension mode. Rectangular specimens with dimensions of 20 mm length, 5 mm width, and 0.07-0.11 mm thickness were prepared. The measurements were performed from -80 to +220°C at a heating rate of 10 °C/min and frequency of 1 Hz. The glass transition temperature (T_g) was determined as the temperature at the maximum of the tan δ vs. temperature curve. The storage modulus (E') in the rubbery plateau region was studied at T_g+60°C to determine crosslink density (ν_e) which is given by Equation 1 derived from the theory of rubber elasticity: where E' is the storage modulus of the thermoset in the rubbery plateau region at T_g+60°C, R is the gas constant, and T is the absolute temperature.[24-25]

$$E' = 3\nu_e RT \qquad (1)$$

A Q500 TGA from TA Instruments was used to study the thermal degradation behavior of the PUs. PU samples were placed in the sample pan and heated from 25 to 800°C under N_2 at a heating rate of 20 °C/min. The measurements were made using 5–15 mg samples, and the weights were recorded as a function of temperature.

6.4. Results and Discussion

6.4.1. Polyol Synthesis

6.4.1.1. Base-catalyzed acid-epoxy reaction

The synthesis of the ester-polyols using the acid-epoxy reaction was catalyzed by 1, 8-diazabicyclo [5.4.0] undec-7-ene (DBU). DBU belongs to the class of amidine compounds having biscyclic structure and amidino functional group, -HN=CNH_2. DBU is not only a curing agent for epoxy resins, but can also function as a curing catalyst for polyurethane.[26]

Acetic acid (AA), propionic acid (PA), and 2-ethylhexanoic acid (EHA) were the carboxylic acids used in this study. The synthesis and characteristics of the ester-polyols synthesized are shown in Table 6.1. The number in the polyol name is the molar ratio of acids to epoxides. Based on the reaction time and final acid number, the reactivity of the carboxylic acids with respect to epoxide is in the order of EHA>AA>PA. EHA was able to reduce the acid number to 12 with an acid/epoxide ratio as high as 0.8:1. In the acid/epoxide ratio of 0.6:1, PA takes 1.5 hours longer than AA to approach the acid number 15. The ester-polyols having acid numbers less than 15 were selected to be used in the subsequent preparation of PUs. The glass transition temperatures of the selected ester-polyols range from -41 to -31°C. Assuming that the carboxylic acids are only consumed by epoxides, the epoxide conversion can be calculated using equation 2, where AN_0 is the initial acid number, AN_f is the final acid number, and C is the molar ratio of acids to epoxides. Due to the existence of unreacted carboxylic acids after reaction, the epoxide conversion is always lower than the acid/epoxide ratio C in each batch of polyol. The

hydroxyl functionality of ester-polyol is given by the epoxide functionality of f-ESS multiplied by the epoxide conversion.

$$Epoxide\ conversion = C \times \frac{(AN_0 - AN_f)}{AN_0} \qquad (2)$$

Biobased acetic acid can be produced by bacterial fermentation of biomass in vinegar production. Compared with PA and EHA, the acetic acid produced ester-polyol shows the lowest viscosity in the acid/epoxide ratio of 0.6:1. Thus, acetic acid is a good option to produce ester-polyols with a high biocontent and low viscosity.

Table 6.1. Ester-sucrose soyate polyols prepared in acid-epoxy reactions

Polyols	Reaction time (hr)	Acid number	Epoxide conversion	Hydroxyl functionality	Viscosity (mPa·s)	T_g (°C)
AA_1	11.0	52	72	7.6	38,000	-
AA_0.9	6.5	37	70	7.4	11,940	-
AA_0.6	4.0	14	53	5.6	4,980	-40
PA_0.6	5.5	15	52	5.5	12,160	-36
EHA_0.9	6.0	24	74	7.8	14,140	-
EHA_0.8	3.25	12	72	7.6	15,100	-33
EHA_0.6	2.5	7.5	56	5.9	12,060	-36
EHA_0.4	0.5	1.0	40	4.2	5,060	-41

Figure 6.2 shows the GPC plots of the f-ESS starting material and the ester-polyols prepared using EHA with acid/epoxide ratios of 0.8:1, 0.6:1, and 0.4:1. It is observed that acid-epoxy reactions result in the molecular weight (MW) slightly increasing from f-ESS to polyols, and the plots of the ester-polyols all show a small higher MW shoulder. The size of the shoulder increases with an increase of the acid/epoxide ratio. The alcohol-epoxide reaction between the newly formed secondary hydroxyls and epoxides can be responsible for the higher MW oligomers.

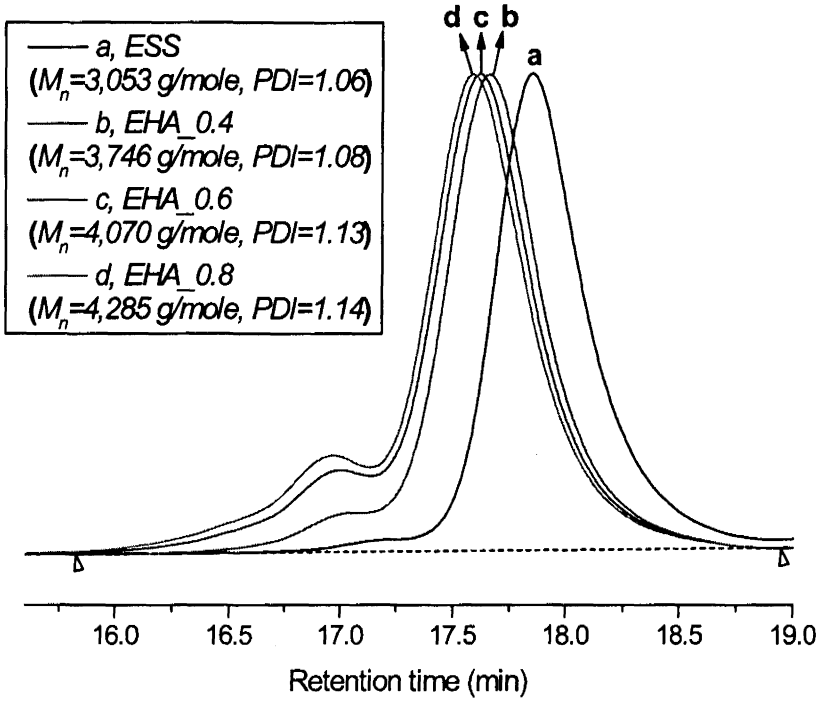

Figure 6.2. GPC plots of the f-ESS starting material and the ester-polyols prepared by reaction with 2-ethylhexanoic acid (EHA) in different acid/epoxide molar ratios

Figure 6.3 shows the FTIR spectra of f-ESS starting material and the ester-polyols prepared using EHA. No hydroxyl adsorption band is observed in the FTIR spectrum of f-ESS. In the FTIR spectra of polyols, the size of hydroxyl adsorption band at 3200-3500 cm^{-1} increases with the acid/epoxide ratio. Consequently, the intensity of the characteristic epoxide adsorption at 826 cm^{-1} decreases.

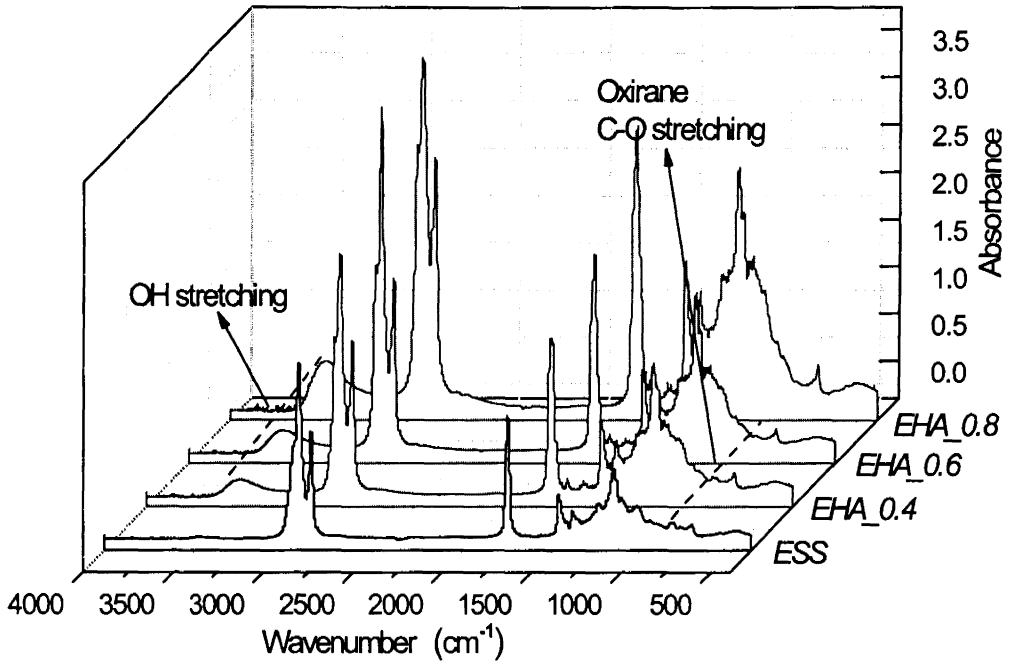

Figure 6.3. FT-IR spectra of the f-ESS starting material and the ester-polyols prepared by reaction with 2-ethylhexanoic acid (EHA) in different acid/epoxide molar ratios

Figure 6.4 shows the overlaid ^{1}H-NMR spectra of the ester-polyols prepared using EHA. The peaks of the protons on the sucrose ring are at 4.0-4.4 ppm, and its quantitative value (area integration, $A_{1\text{-}9}$) is used as a constant for normalization. The peaks of the protons on the epoxides of fatty acids are at 2.86-3.21 ppm, and its quantitative value (area integration, $A_{a\text{-}l}$) is a variable in each spectrum. The ratios of $A_{a\text{-}l}/A_{1\text{-}9}$ for f-ESS, EHA_0.4, EHA_0.6, and EHA_0.8 are designated as A_0, $A_{0.4}$, $A_{0.6}$, and $A_{0.8}$, respectively. The ratio of A_0: $A_{0.4}$: $A_{0.6}$: $A_{0.8}$ is normalized as 1: 0.67: 0.4: 0.2, which can be used to correlate to the epoxide conversion.

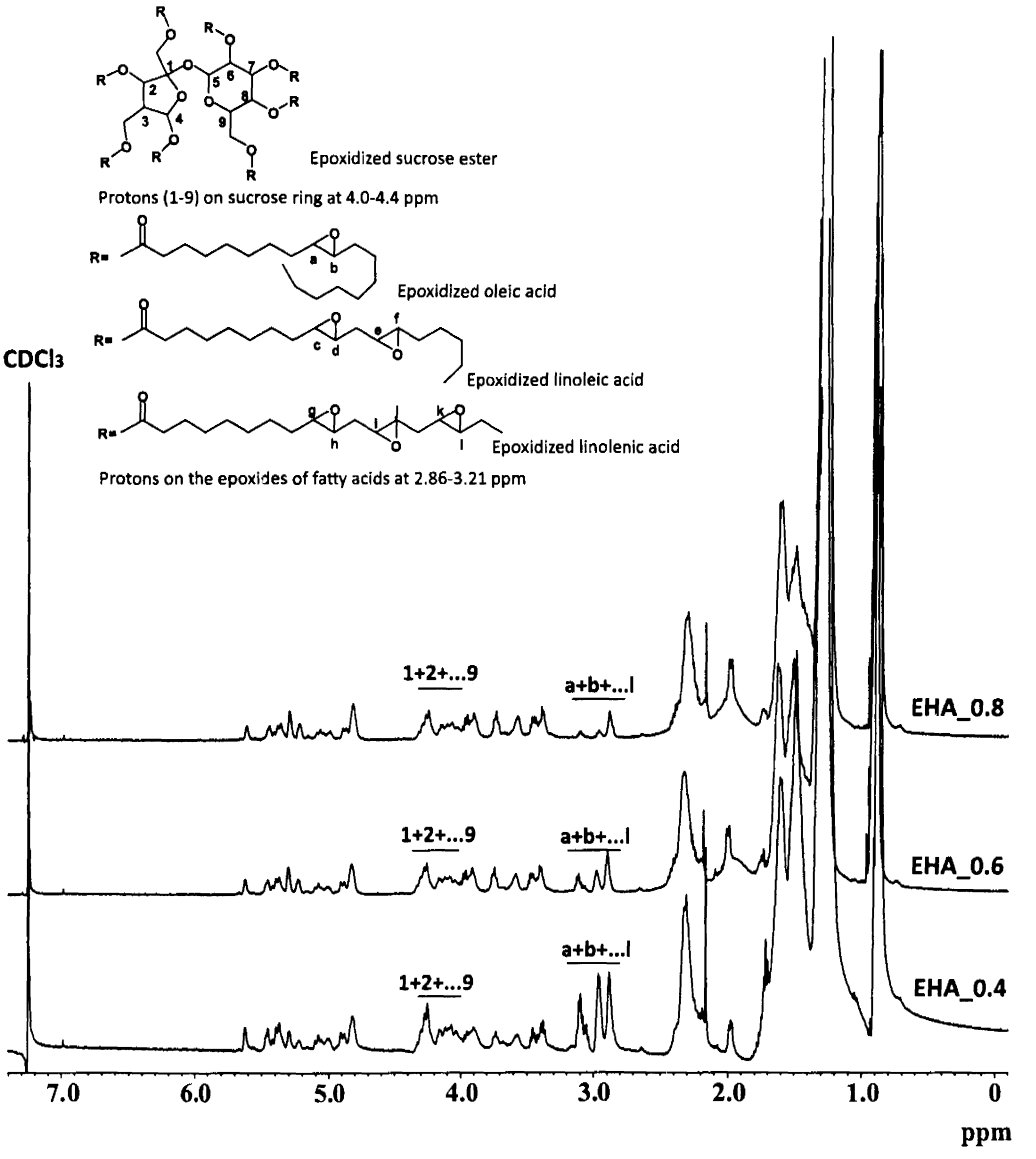

Figure 6.4. The overlaid ^{1}H-NMR spectra of the ester-polyols prepared by reaction with 2-ethylhexanoic acid (EHA) in different acid/epoxide molar ratios

Figure 6.5 shows the epoxide conversions that are calculated using the quantitative information of ^{1}H-NMR and acid number titration. The epoxide conversion has been successfully controlled by the initial acid/epoxide feed ratio, and the results from ^{1}H-NMR match the results from acid number titration. Thus, the amount of newly formed hydroxyls

is proportional to the amount of EHA used in acid/epoxide ratios from 0.4:1 to 0.8:1. It has been observed that the viscosity of the ester-polyols increases with the increase of the acid/epoxide ratio (in Table 6.1).

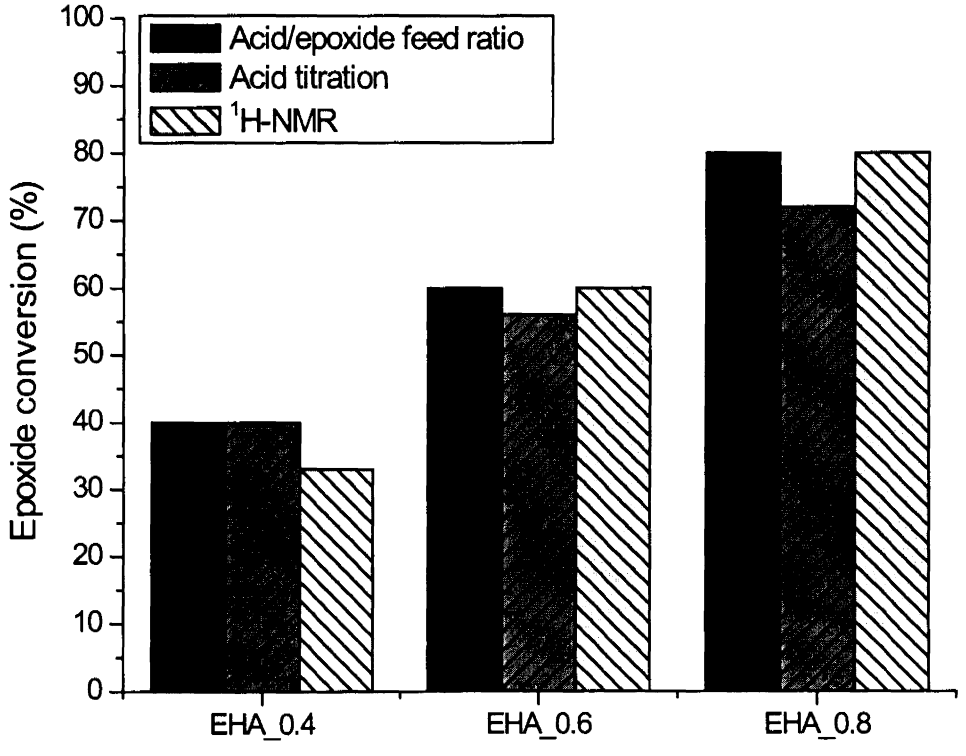

Figure 6.5. The epoxide conversions of the ester-polyols using 2-ethylhexanoic acid (EHA) in different acid/epoxide molar ratios

6.4.1.2.Acid-catalyzed alcohol-epoxy reaction

The acid-catalyzed alcohol-epoxy reaction has been used to prepare biobased soy lubricants based on the reaction between ESO and primary alcohols.[27-28] To obtain good oxidative stability and low pour point, both epoxide ring-opening and transesterification reactions are allowed to take place together in the presence of a sulfuric acid catalyst. However, to maintain an intact sucrose ester structure while producing the ether-polyol,

transesterification is an undesirable side reaction that could cleave the sucrose ester bonds to form alkyl esters of fatty acids. The reaction between epoxides and primary alcohols should be the main reaction. As another possible side reaction, newly formed secondary hydroxyls can also react with epoxides. This oligomerization will lead to a significant increase in the viscosity of ether-polyol.

Following the route of preparing soy triglyceride polyol from ESO, the method of using a methanol-isopropanol solution in the presence of tetrafluoroboric acid catalyst has been employed in this study. Methanol functions as a reactive alcohol that opens the epoxide, and isopropanol functions as solvent to dilute methanol to suppress the transesterification between methanol and sucrose ester. A low reaction temperature of 45-50°C will also suppress transesterification but facilitate the alcohol-epoxy reaction. Dropwise addition of the epoxy solution was used to create a "starved epoxide" condition to suppress oligomerization between the newly formed secondary hydroxyls and epoxides.

The compositions and characteristics of the ether-polyols synthesized are shown in Table 6.2. The effects of methanol/epoxide ratio and the addition rate of the epoxy solution on the properties of the ether-polyols were investigated using f-ESS. A lower methanol/epoxide ratio and slower addition rate of the epoxy solution result in a lower viscosity methoxylated epoxidized sucrose soyate (MESS). ESSB6 was used to prepare methoxylated epoxidized sucrose soyate B6—MESSB6. The viscosity of MESSB6 is about 5 times of the viscosity of MESS made using the same methanol/epoxide ratio and addition rate of epoxy solution. The glass transition temperatures of the ether-polyols range from -38°C to -35°C.

Table 6.2. Ether-sucrose soyate polyols prepared in alcohol-epoxy reactions

Polyol	Epoxy	Methanol/epoxide (molar ratio)	Dropwise rate of epoxy solution (ml/min)	Hydroxyl functionality	Viscosity (mPa·s)	T_g (°C)
MESS_1	f-ESS	6/1	4.0	10.0	54,800	-37
MESS_2	f-ESS	3/1	1.0	10.2	31,600	-38
MESSB6	ESSB6	3/1	1.0	9.40	185,000	-35

Figure 6.6 shows the GPC plots of the ESSs and the ether-polyol products. No peak is observed that indicates that a lower MW product was formed. Thus, the side reaction of transesterification between sucrose ester and alcohol did not occur. The higher MW peaks confirm the occurrence of the side reaction of oligomerization, and the magnitude of the higher MW shoulders of the ether-polyols is larger than that of the ester-polyols. The MW of each ether-polyol was separately determined as the MWs of the mono-sucrose soyate polyol (SSP) and oligomers. The MWs of the oligomers are 2-3 times that of the MWs of the mono-SSP.

Figure 6.7 shows the FTIR spectra of the epoxy starting materials and their ether-polyol products. A small epoxide adsorption band is observed at 826 cm^{-1} in the FTIR spectrum of f-ESS and ESSB6, but completely disappears in the spectra of polyol products. In each spectrum of ether-polyol using f-ESS, a modest hydroxyl adsorption band appears at 3200-3500 cm^{-1}. A hydroxyl adsorption band is observed at 3200-3500 cm^{-1} in the spectrum of ESSB6. The size of the hydroxyl adsorption band increases by the newly formed secondary hydroxyls in MESSB6.

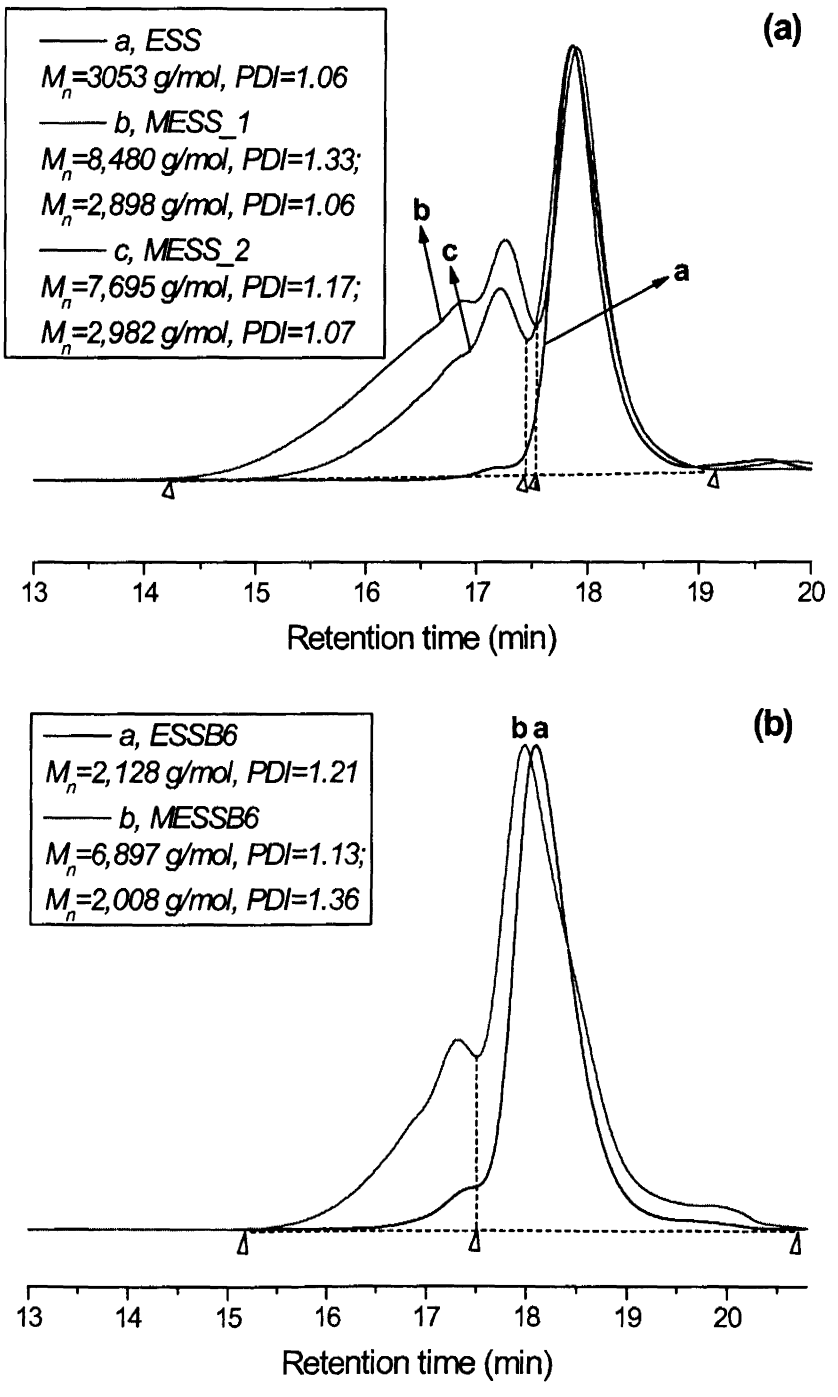

Figure 6.6. GPC plots of the starting material ESSs and ester polyol products: (a) f-ESS and MESSs; (b) ESSB6 and MESSB6

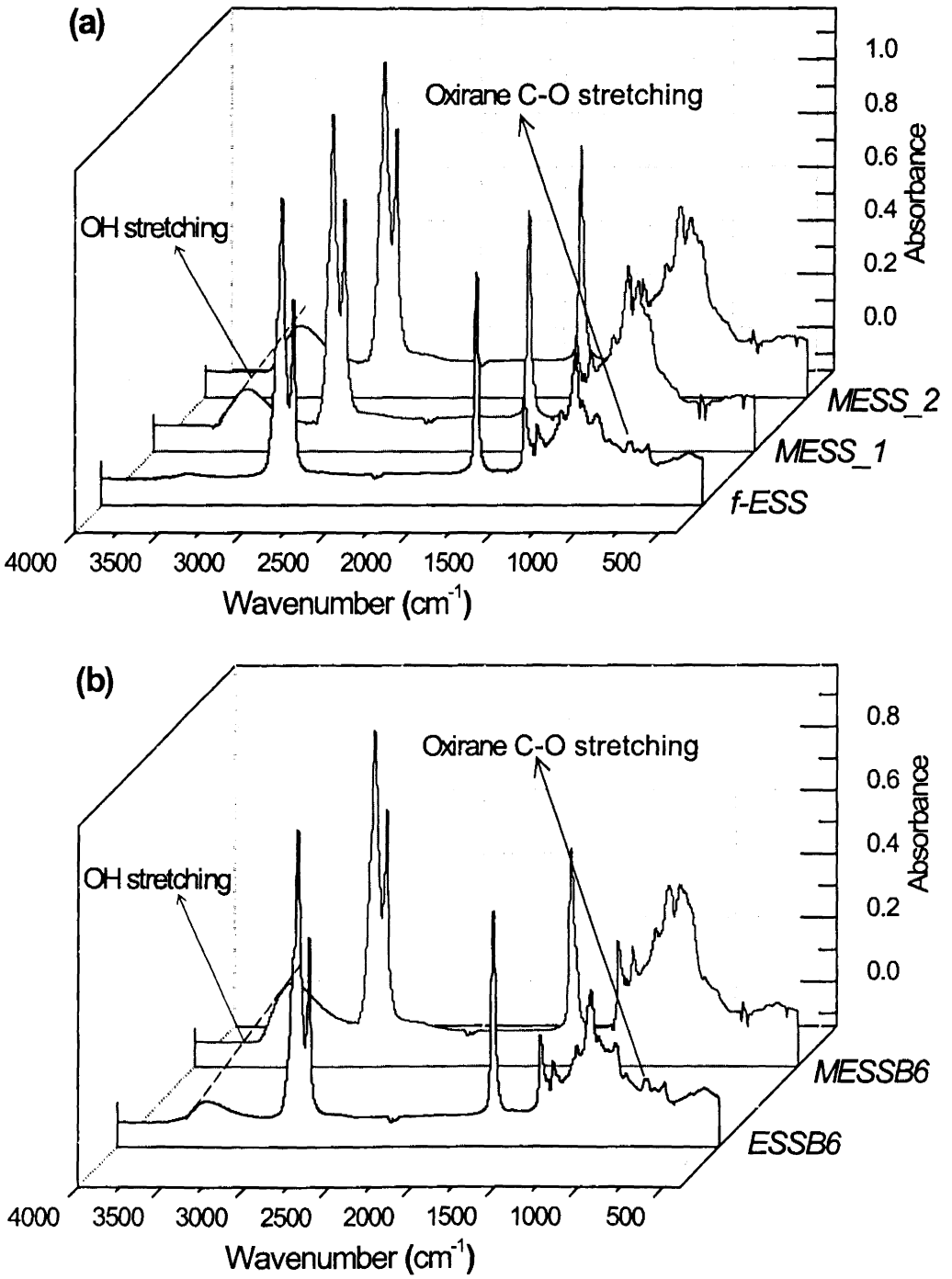

Figure 6.7. FTIR spectra of the starting material ESSs and the ether-polyol products: (a) f-ESS and MESS; (b) ESSB6 and MESSB6

Figure 6.8 shows the overlaid ^{1}H-NMR spectra of f-ESS and its ether-polyol product MESS_1. The peaks of the protons on the sucrose ring are at 4.0-4.4 ppm, and its quantitative value (area integration, $A_{1\text{-}9}$) is used as a constant for normalization. The peaks of the protons on the epoxides of fatty acids are at 2.86-3.21 ppm, and its quantitative value (area integration, $A_{a\text{-}l}$) is the variable in each spectrum. The ratios of $A_{a\text{-}l}/A_{1\text{-}9}$ for f-ESS and MESS_1 are designated as A_0 and A_{MESS_1}. The ratio of A_0: A_{MESS_1} is 1: 0.06, which means that the epoxide conversion of MESS_1 is 94%. The hydroxyl functionality of ether-polyol is determined as the epoxide functionality multiplied by the epoxide conversion.

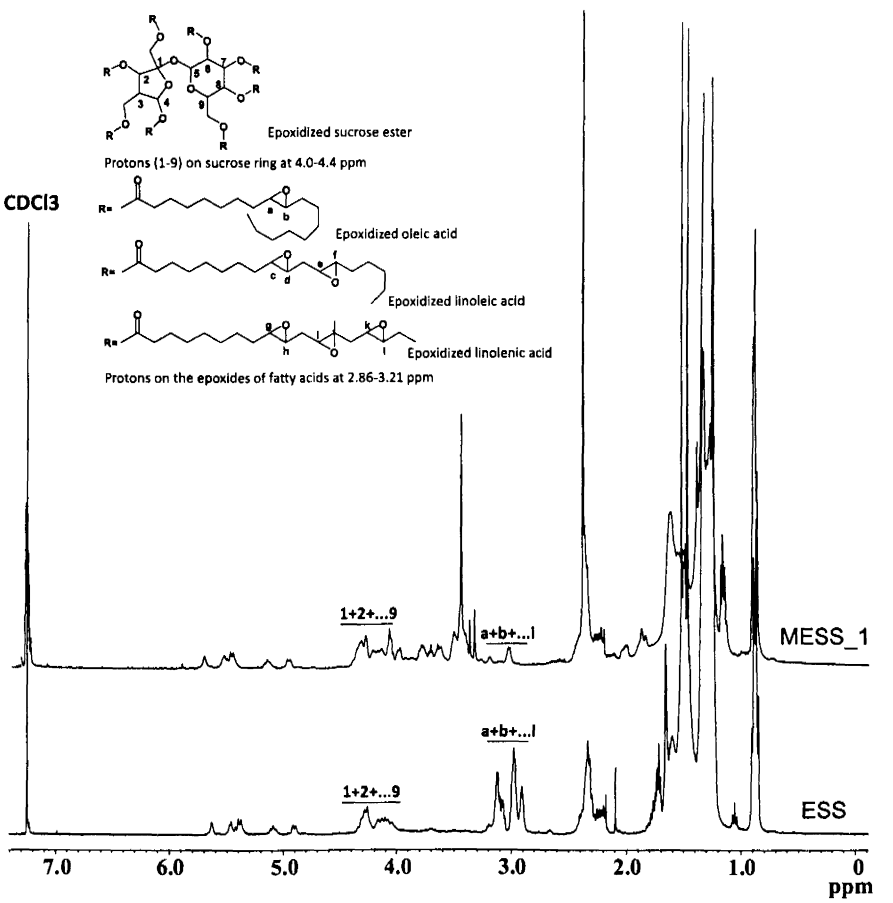

Figure 6.8. ^{1}H-NMR spectra overlaid of the starting material f-ESS and its ether-polyol product MESS_1

6.4.2. Properties of PU Thermosets

Isophorone diisocyanate (IDPI) trimer and hexamethylene disiocyanate (HDI) trimer are both aliphatic diisocyanate based polyisocyanates commonly used as crosslinkers in two component polyurethane coatings (Figure 6.9). While the isocyanate equivalent weight (IEW) of the HDI trimer is lower than that of the IPDI trimer, the IPDI trimer has a more compact and rigid chemical structure which is able to provide a more rigid polyurethane network. In this study, they were used as crosslinkers with the ester/ether-polyols to prepare PU thermosets.

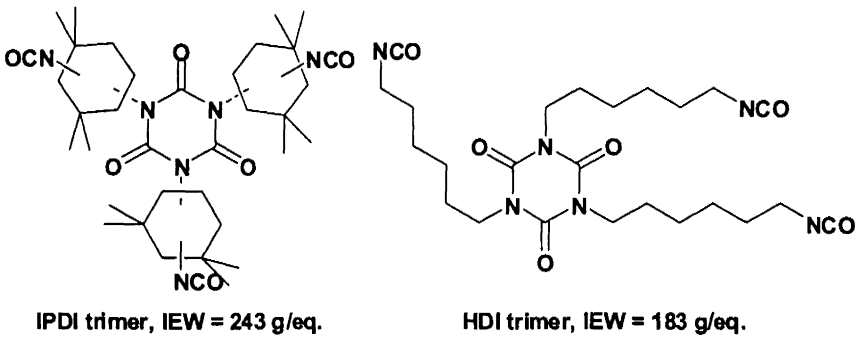

Figure 6.9. Aliphatic diisocyanate trimers

6.4.2.1.Biobased content

The United States Department of Agriculture defines the biobased content of a product as the "amount of biobased carbon in the material or product as a percent of the weight (mass) of the total organic carbon in the product", and radiocarbon analysis in accordance with ASTM D6866-05 is a reliable method for experimentally verifying the biobased content.[29] Thus, the biobased content of a product was simply demonstrated as the percent of the number of biobased carbons in the total organic carbons of the product.

Based on the above definition, sucrose soyates—made of sugar and soybean oil—are 100% biobased. Due to the incorporation of oxygen in epoxidation, epoxidized sucrose soyates are 100% biobased. On a weight basis, an f-ESS is about 77.2% carbon and a petrochemical-based methanol is 37.5% carbon. Assuming that one mol of f-ESS (2,589g) incorporates with 10 mol of methanol (302.4g) with 0% biobased, the biobased content of an ether-polyol is theoretically $\frac{2589\times77.2\%}{2589\times77.2\%+302.4\times37.5}$, which comes out to 94.6%. A typical MESS/IPDI trimer/DBU PU formulation with the NCO/OH ratio of 1.1:1 contains 10g of MESS, 12.6g of IPDI trimer, and 0.23g of DBU. On a weight basis, an IPDI trimer is 56.6% carbon and the DBU is 70.9% carbon. Theoretically, the biobased content of the PU thermoset is $\frac{10\times94.6\%}{10\times94.6\%+12.6\times56.6\%+0.23\times70.9\%}$, which comes out to and overall 56.5%. Therefore, the PU thermosets using the sucrose soyate polyols are high biobased content materials.

6.4.2.2.Coatings properties

FTIR spectroscopy is a simple but powerful technique for the investigation of the curing of polyurethanes. As an example, the ether-polyol MESS_1 was formulated with the IPDI trimer at equivalent ratios of NCO/OH of 1.1:1, 0.8:1, and 0.6:1. After curing for three hours at ambient and one hour in an oven at 80°C, the cured PU samples were studied using FTIR to monitor the characteristic stretching adsorption bands of isocyanate, ester carbonyl, and urethane carbonyl (Figure 6.10). The adsorption bands observed from the FTIR spectra of the cured samples are: 3377-3400 cm^{-1} (urethane N-H stretching), 2928-2930 cm^{-1} (antisymmetric sp^3 C-H stretching), 2856-2857 cm^{-1} (symmetric sp^3 C-H stretching), 2254-2256 cm^{-1} (isocyanate N=C=O stretching), 1741-1750 cm^{-1} (ester

carbonyl C=O stretching), 1687-1698 cm^{-1} (urethane carbonyl C=O stretching), and 1523-1547 cm^{-1} (urethane N-H out-of-plane bending). The wavenumber of the adsorption of ester carbonyl is higher than that of the urethane carbonyl due to the less capability of ester carbonyl to form hydrogen bonding.[30] The adsorption band of isocyanate stretching decreases with the decrease of the equivalent ratio of NCO/OH. The presence of unreacted isocyanates in the formulation of NCO/OH of 0.8:1 after curing is due to the low reactivity of the secondary hydroxyls.

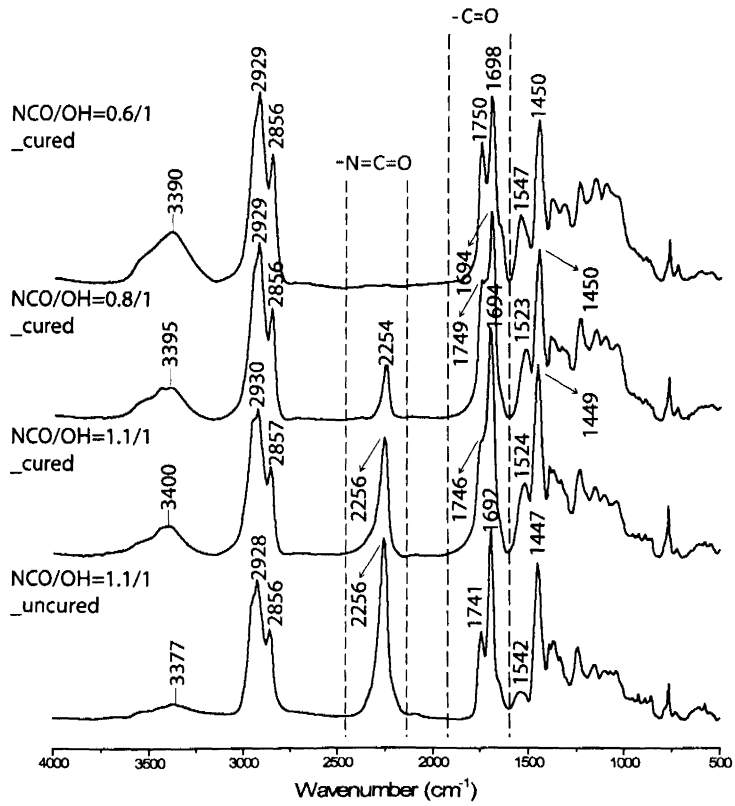

Figure 6.10. The overlaid FTIR spectra of MESS_1/IPDI trimer PU thermosets with different NCO/OH ratios

The properties of the PU coatings are shown in Table 6.3. It is observed that the IPDI-based coatings have higher coating hardness (i.e. pencil and pendulum hardness) and solvent-resistance than the HDI-based coatings, but the HDI-based coatings have greater flexibility and ductility (e.g. impact and bending resistances) than the IPDI-based coatings. EHA produced ester-polyols (i.e. EHA_0.4, EHA_0.6, and EHA_0.8) are cured by the IPDI trimer at an NCO/OH ratio of 1.1:1. Theoretically, a higher amount of hydroxyls will provide a higher degree of urethane crosslinking. Experimentally, the PU coatings using the ester-polyol having higher hydroxyl functionality have higher coating hardness and solvent resistance than the PU coatings using the ester-polyol having lower hydroxyl functionality. In the PU coatings made using the ether-polyols, a higher NCO/OH ratio results in a higher degree of urethane crosslinking and greater coating hardness and solvent resistance. However, the flexibility of the PU coatings decreases with the increase of the NCO/OH ratio.

Table 6.3. Properties of polyurethane coatings

PU formulation (Polyol/Isocyanate)	NCO/OH (molar ratio)	Thickness (μm)	König pendulum hardness (s)	Pencil hardness (gouge)	Cross-hatch adhesion	MEK double rub	Reverse impact (in-lb)	Mandrel bend (elongation-at-break)
EHA_0.8/IPDI	1.1	75 ± 3.4	164	H	3B	215	80	>28%
EHA_0.6/IPDI	1.1	71 ± 5.8	142	F	3B	185	>172	>28%
EHA_0.4/IPDI	1.1	89 ± 5.3	47	3B	5B	90	>172	>28%
PA_0.6/IPDI	1.1	84 ± 9.3	147	HB	1B	190	40	>28%
AA_0.6/IPDI	1.1	66 ± 2.9	159	2H	1B	240	40	<2.5%
AA_0.6/HDI	1.1	73 ± 6.2	10	5B	5B	130	>172	>28%
MESS_2/IPDI	1.1	70 ± 4.6	194	B	1B	>400	<4	<2.5%
MESS_2/IPDI	0.8	67 ± 5.6	179	H	4B	275	16	<2.5%
MESS_2/IPDI	0.6	66 ± 8.1	160	HB	4B	165	32	>28%
MESSB6/IPDI	1.1	71 ± 7.6	200	B	1B	>400	<4	<2.5%
MESSB6/IPDI	0.8	87 ± 8.5	192	HB	2B	350	<4	<2.5%
MESSB6/IPDI	0.6	67 ± 9.6	172	H	4B	270	<4	<2.5%
MESS_2/HDI	1.1	79 ± 5.2	57	H	5B	>400	8	>28%
MESSB6/HDI	1.1	95 ± 6.8	141	H	5B	>400	32	>28%

6.4.2.3.Tensile, dynamic mechanical, and thermal properties of PU films

The tensile properties of the PU films are shown in Table 6.4, including Young's modulus, tensile strength at break, and elongation at break. It is impressive to see that a plant-oil based PU thermoset can have modulus values of 1.0-1.6 GPa in the absence of groups having an aromatic structure. Figure 6.11 (a) shows that the PU thermosets using the ester-polyols are hard and ductile materials. The tensile properties of the PUs made using EHA-based polyols are clearly affected by the hydroxyl functionality of polyols. Figure 6.11 (b) shows that the PU thermosets using the ether-polyols are harder but more brittle than the PU thermosets using the ester-polyols. The tensile properties of PUs using ether-polyols have been effectively adjusted by the NCO/OH ratios. Additionally, the PUs using SSB6-based polyols are more elastic than the PUs using f-ESS-based polyols. Overall, the IPDI-based PUs are more elastic than the HDI-based PUs.

Table 6.4. Young's modulus, tensile strength at maximum load, and elongation at break of polyurethane films in tensile testing

PU formulation (Polyol/Isocyanate)	NCO/OH (molar ratio)	Thickness (mm)	Modulus (MPa)	Tensile strength at Max. Load (MPa)	Elongation at break (%)
EHA_0.8/IPDI	1.1	0.09 ± 0.2	1052 ± 116	25.6 ± 7.1	4.1 ± 1.0
EHA_0.6/IPDI	1.1	0.09 ± 0.5	808 ± 52	29.1 ± 1.1	9.7 ± 2.9
EHA_0.4/IPDI	1.1	0.11 ± 0.03	2.7 ± 0.55	2.03 ± 0.48	97 ± 10.4
PA_0.6/IPDI	1.1	0.09 ± 0.01	931 ± 118	34.3 ± 1.9	6.1 ± 0.4
AA_0.6/IPDI	1.1	0.08 ± 0.01	889 ± 269	40.0 ± 0.9	8.0 ± 1.7
AA_0.6/HDI	1.1	0.09 ± 0.01	6.5 ± 1.50	3.06 ± 0.40	70 ± 5.2
MESS_2/IPDI	1.1	0.07 ± 0.01	1,327 ± 159	38.9 ± 7.1	4.9 ± 1.1
MESS_2/IPDI	0.8	0.08 ± 0.02	916 ± 78	30.7 ± 5.7	5.2 ± 1.0
MESS_2/IPDI	0.6	0.08 ± 0.01	891 ± 177	36.2 ± 1.7	7.3 ± 1.0
MESSB6/IPDI	1.1	0.09 ± 0.08	1,642 ± 237	28.0 ± 6.7	2.9 ± 0.4
MESSB6/IPDI	0.8	0.08 ± 0.01	1,411 ± 64	32.5 ± 2.8	3.7 ± 0.2
MESSB6/IPDI	0.6	0.07 ± 0.01	1,234 ± 104	36.5 ± 2.8	4.6 ± 0.2
MESS_2/HDI	1.1	0.09 ± 0.01	686 ± 25	25.8 ± 1.0	20 ± 3.9
MESSB6/HDI	1.1	0.09 ± 0.02	945 ± 60	34.1 ± 5.2	6.1 ± 1.1

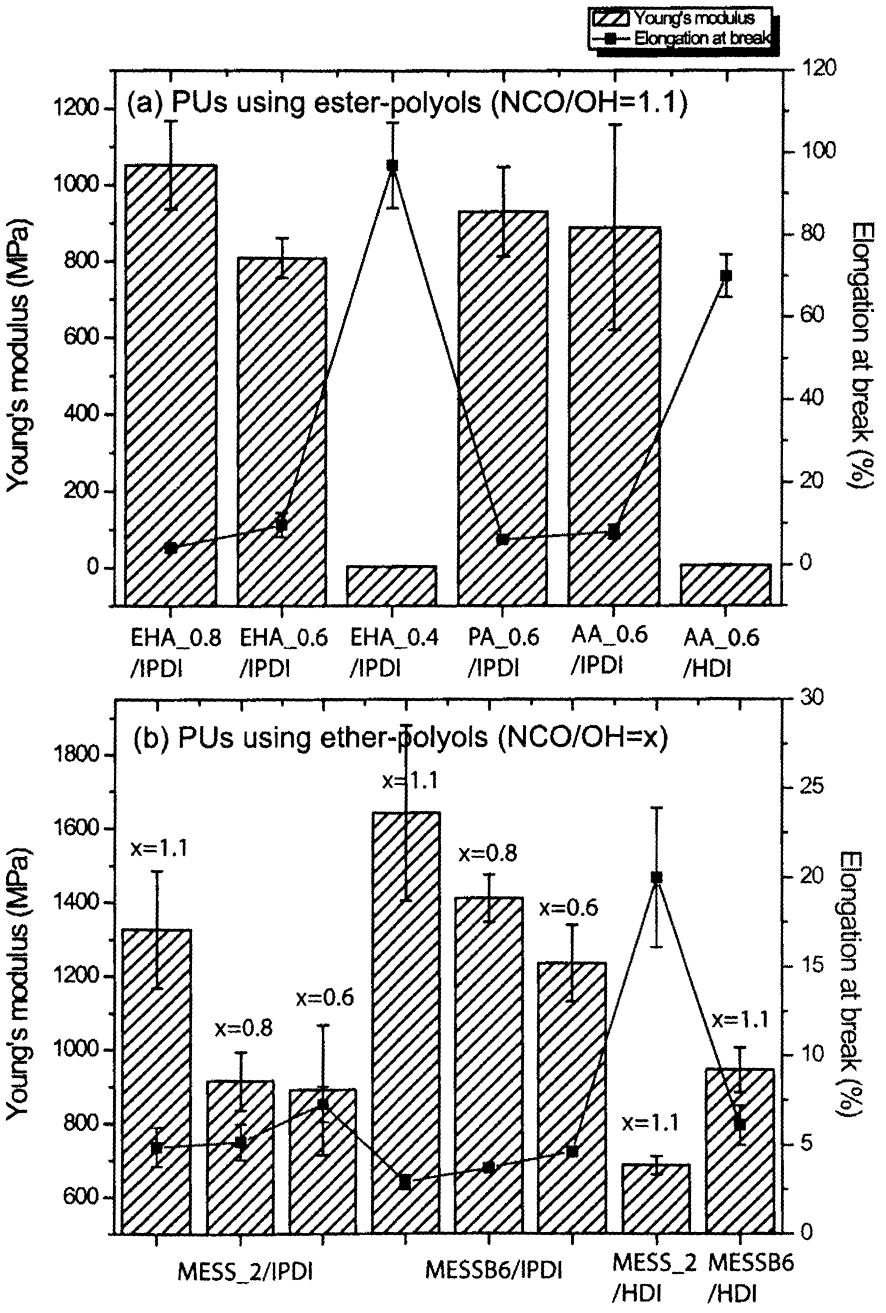

Figure 6.11. Young's moduli and elongations at break of polyurethanes films

The thermal and dynamic mechanical properties of the PUs are shown in Table 6.5. While DSC and DMA produce different glass transition temperature (T_g) values due to

their different principles of measuring T_g, the trend of T_g of PU samples is similar. It is impressive to see that a plant-oil based PU thermoset can have a 100-140°C T_g in the absence of groups having an aromatic structure. It is observed that (a) in the PUs using ester-polyols, the values of T_g, E' and ν_e are proportional to the hydroxyls available in the ester-polyols; (b) in the PUs using ether-polyols, the values of T_g, E' and ν_e are proportional to the NCO/OH ratio; (c) the T_g values of the IPDI-based PUs are higher than those of the HDI-based PUs; and (d) the PUs using SSB6-based polyols have higher T_g than the PUs using f-ESS-based polyols.

Table 6.5. Dynamic mechanical and thermal properties of polyurethane films

PU formulation (Polyol/Isocyanate)	NCO/OH (molar ratio)	DSC T_g (°C)	DMA			
			T_g (°C)	E' at 25°C (MPa)	E' at T_g+60°C (MPa)	ν_e (X 10^3 mol/mm^3)
EHA_0.8/IPDI	1.1	101	127	518.2	11.8	1.05
EHA_0.6/IPDI	1.1	70	107	509.0	9.6	0.90
EHA_0.4/IPDI	1.1	-16	17	9.4	2.1	0.25
PA_0.6/IPDI	1.1	72	115	491.6	8.6	0.79
AA_0.6/IPDI	1.1	85	122	568.7	8.0	0.72
AA_0.6/HDI	1.1	9.8	6.4	10.3	6.7	0.82
MESS_2/IPDI	1.1	141	118	570.3	7.1	0.65
MESS_2/IPDI	0.8	120	91	328.0	3.8	0.37
MESS_2/IPDI	0.6	101	86	262.6	3.6	0.35
MESSB6/IPDI	1.1	142	126	636.0	12.9	1.15
MESSB6/IPDI	0.8	134	123	401.8	9.5	0.85
MESSB6/IPDI	0.6	116	120	395.6	7.4	0.67
MESS_2/HDI	1.1	47	62	274.6	19.9	2.07
MESSB6/HDI	1.1	64	80	274.0	21.5	2.14

Petrovic et al. studied the effect of NCO/OH molar ratio and different isocyanates on the properties of soy triglyceride polyurethanes, in which the soy triglyceride polyols were prepared by reacting epoxidized soybean oil with methanol.[21-22] The T_g values of the PU thermosets were determined by DSC, DMA, and thermomechanical analysis. In an NCO/OH ratio of 1:1, the T_g values of the IPDI-based PUs were in the range of 50-70°C, and the T_g values of the HDI-based PUs were in the range of 10-20°C. Aromatic